Large-amplitude spin dynamics induced by femtosecond laser excitation in iron oxides

Dmytro Afanasiev

Large-amplitude spin dynamics induced by femtosecond laser excitation in iron oxides

Proefschrift

ter verkrijging van de graad van doctor
aan de Radboud Universiteit Nijmegen
op gezag van de rector magnificus,
volgens besluit van het college van decanen
in het openbaar te verdedigen op dinsdag 22 december 2015
om 15:00 uur precies

door

Dmytro Volodymyrovych Afanasiev

geboren op 6 juni 1988
Kremenchuk, Oekraïne

Promotor:	Prof. dr. Th. H. M. Rasing
Copromotor:	Dr. A. V. Kimel

Manuscriptcommissie:

Prof. dr. P.C.M. Christianen (voorzitter)

Prof. dr. V.V. Kruglyak (University of Exeter, Verenigd Koninkrijk)

Prof. dr. A. Maziewski (Uniwersytet w Byalimstoku, Polen)

The work described in this thesis work was supported by the European Community Seventh Framework Programme FP7-NMP-2011-SMALL-281043 (FEMTOSPIN), the European Research Council ERC Grant agreement No.257280 (Femtomagnetism), the Foundation for Fundamental Research on Matter (FOM) as well as the Netherlands Organization for Scientific Research (NWO).

to my mother Tatiana

Preface

Every story has an end but in life every end is just a new beginning. It seems that my story has come to an end. More than four years of diligent work devoted to this PhD work have flown away. One can simply say that this manuscript is something every successful PhD study ends up with. In a personal level, these four years had given me more than previewed - they made me a part of a community. Three years ago on my first conference I felt like an alien and a total stranger. Everything was new and indicted: people, techniques, ideas. Approaching this day that feeling has gradually dissolved and everything is enlightened before me, everything has become over time familiar: the people are friends, the techniques are tools, and the ideas are challenges. Today I agonize towards turning the very last page of this chapter of my life, which hopefully will lead the page towards a new as much precious experience.

During this long journey I faced many challenges, sometimes confrontable but sometimes difficult to cope with. In addition, sometimes felt powerless and unable to find the right solution but sometimes I felt proud that I overcame my distrusts and came back triumphant. All of this would be impossible to be done without the help of many people which I met here, in Nijmegen. Now I would like to ask your attention and with gratitude acknowledge some of these people.

First of all, I would like to acknowledge my supervisor - dr. Alexey Kimel. Four years ago, thanks to you I got the chance to enter the experimental physics group having no experience with physical experiment behind my shoulders. I hope that I have truly managed to justify your trust. Thank you also for introducing the beautiful and versatile world of ultrafast magnetism. I am very grateful that the door of your office was always open for me. From you I learned that a scientist has to be foremost a dreamer. From you, I have learned that the dream gives birth to a wide spectrum of problems which turns into something more visionary which one shapes it as a research project. Today I know that one day dreams come true if one persistently believes into them and gives birth to innovation and visionary projects .

Andrei, I am very grateful for your constant interest in research I was doing here. I am still impressed by your clear perception of physics. You master the method of how to translate the sophisticated into the simple. I have to admit though that, to

discuss with you a new idea was the same as to commit a crash test. Many thanks for this, because in this way I really learned a lot.

I would like to send special thanks to prof. Theo Rasing for giving me the opportunity to work in his group. Your criticism always makes working environment more ambitious and advanced, whether it concerns a simple poster, a presentation or an article. In the end of the process, your approval to me is a mark of excellence and achievement.

Dear Marilou, you solved so many formal and non-formal issues I had here. Your contribution into my successful graduation is enormous. Many thanks for your collaboration.

I wish to thank the team of our technicians: Tonnie, Albert, Andre, Sergey. Your contribution is hard to overestimate properly. It is always hard to turn into reality even the most brilliant idea. However, your responsiveness and quickness make things easier around here and help build the trust that everything is possible.

I am enormously indebted to my former supervisor and friend Prof. Boris A. Ivanov. Every discussion with you improves my understanding of physics. Your stunningly broad knowledge and experience gives a new form to the forgotten primary principles and concepts.

Ruslan, thank you so a lot for being my colleague as well as my friend! Your knowledge in solid state phenomena, especially semiconductors, is very impressive. It was always constructive to discuss physics with you. I promise, that till the end ticket of my life, I will keep checking "effect of the nuclei". Leave aside your performance, you are a very organized person, both in science and in regular life and your fanatic discipline will always serve as an example for me.

Rostislav, I am very happy to have you around. You acquired a very fortunate combination of experimentalist and theoretician, which makes you a unique specialist. It was always a pleasure to hear a critical and precise reasoned opinion from you.

Personally I would like to acknowledge dr. Iliya Razdolskii for teaching me the pump-probe technique and for theendless discussions we had together during the measurements and writing. I am grateful to dr. Sasha Kalashnikova for constant interest in the research I was conducting and for the precious advices she gave me. Many thanks to Dr. Yusuke Hashimoto, who helped me start programming with LabView. I was very lucky to work with Dr. Johan Mentink during my master studies. Johan, many thanks for this fruitful work!

I wish to thank to dr. Mark Strugatsky , who is a well recognized expert in iron borate. Our collaboration was very pleasant for me and finalized in a great publication. During my PhD I was very lucky to get a chance to meet and to work with famous Prof. A. Zvezdin, who is an expert in rare-earth magnetism. Many thanks for the joint efforts. I am very grateful to Prof. Roman V. Pisarev, for the expressed interest and his suggestions.

And of course, I am thankful for all people I met during my PhD. You guys, made my stay here enjoyable and memorable.

Finally, I take this opportunity to express my unlimited gratitude to my mom Tatiana for her unconditional love, unfailing encouragement and support.

Contents

Chapter 1

Introduction

1.1 The frontiers of magnetic data storage

In nowadays electronic technology miniaturization is successfully entering the nanoworld following Moores law, whereas the speed lags behind, creating a so called ultra-fast technology gap [1]. This is also evident in modern PCs that already have a clock speed of a few GHz, whereas the storage on the magnetic hard disk requires a few nanoseconds. Similar problems are encountered by in the recently emerged spintronics-technology and Magnetic Random Access Memory (MRAM) devices, in particular. Although MRAM possesses very strong advantages over its alternatives (Dynamical RAM and Static RAM), such as non-volatility, high density and radiation hardness, the state-of-the-art rate for manipulating magnetic bits in spintronics is remains below the GHz regime. Meanwhile, competing technologies, not based on magnetic media, such as solid stat memory, offer much higher speeds being up to 5 bit/ns.

The reason for this lag is not necessarily found in fundamental limitations, but rather in the lack of our understanding of particular mechanisms allowing faster switching of magnetic moments. Therefore, the search for fundamental and practical solutions to increase the speed of manipulating magnetic bits is an issue of vital importance for modern technology.

Consequently nanoscale magnetization dynamics has become a subject of intense research interest making the search for fundamental limits on the speed of magnetic switching one of the most challenging issues in modern magnetism. It is known that one of the fastest ways to reorient the magnetization $\mathbf{M}$ is the reorientation via a precessional motion, where the magnetic field is applied perpendicularly to $\mathbf{M}$ [2, 3]. The mechanisms and dynamics of magnetization reversal in nanomagnets have been intensively investigated over the last 10 years. However, all these time-resolved studies were performed at time-scales longer than 100 ps. The generation of magnetic field pulses strong enough to reverse magnetization and shorter than 100 ps appears to be

an extremely challenging issue as it involves magnetic field pulses that are both short (<100 fs) and strong (>1T) [1]. As a result, very little is known about the dynamics of magnetization reversal on a sub-100 ps time-scale. Interestingly, the very first time-resolved studies of the laser induced demagnetization of Gd [4] and Ni [5] also declared 100 ps, defined by spin lattice relaxation time, to be the intrinsic limit for the time required to control the magnetization in media. Usually, at this and longer timescales, thermodynamical models can be applied to explain the subsequent processes. Thus this timescale became a limit below which the magnetization dynamics can be referred to as "ultrafast " and "non-equilibrium".

These limitations have triggered an intense search for ways to control the magnetic state of a medium by means others than magnetic fields and on timescale less than 100 ps. The subpicosecond demagnetization of a Ni film by a 60 fs optical laser pulse [6], discovered just a couple of years later, has raised a number of questions about the mechanisms responsible for a laser-induced demagnetization on a time-scale much faster than the spin-lattice relaxation time. Many scenarios suggesting novel mechanisms for ultrafast energy and angular momentum transfer from and/or to the spin system have been suggested.

According to Ref. [7] the effects of a pump pulse on a magnetic system could be classified as belonging to one of the following classes:

Thermal effects. The direct pumping of energy from light to spins is not effective. Instead, light pumps its energy into the electron and phonon system. Internal equilibration processes such as electron-electron, electron-phonon, and electron-spin interactions, determines magnetization changes. Usually this mechanism is effective for itinerant ferromagnets.

Nonthermal (photomagnetic) effects. These effects depend on the absorption of photons, resulting in an effective excitation of the system. In this case the photons are absorbed via certain real electronic states that have a direct influence on the magnetic parameters, such as, for example, the magnetocrystalline anisotropy.

Nonthermal (optomagnetic) effects. Nonthermal optomagnetic effects that do not require the absorption of pump photons but are based on optically coherent stimulated Raman scattering. It was demonstrated that circularly and linearly polarized femtosecond laser pulses can excite and coherently control the spin dynamics in magnets. Moreover, the effect of such ultrashort optical pulse on a magnetic system was found to be equivalent to the effect of a similarly short magnetic field pulse with the strengths of the order of several T. Usually this mechanism is effective in dielectrics.

In this work we limit our study to the interactions of femtosecond laser pulses with iron oxides, which belong to the family of antiferromagnetic dielectrics. Antiferromagnets, though representing the overwhelming majority of magnetically ordered materials, only nowadays start to attract practical interest. Antiferromagnets have no net magnetic moments and as a consequence are much less sensitive to external

magnetic fields. Spin dynamics in antiferromagnets is intrinsically faster (up to two orders of magnitude) than in ferromagnetic materials, because this dynamics is driven by the exchange interaction [8]. Many iron oxides have the bandgap in the range 1.5-3 eV. This fact allows photons with their energy in this range to interact with the oxides without being absorbed. It means that a situation when one photon interacts with several spins is not forbidden.

1.2 Magnetization dynamics in non-collinear antiferromagnets

Antiferromagnetism is often encountered among transition metal compounds, especially oxides. Examples of antiferromagnets include metals (Cr), alloys (FeMn), and oxides (NiO).

The magnetic structure of the antiferromagnets consists of at least two magnetic sublattices oriented antiparallel with respect to each other. As a result, no net magnetic moment is associated with the antiferromagnetic structure. For this reason manipulation of the magnetic structure by an external magnetic field is hindered in antiferromagnets.

To obtain very fast intrinsically magnetization dynamics, the presence of the antiferromagnetic coupling is crucial [8]. To manipulate the magnetic structure by means of a moderate external magnetic field, the presence of the a net magnetization moment is desirable. Non-collinear antiferromagnets (weak ferromagnets) satisfy both requirements. Their magnetic structure consist of two antiferromagnetically coupled magnetic sublattices $\mathbf{M}_1$ and $\mathbf{M}_2$, which are canted due to the relativistic antisymmetric exchange interaction (the Dzyaloshinskii-Moria interaction) [9]. Such a non-collinear structure possesses a small net magnetization.

To describe the spin dynamics of non-collinear antiferromagnets one can start from the equations for the vectors of ferromagnetism $\mathbf{M}$ and antiferromagnetism $\mathbf{L}$:

$$\mathbf{M} = \mathbf{M}_1 + \mathbf{M}_2, \qquad \mathbf{L} = \mathbf{M}_2 - \mathbf{M}_1 \tag{1.1}$$

Such representation suggests the vector $\mathbf{L}$ as the order parameter for the antiferromagnets. In weak-ferromagnets the following statements are valid:

$$\mathbf{M} \perp \mathbf{L}, \qquad |\mathbf{M}| \ll |\mathbf{L}| \tag{1.2}$$

The equations of motion for the vectors $\mathbf{M}$ and $\mathbf{L}$ can be easily obtained from the Landau-Lifshitz equations for the sublattice magnetizations $\mathbf{M}_1$ and $\mathbf{M}_2$:

$$\frac{\partial \mathbf{M}}{\partial t} = \gamma \left[\mathbf{M}, \mathbf{H}_{\mathrm{M}}\right] + \gamma \left[\mathbf{L}, \mathbf{H}_{\mathrm{L}}\right] \tag{1.3}$$

$$\frac{\partial \mathbf{L}}{\partial t} = \gamma \left[\mathbf{M}, \mathbf{H}_{\mathrm{L}}\right] + \gamma \left[\mathbf{L}, \mathbf{H}_{\mathrm{M}}\right] \tag{1.4}$$

Here γ is the gyromagnetic ratio. The fields $\mathbf{H}_{\mathrm{M}}$ and $\mathbf{H}_{\mathrm{L}}$ are called effective magnetic fields and defined as:

$$\mathbf{H}_{\mathrm{M}} = -\frac{\delta\Phi}{\delta\mathbf{M}}, \qquad \mathbf{H}_{\mathrm{L}} = -\frac{\delta\Phi}{\delta\mathbf{L}} \tag{1.5}$$

The general expression for the magnetic free energy of a non-collinear antiferromagnet Φ has the form:

$$\Phi = \frac{1}{2}\mathcal{J}M^2 + \mathbf{D}\cdot[\mathbf{L}\times\mathbf{M}] + \Phi_a - \mathbf{M}\cdot\mathbf{H} \tag{1.6}$$

Here $\mathcal{J} > 0$ so that the first term represents the isotropic exchange energy. Positive sign of $\mathcal{J}$ favors anticollinear spin alignment. The term proportional to $\mathbf{D}$ is the energy of the antisymmetric exchange or the Dzyaloshinkii-Moria energy, which favors the magnetizations canting. Φ_a is determined by magnetic symmetry group of the antiferromagnet. The very last term is the Zeeman interaction with external magnetic field $\mathbf{H}$.

It is worth mentioning that since in general effective fields depend on $\mathbf{M}$ and the product of these quantities appears in the right-hand side part of Eq. (1.3), Eq. (1.4) this equations are intrinsically nonlinear.

Substitution of free energy Eq. (1.6) in Eq. (1.4) allows to represent $\mathbf{M}$ as unambiguous function of $\mathbf{L}$ and $\mathbf{H}$:

$$\mathbf{M} = \frac{1}{\mathcal{J}}\left\{[\mathbf{D}\times\mathbf{L}] + \mathbf{H} + \frac{1}{\gamma}\left[\mathbf{L}\times\frac{\partial\mathbf{L}}{\partial t}\right] - \mathbf{L}\,(\mathbf{L}\cdot\mathbf{H})\right\} \tag{1.7}$$

Interestingly, Eq. (1.7) shows that even in compensated collinear antiferromagnet with no antisymmetric exchange a net magnetization emerges once the dynamics is triggered. It is seen also that in presence of the Dzyaloshinskii-Moria interaction a built-in net magnetization is present in the media. Effect of the static external field in antiferromagnets is substantially reduced by the exchange parameter $\mathcal{J}$ and in many cases may be neglected.

It is reasonable, based on inequality $|\mathbf{M}| \ll |\mathbf{L}|$, to assume that anisotropy energy is a function only of the components of the antiferromagnetic vector L_i, $\Phi_a = \Phi_a\,(L_j)$. The equation which describes motion of the vector $\mathbf{L}$ is:

$$\frac{1}{\gamma^2}\left[\mathbf{L}\times\frac{\partial^2\mathbf{L}}{\partial^2 t}\right] = \left[\mathbf{L}\times\left(-\mathcal{J}\frac{\delta\Phi_e}{\delta\mathbf{L}}\right)\right] + \frac{1}{\gamma}\left\{2\,(\mathbf{L}\cdot\mathbf{H})\,\frac{\partial\mathbf{L}}{\partial t} + \left(\mathbf{L}\left(\mathbf{L}\cdot\frac{\partial\mathbf{H}}{\partial t}\right) - \frac{\partial\mathbf{H}}{\partial t}\right)\right\} \tag{1.8}$$

$$\Phi_e = \Phi_a\,(L_j) + \mathbf{L}\cdot[\mathbf{D}\times\mathbf{H}] + \frac{1}{2}\,(\mathbf{L}\cdot\mathbf{H})^2 + \frac{1}{2}\,(\mathbf{L}\cdot\mathbf{D})^2 \tag{1.9}$$

Eq. (1.8) is a particular case of more general spatially inhomogeneous the Andreev-Marchenko equation, which describes magnetization dynamics in antiferromagnets [10]. It is of second order, so that can demonstrate features of the inertial dynamics. This is in contrast to ferromagnets, where dynamics of the magnetization is described by a first-order differential equation. In systems described by first-order equations the dynamics can be driven only when external stimulus is present. Once stimulus is gone

system relaxes back to the equilibrium. For this reason excitation of ferromagnets by impulsive perturbation is inefficient. In antiferromagnets energy can be stored in the form of kinetic energy proportional to the first derivative of the antiferromagnetic vector $\frac{\partial L_i}{\partial t}$.

Eq. 1.8 clearly shows that magnetization dynamics can be triggered by means of external magnetic field. Interesting, that both terms $\mathbf{H}$ and $\frac{\partial \mathbf{H}}{\partial t}$ can contribute to the magnetization dynamics. In case of the static fields the term proportional to the derivative of the field can be neglected. However account for this term becomes especially important, when one deals with short pulses of magnetic field. The Eq. (1.8) in absence of the external magnetic field is:

$$\frac{1}{\gamma^2}\frac{\partial^2 L_i}{\partial^2 t} + \mathcal{J}\frac{\partial \Phi_a\left(L_j\right)}{\partial L_i} = 0 \tag{1.10}$$

Consider the simplest case of the magnetic anisotropy in the form:

$$\Phi_a\left(L_j\right) = -\frac{1}{2}K_2 L_j^2 = -\frac{1}{2}K_2\left(L_0^2 - \sum_{i\neq j} L_i^2\right). \tag{1.11}$$

Here K is magnetic anisotropy parameter. In this case preferred direction of the vector L is the j axis. The Eq. (1.10) for the transverse component L_i takes the form of the mathematical pendulum:

$$\frac{\partial^2 L_i}{\partial^2 t} + \left(\gamma^2 \mathcal{J} K_2\right)\cdot L_i = 0 \tag{1.12}$$

It is seen that frequency of oscillations $\omega_0 = \gamma\sqrt{\mathcal{J}K_2}$. Importantly, ω_0 is given not only by anisotropy parameter but by of the geometric mean of exchange and anisotropy parameters. For this reason dynamics of antiferromagnets is intrinsically faster than in ferromagnets.

1.3 Inverse magneto-optical effects

Among the large variety of non-dissipative optomagnetic effects, the most prominent are the Inverse Faraday Effect and the Inverse Cotton-Mouton Effect [7].

Recently, it has been reported [11] that spin precession was induced by a circularly polarized pulse in antiferromagnetic $DyFeO_3$ with a weak ferromagnetic moment. The phase of the spin precession changed over π on reversal of the pump polarization helicity. The interpretation of this phenomenon is that an effective magnetic field pulse $\mathbf{h}^{eff}$ parallel to the pump wave vector is induced by the circularly polarized light pulse, giving rise to the precession:

$$\mathbf{h}^{eff} = -i\frac{\chi}{16\pi}\left[\boldsymbol{\mathcal{E}} \times \boldsymbol{\mathcal{E}}^*\right] \tag{1.13}$$

Equation (1.13) is given in the Gaussian system of units, χ is the magneto-optical susceptibility. $\boldsymbol{\mathcal{E}}$ and $\boldsymbol{\mathcal{E}}^*$ are the electric field of the light wave propagating along the z-direction and its complex conjugate, respectively.

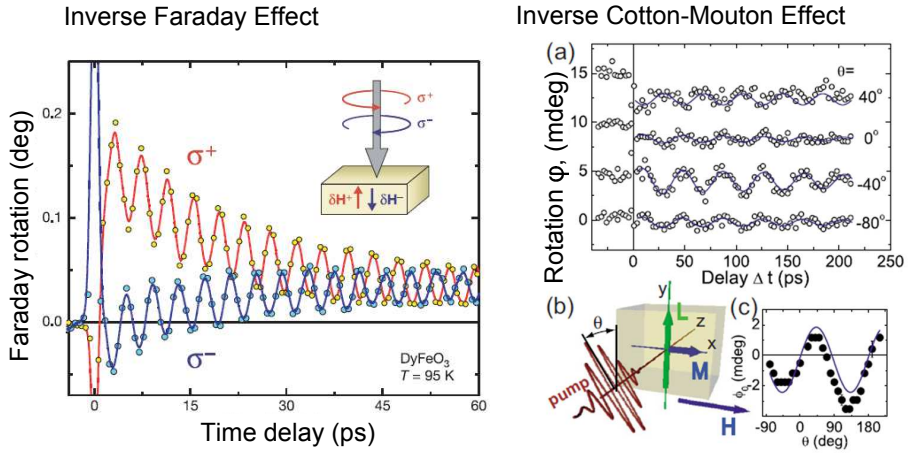

Figure 1.1: (a) Optomagnetic excitation of spin precession in $DyFeO_3$ by a circularly polarized femtosecond laser pulse via the Inverse Faraday Effect. (b) Optomagnetic excitation of spin precession in $FeBO_3$ by a linearly polarized femtosecond laser pulse via the Inverse Cotton-Mouton Effect.

$$\boldsymbol{\mathcal{E}} = \boldsymbol{\mathcal{E}}_0 \exp\left[-i\left(\omega t - kz\right)\right] \tag{1.14}$$

Here $\boldsymbol{\mathcal{E}}_0$ is amplitude of the electric field of the light wave, ω and k are the frequency and wavevector of the wave, respectively.

Spin precession can be also excited with the help of a linearly polarized pump pulse via the Inverse Cotton-Mouton effect (ICME) [12]. ICME can be interpreted as an instantaneous light-induced magnetic anisotropy axis, the direction of which coincides with the light polarization. If such an axis is parallel or orthogonal to the initial directions of the spins, there will be no effect of light on the spins. Otherwise the light induces a torque which effectively launches the spin precession.

The ultrafast IFE and ICME are also interpreted as an impulsive stimulated Raman scattering (ISRS) process. An electron in the ground state is excited by the pump pulse into a virtual state. This fact changes the orbital momentum of the electron. Due to the non-zero orbital momentum and spin-orbit coupling in the virtual state the electron spin flips. The excited electron radiates a photon and relaxes to the final state. The energy gap between the final and initial states corresponds to the energy of a magnon at the center of the Brillouin zone.

Linear magneto-optical properties of media and their modifications in external magnetic fields (the Faraday effect, magnetic dichroism, etc.) are described in terms of the dielectric permittivity tensor ε_{ij}. By virtue of the Onsager principle, if absorption is negligible, ε_{ij} can be divided into symmetric (ε^s_{ij}=ε^s_{ji}) and antisymmetric parts, (ε^a_{ij}=-ε^a_{ji}) with real and imaginary components, respectively.

The energy per unit volume of the interaction between the electric component of the electromagnetic wave and the magnetic medium is given by:

$$\Phi_{lm} = \frac{\varepsilon_{ij}}{16\pi}\mathcal{E}_i\mathcal{E}_j^* \tag{1.15}$$

$\mathcal{E}_{i,j}$ are time-dependent components of the electric field of the pump light. The interaction of the light with the magnetic system can be described as an expansion of ε_{ij} with respect to $\mathbf{L}$ and $\mathbf{M}$:

$$\varepsilon_{ij} = \varepsilon_{ij}^0 + ig_{ijk}L_k + a_{ijkl}M_kM_l + b_{ijkl}L_kL_l + c_{ijkl}M_kL_l + \dots \tag{1.16}$$

The tensors g_{ijk}, a_{ijkl}, b_{ijkl} and c_{ijkl} have to satisfy symmetry operations of the magnetic and crystal point groups.

A circularly polarized wave propagating along the $z-$axis can be presented in the form:

$$\begin{pmatrix}\mathcal{E}_x\\ \mathcal{E}_y\end{pmatrix} = \frac{1}{\sqrt{2}}\mathcal{E}_0\begin{pmatrix}1\\ \pm i\end{pmatrix} \tag{1.17}$$

Here the $\pm$ signs indicate the opposite senses of the helicity and $\mathcal{E}_0$ is the amplitude of the electric field of the incident light.

The energy of the interaction between media and the circularly polarized light wave is given by:

$$\Phi_{\sigma\pm} = \frac{1}{32\pi}\mathcal{E}_0\mathcal{E}_0^*\left(\varepsilon_{xx}^s + \varepsilon_{xx}^s \mp 2i\varepsilon_{xy}^a\right) \tag{1.18}$$

A linearly polarized light wave with the polarization inclined at an angle ϕ with respect to the x axis can be presented in the form:

$$\begin{pmatrix}\mathcal{E}_x\\ \mathcal{E}_y\end{pmatrix} = \mathcal{E}_0\begin{pmatrix}\cos\phi\\ \sin\phi\end{pmatrix} \tag{1.19}$$

The energy of the interaction of the linearly polarized wave and the media is given by:

$$\Phi_{\phi} = \frac{1}{16\pi}\mathcal{E}_0\mathcal{E}_0^*\left(\varepsilon_{xx}^s\cos^2\phi + \varepsilon_{yy}^2\sin^2\phi + \varepsilon_{xy}^s\sin 2\phi\right) \tag{1.20}$$

To show how light can perturb a magnetic system, the effective fields need to be introduced according to the following rule:

$$\mathbf{h}_{\mathrm{M}}^{eff} = -\frac{\delta\Phi_{lm}}{\delta\mathbf{M}} \qquad \mathbf{h}_{\mathrm{L}}^{eff} = -\frac{\delta\Phi_{lm}}{\delta\mathbf{L}} \tag{1.21}$$

Thus, such an approach allows to include light-matter interactions in the conventional Landau-Lifshitz equation as extra terms in the effective fields. For the case of ultrashort laser pulses, the effective fields are pulsed with a duration defined by the temporal width of the optical pulse.

1.4 Impulsive excitation

If the duration of the pulse of the effective field Δt satisfies the inequality $\Delta t \ll \frac{1}{\omega_0}$, the pulse of effective field $\mathbf{h}^{eff}$ can be considered as aδ-function in the time domain. Such a excitation is called impulsive and acts instantaneously. Usually it is relevant for the optomagnetic effects. The Eq. (1.12) can be written as:

$$\frac{\partial^2 L_i}{\partial t^2} + \omega_0^2 L_i = C_i \cdot \delta(t) \tag{1.22}$$

or:

$$\frac{\partial^2 L_g}{\partial t^2} + \omega_0^2 L_g = C_g \cdot \frac{\partial}{\partial t}\delta(t) \tag{1.23}$$

Here L is used to denote a oscillatory component of the vector $\mathbf{L}$.

The mechanisms of excitation described by Eqs. (1.22) and (1.23) are called inertial and gyroscopic, respectively [13]. Which one depends how light acts on a magnetic media: as a effective field itself or as its derivative. The parameters C_i and C_g are proportional to the intensity of the laser radiation. It can be easily shown that the action of the driving force is equivalent to the establishment of the initial conditions, namely:

$$L_i(0) = 0 \qquad \frac{\partial L_i}{\partial t}(0) = C_i \tag{1.24}$$

$$L_g(0) = C_g \qquad \frac{\partial L_g}{\partial t}(0) = 0 \tag{1.25}$$

It is not difficult to obtain from Eqs. (1.24) and (1.25) that the amplitudes of the excited precession with the eigenfrequency ω_0 are:

$$L_i^0 = \frac{C_i}{\omega_0} \qquad L_g^0 = C_g \tag{1.26}$$

There is a fundamental difference between the inertial and the gyroscopic dynamics. For the case of the gyroscopic mechanism, the amplitude of the oscillation is not sensitive to any internal parameters of the material and is defined only by the pump. For the inertial mechanism, the amplitude is inversely proportional to the eigen frequency of the oscillation, which is a function of the magnetic media.

This can be easily understood in terms of the energy conservation law applied to Eq. (1.12):

$$\frac{1}{2}\left(\frac{\partial L}{\partial t}\right)^2 + \frac{1}{2}\omega_o^2 L^2 = const \tag{1.27}$$

Here the first and the second term represent the kinetic and the potential energy of the system, respectively. The inertial excitation mechanism of spins relies on light-induced contributions to the kinetic energy, while the gyroscopic mechanism contributes to the potential energy.

1.5 Displacive excitation

A displacive excitation can be introduced as an instantaneous and long-living change of the magnetic parameters of the magnetic system. It is relevant mostly for absorptive photomagnetic effects, such as the photo-induced magnetic anisotropy [14]. On the basis of Eq. (1.12) it can be introduced as a step-function $\theta(t)$:

$$\frac{\partial^2 L_d}{\partial t^2} + \omega_0^2 L_d = C_d \cdot \theta\,(t) \tag{1.28}$$

A general solution of this equation is:

$$L_d = \frac{C_d}{\omega_0^2} \cdot (1 - \cos \omega t) \tag{1.29}$$

It is seen that in addition to the oscillations, the amplitude L_d^0 of which is given by:

$$L_d^0 = \frac{C_d}{\omega_0^2}, \tag{1.30}$$

the system acquires a permanent displacement.

Another case of a displacive excitation is a periodic driving force which acts at a frequency $\omega \ll \omega_0$. On the basis of Eq. (1.12) it can be introduced as an equation of a driven harmonic oscillator:

$$\frac{\partial^2 L_h}{\partial t^2} + \omega_0^2 L_h = C_h \sin \omega t \tag{1.31}$$

The amplitude of the driven oscillations is given by:

$$L_h^0 = \frac{C_h}{\omega^2 - \omega_0^2} \tag{1.32}$$

Thus it shows a typical resonant behavior.

1.6 Large-amplitude magnetization dynamics and anharmonicity

The possibility to excite coherent spin precession by means of ultrashort laser pulses paves the way to coherent control of the spin precession. This includes the controllable amplification and suppression of the spin oscillation with the help of pump pulses. The most exciting application of such a concept is the oscillatory magnetization reversal (Fig. 1.2).

In order to perform a magnetization reversal one needs to overcome the potential barrier created by the magnetic anisotropy. The barrier separates states with their magnetization directed "up" and "down". The essential part of this scenario is high-amplitude spin oscillations launched by ultrashort laser pulses. As it was mentioned,

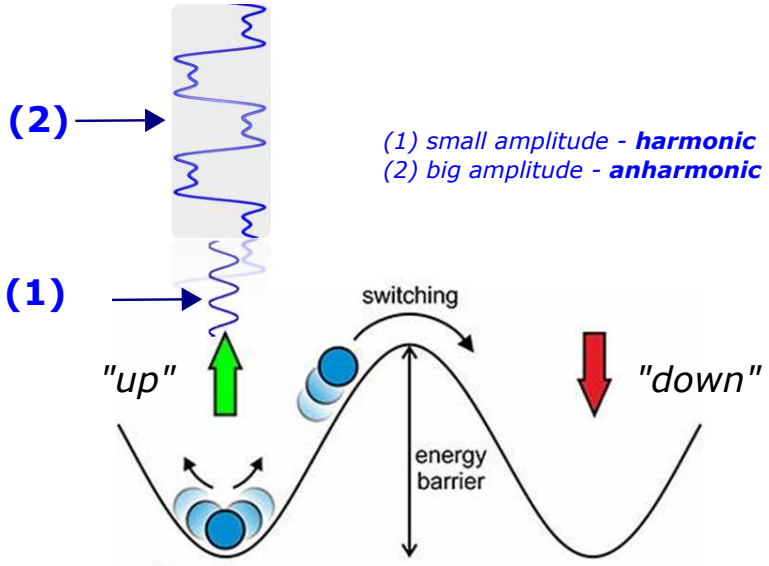

Figure 1.2: Scenario for oscillatory magnetization reversal. It is shown that anharmonicity always accompanies large amplitude spin precession and precedes the magnetization reversal.

the equation of spin motion is essentially non-linear and has to demonstrate anharmonic behavior for high amplitudes of the spin deviations. Hence an anharmonicity has to precede the magnetization reversal.

The generalized equation to describe the non-linear motion of a particle in a complex potential $U(x)$ is given by:

$$\frac{\partial^2 x}{\partial t^2} + f(x) = 0 \tag{1.33}$$

where $f(x) = \frac{\partial U}{\partial x}$. Expanding $f(x)$ in a Taylor series up to terms of the 3^{rd} order gives:

$$\frac{\partial^2 x}{\partial t^2} + \omega_0^2 x + \alpha x^2 + \beta x^3 = 0 \tag{1.34}$$

The nonlinear terms in Eq. (1.33) lead to the emergence of the first, the second and the third harmonic of the main frequency ω. The solution of this equation can be found in the following form:

$$x = A\exp(i\omega t) + a\exp(i2\omega t) + b\exp(i3\omega t) + c.c. + C \tag{1.35}$$

Substitution of Eq. (1.35) in Eq. (1.34) and assuming that $A \gg a, b, C$ gives:

$$\left[\left(\omega_0^2 - \omega^2\right)A + 3\beta A^2 A^*\right]\exp(i\omega t) + \left[\left(\omega_0^2 - 4\omega^2\right)a + \alpha A^2\right]\exp(i2\omega t) + \left[\left(\omega_0^2 - 9\omega^2\right) + \beta A^3\right]\exp(i3\omega t) + c.c. + \omega_0^2 C + 2\alpha A A^* \approx 0 \tag{1.36}$$

Solving this equation one can get the following relations:

$$\omega = \omega_0 + \frac{3\beta AA^*}{2\omega_0} \qquad a = \frac{\alpha A^2}{3\omega_0^2} \qquad b = \frac{\beta A^3}{8\omega_0^2} \qquad C = -\frac{2\alpha AA^*}{\omega_0^2} \tag{1.37}$$

Interestingly, the frequency of the oscillations is a function of the amplitude of the spin precession. This phenomena is called non-isochronism and is a mark of anharmonic behavior. In this particular case it originates from the cubic non-linearity β.

It is interesting to apply the analysis set out above to the dynamics of the magnetization in an antiferromagnet.

To do so, we use instead of the vectors $\mathbf{M}$ and $\mathbf{L}$, their normalized values $\mathbf{m}$=$\mathbf{M}/2M_0$ and $\mathbf{l}$=$\mathbf{L}/2M_0$. For them relations hold:

$$\mathbf{m} \ll \mathbf{l}, \qquad \mathbf{l}^2 = 1 - \mathbf{m}^2 \cong 1 \tag{1.38}$$

Thus one can operate with vector $\mathbf{l}$ as with an unit vector.

$$\mathbf{l} = \begin{cases} l_x = \sin\theta\cos\phi, \\ l_y = \sin\theta\sin\phi, \\ l_z = \cos\theta. \end{cases} \tag{1.39}$$

Here ϕ is in-plane angle which vector $\mathbf{l}$ makes with the x coordinate axis, θ is angle which vector $\mathbf{l}$ makes with the z coordinate axis.

The role of the energy potential $U(x)$ in the case of a magnetic system is played by the magnetic anisotropy energy $\Phi_a(\theta, \phi)$. In the simplest case this energy, which favors orientation of the spins along the $z-$axis, can be written as:

$$\Phi_a(\theta) = K_2 \cos^2\theta \tag{1.40}$$

Here K_2 parameter characterizes magnetic anisotropy energy ($K_2 < 0$). Consequently, a non-linear equation for the spin precession is:

$$\frac{\partial^2\theta}{\partial t^2} + \gamma\mathcal{J}K_2 \cdot \sin(2\theta) = 0 \tag{1.41}$$

So we showed that the equation of motion of the angle can be reduced to the case of mathematical pendulum [15]. This equation becomes substantially anharmonic for large amplitudes of θ. Expansion of $\sin(2\theta)$ in the Taylor series gives:

$$\sin(2\theta) = (2\theta) - \frac{1}{6}(2\theta)^3 + \frac{1}{120}(2\theta)^5 - \ldots \tag{1.42}$$

It is important that this function contains only odd powers of θ. Thus for magnetization dynamics $\alpha = 0$.

We can summarize the main non-linear features of the magnetization dynamics in a magnet with an uniaxial anisotropy. First, the dynamics of the magnetization does not contain even harmonics. The present harmonics are exclusively odd. Second,

the non-isochronic shift of the resonant frequency $\omega_0\left(|\theta_0|^2\right)$ has to be present in magnetization dynamics. One can conclude that the presence of the higher harmonics as well as dependent on amplitude of the oscillation shift of the frequency are genuine physical property of the non-linear magnetization motion and an evidence of the highly efficient perturbation. The phenomena of non-isochonism is well know from the experiments of the non-linear ferromagnetic resonance [16].

A variety of reports about the optical excitation of spin precession in magnetic dielectrics were published so far [11, 14, 17]. The biggest achieved amplitude of the spin precession of 10 % was reported in the experiments [18] where the magnetization dynamics was excited by *ps* acoustic strain pulses. However, the spin dynamics was well described by a harmonic function with a single frequency and exponential damping.

1.7 Coupled magnetic and acoustic excitations

Resonant excitation of spin precession (see Eq. (1.32)) can be very effective way to drive high-amplitude magnetization dynamics. Recently, resonant excitation of the magnetization dynamics via single-cycle terahertz pulses was demonstrated in Ref. [19]. However, as a matter of fact, the triggered dynamics could be explained without the involvement of any nonlinearities.

The problem is that the duration of such an excitation is limited to 10 ps. Thus, it is difficult to effectively drive the spin resonance up to the point where non-linearity appears.

It is well known that ultrafast laser pulses can launch not only magnetization dynamics but also other elementary excitations. Phonons are of special interest, because they can resonantly couple to spin modes. Indeed, the dispersion spectra of the spin waves and phonons often intersect and in the intersection points a strong magneto-elastic interaction emerges (Fig. 1.3a). At such a point the resonance conditions between magnetic (magnons) and elastic (phonons) elementary excitation are satisfied:

$$\omega_{ph}\left(k_i\right) = \omega_m\left(k_i\right) \tag{1.43}$$

Here ω_{ph} and ω_m are the frequencies of magnons and phonons, respectively, for a particular wavevector k_i where the crossing occurs.

It is well known that the lifetime of acoustic phonons is extremely long and can last up to μs. If one can optically excite phonons with a frequency equal to that of a spin resonance, it is reasonable to expect that in that case an efficient transfer of energy between these two excitations will occur. A similar phenomenon was observed for a ferromagnetic metal Gd(0001) surface, where an optically excited phonon mode displacively drove coherent spin precession [20]. A significant limitation of the suggested mechanism is the non-zero value of the wavevector k_i, where the required resonant coupling occurs. The problem is that the k -vector of light is very small and a coupling the the short-wavelength excitations is unlikely. At the same time

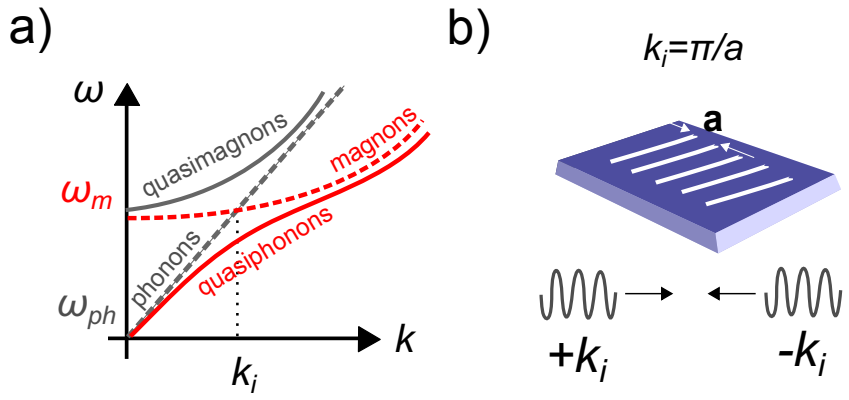

Figure 1.3: (a) Schematics of the dispersion curves for magnons and phonons in a ferromagnet . Dashed lines: no magneto-elastic interaction. Solid lines: with magneto-elastic interaction. The dispersion branches correspond to the quasimagnons and quasiphonons. (b) The periodic spatial pattern (period is denoted with a) on the top of a film, which after spatially homogeneous excitation can serve as a excitation source with $k = \frac{\pi}{a}$.

the spectrum of acoustic phonons is essentially gapless. However, the problem can be solved utilizing concept of the standing waves. A standing wave is a confined excitation, which has finite frequency, but its effective k-vector is zero. It can be seen as the wave effectively consists of two counter-propagating waves of non-zero k. This confinement can be achieved by sputtering or making grooves on the sample surface following a periodic pattern. Alternatively, sample faces can be also used for confinement. In this case even a spatially homogeneous laser excitation (k=0) can serve as a source of a excitation with non-zero wavevector equal to $\frac{\pi}{a}$, where a is a period of introduced pattern.

It is interesting to analyze the strength of the lattice-mediated effect of light on spins in materials with a strong magneto-elastic coupling such as $FeBO_3$ or $\alpha{-}Fe_2O_3$. Can such a resonant coupling be an effective way to trigger high-amplitude magnetization dynamics?

1.8 Magnetic phase transitions

Excitation of high-amplitude magnetization dynamics by a femtosecond laser is not limited to resonant coupling of light to spin modes. Triggering magnetic phase transitions is another way to induce significant changes in the magnetic structure and achieve non-linear regimes of magnetization dynamics.

A phase transition is a transformation of a thermodynamic system from one phase or state of matter to another via a change of external parameters. The phases can show significantly different properties. A very prominent example of such transitions can be demonstrated in the vicinity of the triple point of water, when slight changes in pressure and temperature can provoke transformation between liquid, solid and

vapor phases [21].

It is common to distinguish between first- and second-order phase transitions. This classification can be done with the help of Landau's theory of phase transitions. According to that, the free energy Φ of a system characterized by an order parameter $\mathcal{P}$ in the vicinity of a phase transition and can be presented as an expansion in powers of $\mathcal{P}$:

$$\Phi = \Phi_0 + \frac{1}{2}\alpha\mathcal{P}^2 + \frac{1}{4}\gamma\mathcal{P}^4 + \frac{1}{6}\delta\mathcal{P}^6 + \dots \tag{1.44}$$

The expression for this energy has to satisfy the symmetry operations of the material. The same approach is used to write the free energy of the antiferromagnet Eq. (1.6), where as the order parameters even powers of $\mathbf{L}$ and $\mathbf{M}$ are chosen. Parameter γ is of special importance because it defines the profile of the energy landscape and the type of the phase transition.

If γ <0 the transition is of 2^{nd} order and accompanied by a gradual transformation of the order parameter $\mathcal{P}$ via thermodynamically stable states. The energy minima, which correspond to the two phases, gradually transform one into another (see Fig. 1.4a). For this reason, a second-order phase transitions are also called continuous phase transitions. An example of second-order phase transitions is the transition from a ferromagnetic to a paramagnetic state or from a superconducting to a normal state state.

If γ >0, the transition is of 1^{st} order and accompanied by an sudden change of the order parameter. Interestingly, when such transition occurs, two minima are present simultaneously (Fig. 1.4b). One corresponds to a thermodynamically stable phase, the second corresponds to a metastable state. Both these states are separated by potential barrier all along the phase transition. In other words, the phases coexist. This leads to the presence of hysteresis behavior of the transition in response to external stimuli. Familiar examples are the melting of ice, the boiling of water.

The properties of first-order phase transitions suggest that such transitions are very attractive for induction of the strongly non-equilibrium states and the generation of non-linear magnetization dynamics. These transitions can also be employed for fundamental studies of novel mechanisms of ultrafast magnetic switching. The phases coexistence leads to the appearance of highly inhomogeneous, non-trivial mixtures of phases. For example, the water does not instantly turn into vapor, but forms a turbulent mixture of liquid water and vapor bubbles. However, overheated water turns into a vapor explosively (i.e. ultrafast) upon the appearance of a single bubble. It is interesting to search for similar scenarios of explosive first-order phase transitions in magnetic materials. A thermodynamic equilibrium between two different phases is established by the condition:

$$\Phi_1\left(T, H, p, \dots\right) = \Phi_2\left(T, H, p, \dots\right) \tag{1.45}$$

Here Φ_1 and Φ_2 are specific free energies of the two phases. These energies can be functions of temperature T, magnetic field H, pressure p, etc. Varying these parameters one can transfer the system from one thermodynamically stable phase P_1 to another stable phase P_2. The phase diagram of the competing phases P_1 and P_2 in

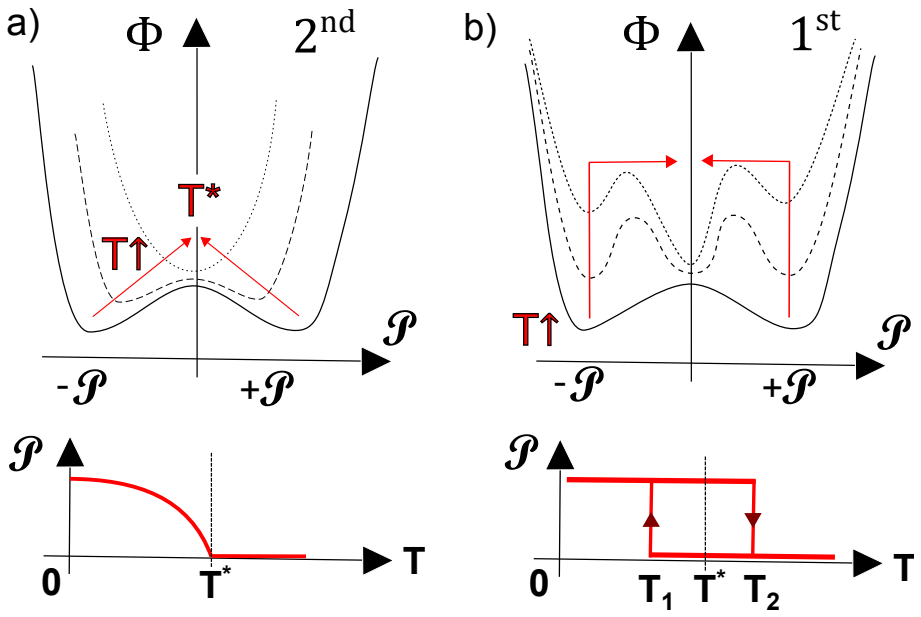

Figure 1.4: (a) Transformation of the free energy potential across a 2^{nd}-order phase transition. (b) Transformation of the free energy potential across a 1^{st}-order phase transition.The red lines demonstrate the evolution of the thermodynamically stable states as function of the bias temperature T. It is seen that a 2^{nd} order phase transition happens via a continuous set of thermodynamically stable states. The 1^{st} order phase transition has only two states one of which is stable and second one is degenerate and metastable. For this reason it is characterized by a temperature hysteresis existing in the temperature interval T_1-T_2, where coexistence of the states is possible.

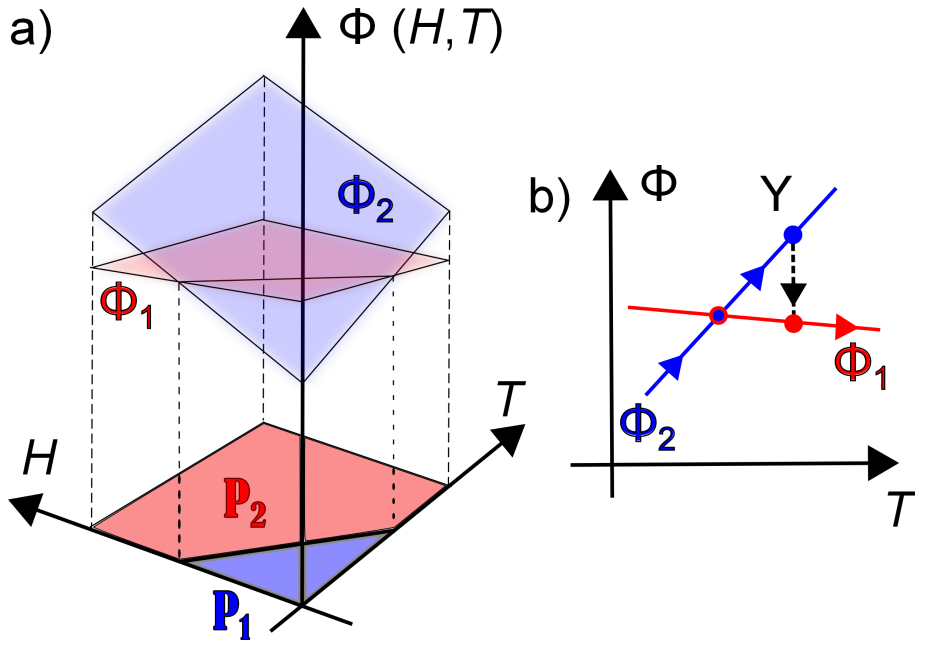

Figure 1.5: (a) The planes show the free energies of the magnetic phases P_1 and P_2, the intersections of the planes correspond to the (H,T) conditions needed to maintain equilibrium between the phases, $\Phi_1 = \Phi_2$. (b) A section through Φ surface in the plane of constant H showing that system can be in metastable state Y. The arrows indicate an free energy landscape which system follows during the phase transition.

the $H-T$ coordinates is shown in Fig. 1.5a. It is seen that for small values of H and T the phase P_1 is thermodynamically stable. An increase of the parameters induces a transition and the phase P_2 becomes favorable. However, this process frequently is complicated by presence of metastable states. Let us examine sections through the Φ surfaces. Figure 1.5b shows a section in plane of constant H. Since, for a given H and T, the stable state is that with the lowest Φ, states such as Y are not stable, but may often be realized as metastable states. For, example, if a liquid is very pure (no places for nucleation of gas phase bubbles) it might be heated well above its boiling point without boiling taking place to produce a superheated liquid.

The possibility to induce a phase transition by an external stimulus is very intriguing and attracts a lot of attention. It has the potential to be used in data storage, where the distinct difference between the states can for example be employed for the representation of the bit values ”0” and ”1”.

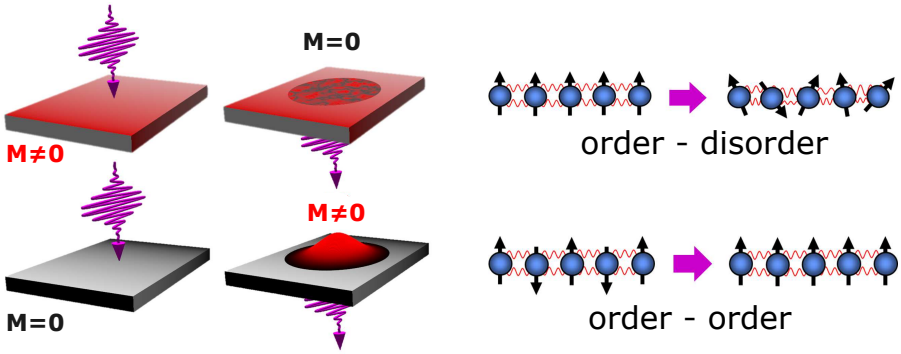

Figure 1.6: Effects on the ultrashort laser pulse on a magnetic media. (a) Ultrafast demagnetization provokes order (ferromagnetic state) to disorder (paramagnetic state) phase transition. (b) Ultrafast generation of the net magnetization via order (antiferromagnetic state) to order (ferromagnetic state) phase transition.

Material	Crystal structure	Temperature, K
Mn_3Ge_2	Tetragonal	148
MnP	Rhombohedral	50
FeRh	Cubic	350
α-Fe_2O_3	Rhombohedral	250
$DyFeO_3$	Rhombohedral	40
CrS	Hexagonal	158
$MnSn_2$	Tetragonal	73
$Mn_{0.9}Li_{0.1}Se$	Cubic	71

Table 1.1: Magnetic phase transitions between antiferromagnetic and ferromagnetic phases. The data are taken from Ref. [22].

1.9 Ultrafast magnetic phase transitions

The most studied phenomenon in ultrafast magnetism is ultrafast demagnetization. It results in the abrupt and drastic decrease of the net magnetization and can be considered as a order-disorder phase transition.

Transitions which involve the transformation of the magnetic structure, so called order-order phase transitions, are less studied but offer a rich playground for studying and understanding ultrafast magnetization dynamics. Among the rich variety of magnetic order-order phase transitions, especially interesting are those, during which the exchange and anisotropy parameters undergo changes [22]. Some of these materials can spontaneously acquire the net magnetization. In particular, those are transitions which show a rearrangement of spins from a pure antiferromagnetic structure with no net magnetization (compensated antiferromagnet) to structures with the net magnetization (ferromagnet or weak ferromagnet).

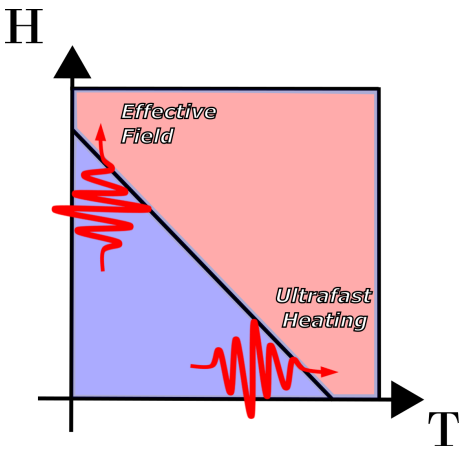

Figure 1.7: An ultrashort laser pulse can act as an effective magnetic field and simultaneously provide ultrafast heating of the magnetic system. Both effects can independently induce the magnetic phase transition.

The sensitivity of the magnetic phase transition to external stimuli, such as magnetic field, temperature and pressure, allows one to control the phase transitions by external stimuli.

It is known that an action of a femtosecond laser pulse can contribute to ultrafast heating [6], mechanical stress [23] and even can act as a directional effective magnetic field [11]. With the help of such a stimulus one can explore the whole phase diagram of magnetic phase transitions in the ultrafast regime. Interestingly, because of the polarization sensitivity of the optomagnetic effects, their contribution can be easily controlled. For this reason dissipative and non-dissipative paths can be chosen. An even more intriguing opportunity emerges if one can selectively pump electronic excitations, responsible for the very existence of the phase transition. An intense pumping of the electronic excitations by femtosecond laser pulses may initiate ultrafast magnetic changes and possibly bring the magnetization dynamics into a non-linear regime.

1.10 Orientational phase transitions in $RFeO_3$

The rare-earth orthoferrites $RFeO_3$ (where R^{+3} indicates a rare-earth element) form a broad class of antiferromagnetic materials which posses a vast variety of magnetic phase transitions (see Fig. 1.8). Most of them are accompanied by spin reorientations between crystallographic directions and originate from the anisotropic exchange interaction between the rare-earth and the transition ions. This interaction effectively plays the role of magnetic anisotropy. It is strongly temperature dependent and, as a consequence, results in spontaneous spin-reorientation phase transitions. Among all the undoped orthoferrites only $DyFeO_3$ demonstrates a spin-reorientation, accompa-

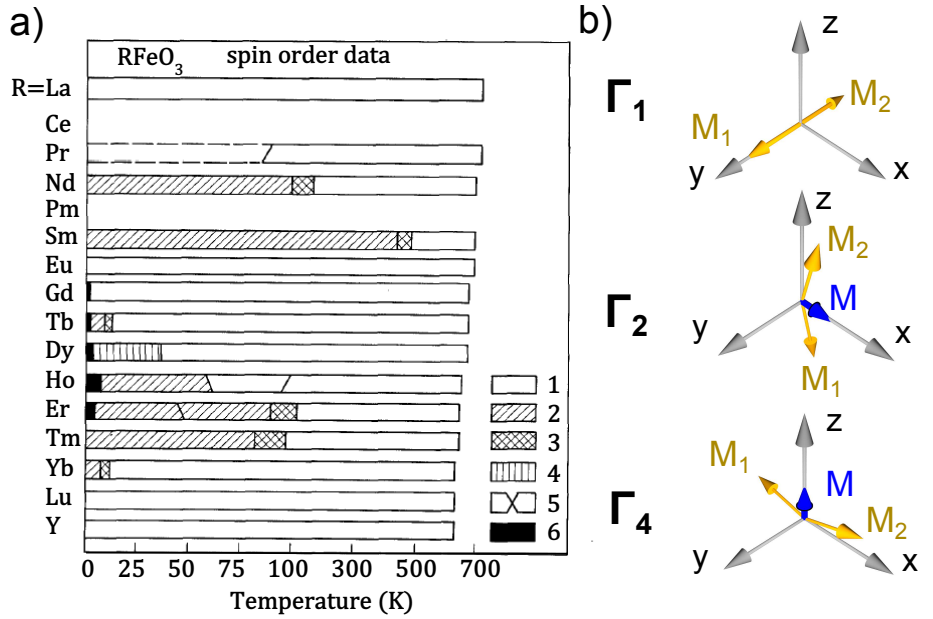

Figure 1.8: (a) Diagram, indicating the magnetic phases of orthoferrites and spontaneous phase transitions between them [24]: 1. Γ_4 phase, 2. Γ_2 phase, 3. Spin reorientation region, 4.Γ_1 phase, 5. Compensation point, where the net magnetic moment of rare-earth ion is equal to the net magnetic moment of the iron sublattices and oriented against it, 6. R^{3+} ions are ordered. (b) Magnetic phases of the rare-earth orthoferrites.

nied by the emergence of a net magnetization. This is a first-order phase transition.

It has been recently demonstrated that in $HoFeO_3$ and $DyFeO_3$ the optically generated effective magnetic field (>1 T) may exceed the magnetic anisotropy field and even trigger a spin reorientation phase transition [11, 25]. These observations open up the opportunity to verify intriguing predictions of a fundamentally novel mechanism of magnetization reversal via an ultrafast expansion (that can be called explosion) of domain walls [26]. It was predicted that short pulses of magnetic fields higher than the magnetic anisotropy field can break the stability of the initial phase and create the conditions for the ultrafast propagation of magnetic-moment-flip waves. Experimentally the intriguing observation of an ultrafast expansion of domain-walls with a velocity up to 60 km/s was reported for garnets, where normally the velocity does not exceed 100 m/s and the phase velocity of magnons equals 3 km/s [27]. A realization of this phenomenon in the orthoferrites, where the normal domain velocity reaches 20 km/s, for the impulsive fields up to 0.1 T showed increase of the domain wall speed up to 60 km/s, characterized by loss of the stationary motion. A realization of such scenario with a help of 100 fs pulses of laser-induced effective field is a promising approach to reach a record-breaking speed of magnetization reversal.

1.11 Scope of this Thesis

This thesis is focused on the investigations of novel approaches to trigger and manipulate large-amplitude magnetization dynamics by means of ultrashort laser pulses. As a playground for this research we chose the dielectric iron-based antiferromagnetic oxides $FeBO_3$ and $DyFeO_3$. In order to significantly influence the magnetic states of these media, we used three different physical effects, which can be launched by laser radiation: magneto-elastic coupling, magnetic phase transitions and photo-ionization of the rare-earth ions. Therefore this Thesis is divided in four different chapters:

Chapter 2 deals with the experimental methods to probe and excite magnetization dynamics with laser light. A novel experimental scheme for optical single-shot measurements of magnetically irreversible processes is described. The scheme has femtosecond temporal and micrometer spatial resolution and has been implemented for studies of ultrafast magnetic phase transitions.

In Chapter 3 we suggest a fundamentally novel approach to steer the magnetization using optically generated sound waves which are strongly coupled to spins in the medium. We trigger oscillations of the magnetization in $FeBO_3$, which are characterized by a large amplitude and a very small damping and the efficiency of the excitation is high enough to push the spin dynamics into an anharmonic regime.

In Chapter 4 we demonstrate that excitation of antiferromagnetic iron oxide $DyFeO_3$ with a single 60 fs laser pulse triggers a transition across the Morin point by pushing the antiferromagnet from a collinear to a non-collinear spin state, inducing a net magnetization. Time-resolved imaging reveals that the pulse first excites antiferromagnetic spin precession. Upon the damping of the precession, the non-collinear spin state with a net magnetization emerges. We show that the direction of the photo-induced net magnetization can be controlled by the pump polarization and the direction of the antiferromagnetic vector in the initial collinear spin state.

In Chapter 5 we report about a long-living effect of intense laser radiation on the critical temperature of the Morin transition in $DyFeO_3$. We show that optical excitation of the antiferromagnet with at least 10 femtosecond laser pulses leads to a shift of the transition temperature over 1 K to higher values, as if the light effectively cools the irradiated area. It is suggested that the observed effect is a result of the photo-ionization of the Dy^{3+} ions.

References

[1] J. Stöhr and H. C. Siegmann, "Magnetism," *Solid-State Sciences. Springer, Berlin, Heidelberg*, p. 5, 2006.

[2] C. Back, R. Allenspach, W. Weber, S. Parkin, D. Weller, E. L. Garwin, and H. Siegmann, "Minimum field strength in precessional magnetization reversal," *Science*, vol. 285, no. 5429, pp. 864–867, 1999.

[3] T. Gerrits, H. Van Den Berg, J. Hohlfeld, L. Bär, and T. Rasing, "Ultrafast precessional magnetization reversal by picosecond magnetic field pulse shaping," *Nature*, vol. 418, no. 6897, pp. 509–512, 2002.

[4] A. Vaterlaus, T. Beutler, and F. Meier, "Spin-lattice relaxation time of ferromagnetic gadolinium determined with time-resolved spin-polarized photoemission," *Phys. Rev. Lett.*, vol. 67, pp. 3314–3317, Dec 1991.

[5] M. Agranat, S. Ashitkov, A. Granovskıi, and G. Rukman, "Interaction of picosecond laser pulses with the electron, spin, and phonon subsystems of nickel," *Zh. Eksp. Teor. Fiz*, vol. 86, pp. 1376–9, 1984.

[6] E. Beaurepaire, J.-C. Merle, A. Daunois, and J.-Y. Bigot, "Ultrafast spin dynamics in ferromagnetic Nickel," *Phys. Rev. Lett.*, vol. 76, pp. 4250–4253, May 1996.

[7] A. Kirilyuk, A. V. Kimel, and T. Rasing, "Ultrafast optical manipulation of magnetic order," *Rev. Mod. Phys.*, vol. 82, pp. 2731–2784, Sep 2010.

[8] A. V. Kimel, A. Kirilyuk, A. Tsvetkov, R. V. Pisarev, and T. Rasing, "Laser-induced ultrafast spin reorientation in the antiferromagnet $TmFeO_3$," *Nature*, vol. 429, pp. 850–853, June 2004.

[9] T. Moriya, "Anisotropic superexchange interaction and weak ferromagnetism," *Phys. Rev.*, vol. 120, pp. 91–98, Oct 1960.

[10] A. F. Andreev and V. I. Marchenko, "Symmetry and the macroscopic dynamics of magnetic materials," *Physics-Uspekhi*, vol. 23, no. 1, pp. 21–34, 1980.

[11] A. V. Kimel, A. Kirilyuk, P. A. Usachev, R. V. Pisarev, A. M. Balbashov, and T. Rasing, "Ultrafast non-thermal control of magnetization by instantaneous photomagnetic pulses," *Nature*, vol. 435, pp. 655–657, June 2005.

[12] A. M. Kalashnikova, A. V. Kimel, R. V. Pisarev, V. N. Gridnev, A. Kirilyuk, and T. Rasing, "Impulsive generation of coherent magnons by linearly polarized light in the easy-plane antiferromagnet $FeBO_3$," *Phys. Rev. Lett.*, vol. 99, p. 167205, Oct. 2007.

[13] B. A. Ivanov, "Spin dynamics of antiferromagnets under action of femtosecond laser pulses (review article)," *Low Temperature Physics*, vol. 40, no. 2, pp. 91–105, 2014.

[14] F. Hansteen, A. Kimel, A. Kirilyuk, and T. Rasing, "Nonthermal ultrafast optical control of the magnetization in garnet films," *Phys. Rev. B*, vol. 73, p. 014421, Jan 2006.

[15] S. Gil, A. E. Legarreta, and D. E. Di Gregorio, "Measuring anharmonicity in a large amplitude pendulum," *American Journal of Physics*, vol. 76, no. 9, pp. 843–847, 2008.

[16] T. Gerrits, P. Krivosik, M. L. Schneider, C. E. Patton, and T. J. Silva, "Direct detection of nonlinear ferromagnetic resonance in thin films by the magneto-optical kerr effect," *Phys. Rev. Lett.*, vol. 98, p. 207602, May 2007.

[17] T. Satoh, S.-J. Cho, R. Iida, T. Shimura, K. Kuroda, H. Ueda, Y. Ueda, B. A. Ivanov, F. Nori, and M. Fiebig, "Spin oscillations in antiferromagnetic NiO triggered by circularly polarized light," *Phys. Rev. Lett.*, vol. 105, p. 077402, Aug 2010.

[18] M. Bombeck, J. V. Jäger, A. V. Scherbakov, T. Linnik, D. R. Yakovlev, X. Liu, J. K. Furdyna, A. V. Akimov, and M. Bayer, "Magnetization precession induced by quasitransverse picosecond strain pulses in (311) ferromagnetic (Ga,Mn)As," *Phys. Rev. B*, vol. 87, p. 060302, Feb 2013.

[19] T. Kampfrath, A. Sell, G. Klatt, A. Pashkin, S. Mahrlein, T. Dekorsy, M. Wolf, M. Fiebig, A. Leitenstorfer, and R. Huber, "Coherent terahertz control of antiferromagnetic spin waves," *Nat Photon*, vol. 5, pp. 31–34, Jan. 2011.

[20] A. Melnikov, I. Radu, U. Bovensiepen, O. Krupin, K. Starke, E. Matthias, and M. Wolf, "Coherent optical phonons and parametrically coupled magnons induced by femtosecond laser excitation of the Gd(0001) surface," *Phys. Rev. Lett.*, vol. 91, p. 227403, Nov 2003.

[21] G. Sutton, R. Underwood, L. Pitre, M. de Podesta, and S. Valkiers, "Acoustic resonator experiments at the triple point of water: first results for the boltzmann constant and remaining challenges," *International Journal of Thermophysics*, vol. 31, no. 7, pp. 1310–1346, 2010.

[22] N. P. Grazhdankina, "First-order magnetic phase transitions," *Sov. Phys. Usp.*, vol. 11, p. 727, 1969.

[23] D. Afanasiev, I. Razdolski, K. M. Skibinsky, D. Bolotin, S. V. Yagupov, M. B. Strugatsky, A. Kirilyuk, T. Rasing, and A. V. Kimel, "Laser excitation of lattice-driven anharmonic magnetization dynamics in dielectric $FeBO_3$," *Phys. Rev. Lett.*, vol. 112, p. 147403, Apr 2014.

[24] R. L. White, "Review of recent work on the magnetic and spectroscopic properties of the rare-earth orthoferrites," *Journal of Applied Physics*, vol. 40, no. 3, pp. 1061–1069, 1969.

[25] A. V. Kimel, B. A. Ivanov, R. V. Pisarev, P. A. Usachev, A. Kirilyuk, and T. Rasing, "Inertia-driven spin switching in antiferromagnets," *Nat Phys*, vol. 5, pp. 727–731, Oct. 2009.

[26] V. Eleonskii, N. Kirova, and N. Kulagin, "Exact solutions of the Landau-Lifshitz equations for weak ferromagnets," *Soviet Journal of Experimental and Theoretical Physics*, vol. 52, p. 162, 1980.

[27] A. Logginov and G. Nepokoichitskii, "Ultrafast magnetic-moment-flip waves in iron garnet films," *JETP Lett*, vol. 35, no. 1, 1982.

Chapter 2

Experimental techniques

2.1 Ultrafast pump-probe set-up for magneto-optical measurements

To study the temporal dynamics of any nature one needs a pulsed external stimulus which can perturb a system and in such a way initiate the dynamics. It is commonly accepted to call this perturbation as pump. To monitor a specific property of a material after the excitation one can employ a time-delayed probe pulse. Here we are mainly interested in the magnetization dynamics, which can be monitored with the help of the magneto-optical Faraday effect. The Faraday effect causes a rotation of the polarization plane θ_F of light. The rotation is proportional to the component of the magnetization in the direction of propagation:

$$\theta_F = \chi \cdot (\mathbf{M}\mathbf{e}_\mathbf{k}) \,. \tag{2.1}$$

Here χ is the magneto-optical susceptibility and $\mathbf{e}_\mathbf{k}$ is the unit vector in the direction of the probe light propagation. To perform time-resolved measurements one has to synchronize the pump and probe pulses and be able to vary the delay between them. If both pump and probe pulses originate from a single pulse, the temporal resolution of such a scheme is defined by the duration of the light pulse and is usually limited up to a few tens of femtoseconds. To date, it is known that the fastest fundamental processes and dynamics in complex materials occur on timescales from femtoseconds to picoseconds. This timescale is covered by such an all-optical technique.

In an ultrafast pump-probe experiment, the output pulse train from a fs laser system is divided into two beams: the sample is excited by one pulse train (pump) and the changes it induces in the sample are probed by the second pulse train (probe), which is suitably attenuated and delayed with respect to the pump. The delay is set mechanically (making use of the speed of light) and then recalculated in the time domain. Some properties related to the probe, such as transmission and the Faraday

rotation are then monitored to investigate the changes produced by the pump in the sample.

A femtosecond laser system is a key element of a set-up for time-resolved all-optical measurements. The main blocks of such system are:

The seed laser is a source of temporally compressed broadband laser pulses. The seed laser used in our experiment is a commercial Ti:Sapphire laser. The emission originates from the fluorescence of excited Ti^{3+} ions (600-1000 nm). The laser operates in the near-infrared spectral range with a central wavelength of 800 nm and a pulse width of 40 fs. The repetition rate of the seed laser in our system is 82 MHz.

The amplifier consist of a cavity pumped by an external laser in order to create population inversion. A single pulse from the seed laser is used to provoke stimulated emission. The essential part of the amplifier system is a stretcher which initially temporally broadens the laser pulse. This is done to reduce the pulse power and not to destroy the active medium and optics upon amplification of the pulses. After the amplification a compression restores the duration of the pulse. The repetition rate of the amplifier is determined by the repetition rate of the external laser and in our experiment was set to f=1 kHz. The maximal energy per single pulse is 2 mJ.

Optical Parametric Amplifier is an optional element of the scheme which provides wavelength tunability and can be used either for pumping or for probing. The operational principle is based on Optical Parametric Generation.

The pump and the probe pulses are made from a single amplified pulse by splitting the pulse with a wedged beam splitter (BS) (see Fig. 2.1a). One of the pulses is reflected by a retroreflector fixed on a controllable mechanical delay line. Indications of the delay line then are translated to the time domain according to the conversion 1 mm = 6.67 ps. The pump and probe beams are focused into spots with the help of the lenses L_1 and L_2. The diameter of the pump spot at the sample is slightly bigger than that for the probe in order to provide homogeneity of the probing area. The probe beam is then collected with a short focus lens L_3 and focused on the balanced detector. The vital part of the balanced detector is the Wollaston prism (WP). With the help of the WP the incident beam splits into two orthogonally polarized rays S and P. Both beams are sent to photodiodes D_1 and D_2 which transform the light pulses into pulses of electric current. The difference $I^- = I_S - I_P$ and sum $I^+ = I_S + I_P$ of these signals from the two diodes are measured in the experiment. In order to balance the detector the difference signal is set to zero turning the optical axis of the WP, such that angle between the incident polarization and optical axis of the WP is equal to $\frac{\pi}{4}$.

The pump excitation affects optical properties of the sample. This results in time dependent transmission $I_0\,(t)$ and polarization $\theta_F\,(t)$ changes of the probe pulse. For small angles $\theta_F\,(t)$ ($\theta_F \ll 1$) one gets:

$$I^{-} = I_0(t)\cos^2\left(\frac{\pi}{4} + \theta_F(t)\right) - I_0(t)\sin^2\left(\frac{\pi}{4} + \theta_F(t)\right) \cong I_0(t) \cdot 2\theta_F(t) \tag{2.2}$$

$$I^{+} = I_0(t)\cos^2\left(\frac{\pi}{4} + \theta_F(t)\right) + I_0(t)\sin^2\left(\frac{\pi}{4} + \theta_F(t)\right) = I_0(t) \tag{2.3}$$

Thus measuring the difference signal I^{-} one can get information about the pump-induced rotation of the probe polarization plane. The measurements of the sum signal reveal changes in the transmission.

In order to increase the sensitivity of the measurements scheme, a chopper CH synchronized with the pump and operating at the half frequency $\frac{1}{2}f$ of the laser system is inserted in the pump path. In such a scheme the signal from the photodiodes is formed by a sequence of light-induced pulses of voltage, measured for the sample in presence of the pump pulse and without (see digital time diagram *Diode* in Fig. 2.1b). The detection of the signal at the frequency $\frac{1}{2}f$ allows to measure only the pump-induced changes and substantially reduces the noise. To detect the amplitude of a signal at a given frequency $1/2f$, normally a lock-in technique is used. It should be noted, however, that the signal generated by the photodiodes in these measurements are nearly delta-functions separated by ms intervals. A Fourier transform of such a signal in the time domain has a very broad spectrum. The operational principle of a lock-in amplifier allows one to sence only narrow spectral lines and thus a large part of the actual useful signal is lost. In order to improve this we use a boxcar integrator, which integrates the values of the obtained signal from pulse to pulse and preserves them up to the next pulse (see digital time diagram *Integrator* in Fig. 2.1b). Thus a square wave signal is obtained. For such a signal the lock-in technique can be implemented with much more higher efficiency (see digital time diagram $Lock-in$ in Fig. 2.1c).

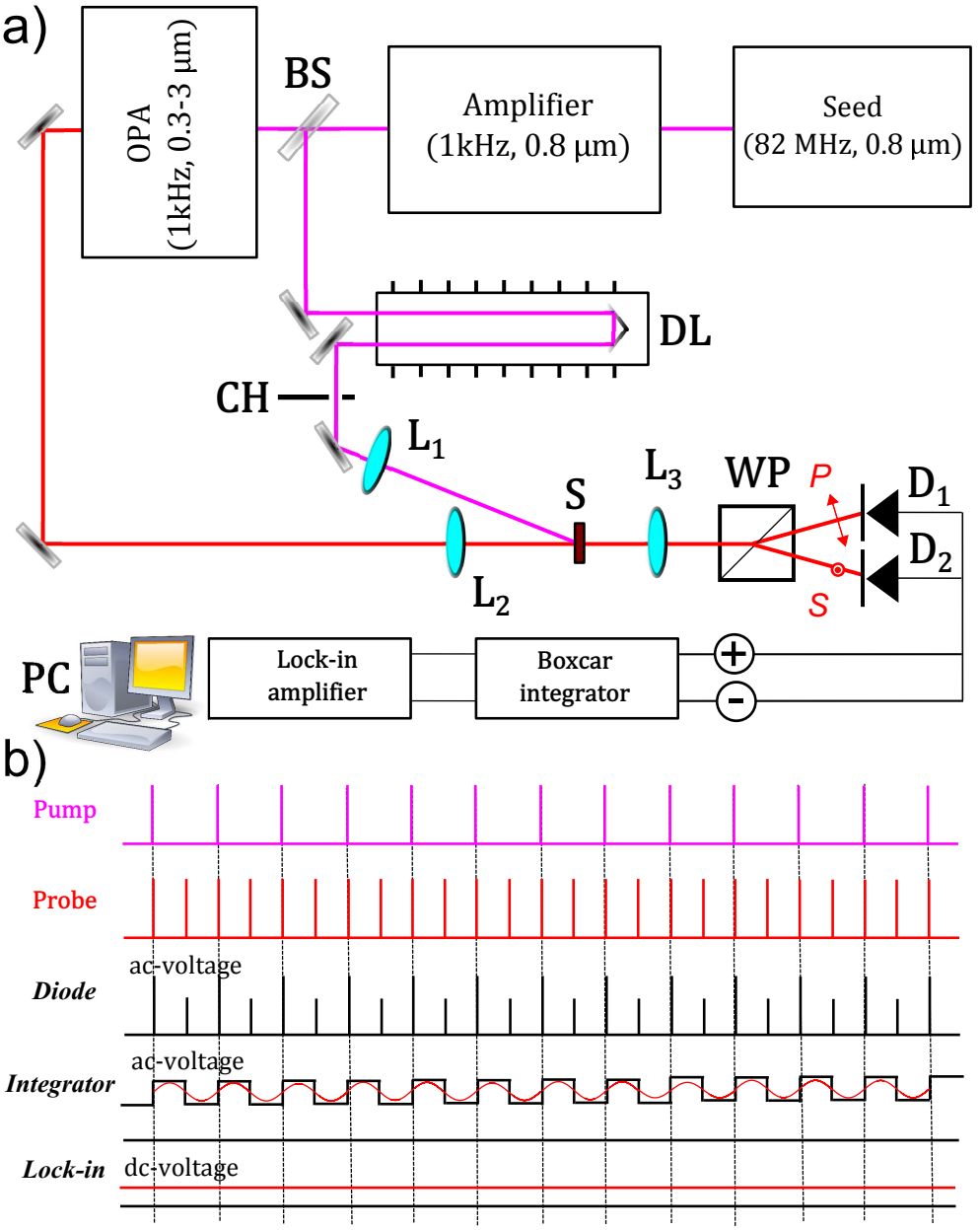

Figure 2.1: (a) Optical pump-probe set-up for measurements of the photo-induced dynamics. BS is a beam splitter. DL is a precision mechanical delay line. CH is mechanical chopper which usually operates at 500 Hz frequency. L_1 and L_2 lenses to focus pump and probe beams, respectively. S is sample under the study. L_3 is a lens to focus divergent probe beam to the photodiodes. WP is a Wollaston prism. *P* and *S* denotes polarizations of the beams spatially separated by WP. D_1 and D_2 are Si-based photodiodes. PC is a personal computer. (b) Digital time diagram of the signals. *Diode* is a signals obtained on the photodiode D_1 or D_2. It is formed by a sequence of light-induced pulses of voltage, measured with pump and with no pump presence. *Integrate* is a integrated pulse-to-pulse signal, obtained from the photodiodes. *Integrator* is a integrated pulse-to-pulse signal, obtained from the photodiodes. $Lock-in$ is a dc-voltage signal proportional to the amplitude of the oscillatory component of the *Integrator* signal.

2.2 Ultrafast imaging of the magnetization dynamics with femtosecond resolution

To date, it is known that the fundamental processes and interactions that determine the magnetization dynamics in complex materials occur on timescales of femtoseconds-to-picoseconds and on length scales of micrometers-to-nanometers. The use of pump-probe techniques with ultrashort pulsed light sources gives easily a time-resolution of subpicoseconds, so that the temporal evolution of the magnetization after impulsive excitation has been extensively investigated. In contrast, only few studies were devoted to the spatial distribution of the excited magnetic state [1], even though the spatial spin flow has been one of the most studied topics in spintronics research. Therefore, it is important to develop an experimental setup which would allow to study laser-induced magnetization dynamics with both subpicosecond temporal and high enough spatial resolution.

Essentially, the setup for time-resolved imaging duplicates the conventional pump-probe one (see Fig. 2.2a). However, there are important differences. The probe size has to be significantly bigger than the pump size in order to monitor spatial changes induced by the pump. The spatial magnification is achieved with the help of the objective O. While for the conventional pump-probe set-up the two-color scheme is optional, for the imaging set-up it is absolutely necessary. The pump scattered by the sample and optical components has to be filtered out with the help of a color filter F. The magneto-optical contrast in the imaging set-up is achieved using nearly crossed polarizer P and analyzer A and recorded with the help of a CCD camera.

The repetition rate of the conventional regenerative amplifier significantly exceeds the acquisition rate of the commercially available high-resolution cameras. A simple calculation shows that a camera, which operates in full frame mode (resolution 1392×1040 pixels) with a readout rate of 20 MHz can take no more than 14 images per second. This value is two orders of magnitude lower than the repetition rate of the laser pulses in our experiments. A natural solution is to integrate the images, increasing the time of exposition. However, in our case it would also increase the noise. The noise is integrated during the exposition time, while the signal is only present within a very short period given by the duration of the probe pulse.

Moreover, high repetition rates of the pumping events substantially contribute to permanent DC heating [2]. For instance, it is known that the spontaneous magnetic phase transition from the collinear to the non-collinear antiferromagnetic phase (the Morin transition) in $DyFeO_3$ (see Chapter 3) is observed in the vicinity of T_M=29 K. The low-temperature antiferromagnetic phase of $DyFeO_3$ has rather unique magnetic properties, such as multiferroelectricity [3]. Nonetheless, this phase has never been detected in time-resolved experiments [4, 5]. To figure out how large the DC-heating is in our experiments, we used the Morin temperature as a reference. We determined the actually observed Morin temperature as a function of the pump repetition rate. The data is presented in Fig. 2.3. It is seen how the pump pulses significantly affect the systematic error in the determination of the temperature of the Morin transition. In order to get rid of this error and decrease the cumulative heating effect, the pump

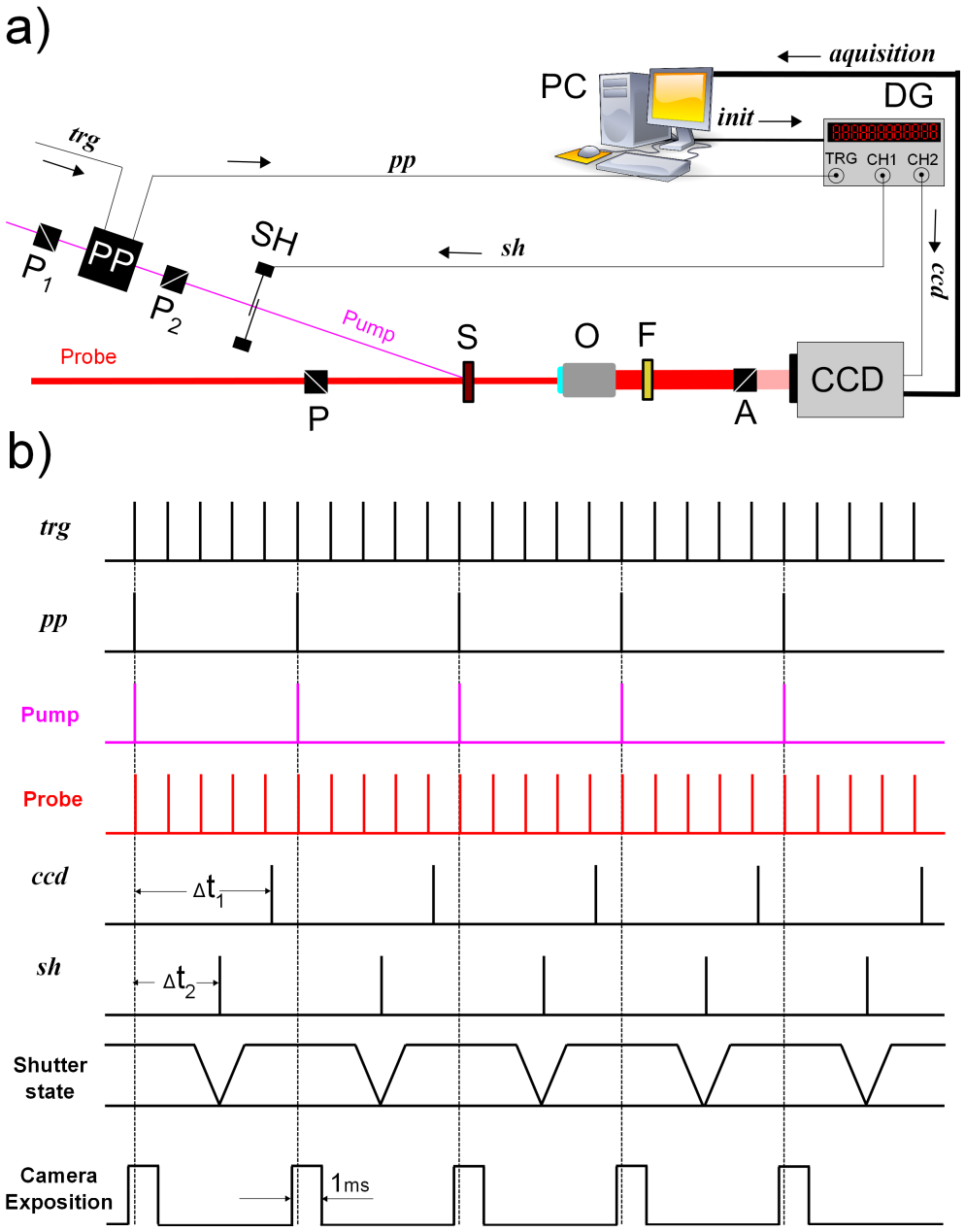

Figure 2.2: (a) Operating scheme of the femtosecond magneto-optical imaging set-up with spatial resolution. P_1, P_2 are crossed polarizers in the pump optical path. PP is pulse picker based on the Pockels effect. SH is a mechanical shutter. P and A are slightly uncrossed polarizer and analyzer in the probe optical path. O is a objective to obtain spatial resolution. F is a dichroic filter. S is a sample under the study. CCD is a externally triggered camera. DG is a electrical delay generator. PC is a personal computer. (b) Digital timing diagram of the signals used for the synchronization. *trg* is a native laser system sync signal. *pp* is a sync signal produced by the pulse picker electronic, and synchronized with the new pump repetition rate. *sh* sync signal to trigger the shutter opening event. *ccd* sync signal to trigger the camera exposition event. *init* is a signal from computer which initiates data acquisition.

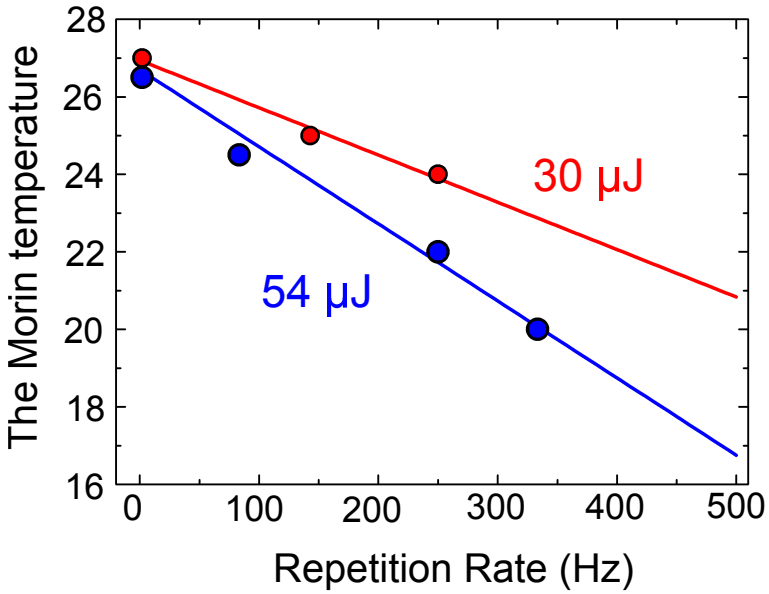

Figure 2.3: Measured temperature of the Morin point in $DyFeO_3$ as a function of the pump repetition rate for two different pump energies.

repetition rate must be reduced.

The most interesting light-induced effects from a practical point of view are those which lead to long-living changes of the magnetic structure. These effects do not relax within the time set by the repetition rate of the pump pulses and even can be thermodynamically stable.

A prominent example of this is the magnetization reversal in GdFeCo alloys, where a single ultrafast laser pulse can induce the permanent reversal of the net magnetization [6]. In order to study this process stroboscopically with a high temporal resolution, an external stimulus (magnetic field) has to be applied to restore the initial state after reversal and before next pumping event. It also introduces limitations on the repetition rate in the experiment. If the reversed state does not relax at all, one needs to be able to perform time-resolved measurements with a single pump pulse.

In order to obtain flexibility and satisfy all above mentioned requirements we developed a single-shot imaging technique with a synchronization scheme which employs a pulse picker and a mechanical shutter steered by a delay generator.

A Pulse Picker (PP) is used to pick out single optical pulses of picosecond or femtosecond duration from a sequence of pulses. Operation of the pulse picker is based on the linear electrooptic effect (Pockels effect). An electro-optical non-centrosymetric uniaxial crystal (e.g. potassium-dideuterium phosphate (KDP)), is placed between two polarizers P_1 and P_2 with the axes oriented at 90^o angle to each other (see Fig. 2.4). Linearly polarized light passes through the first polarizer. By applying a high voltage (∼10 kV) pulse to the electro-optical crystal, birefringence is induced

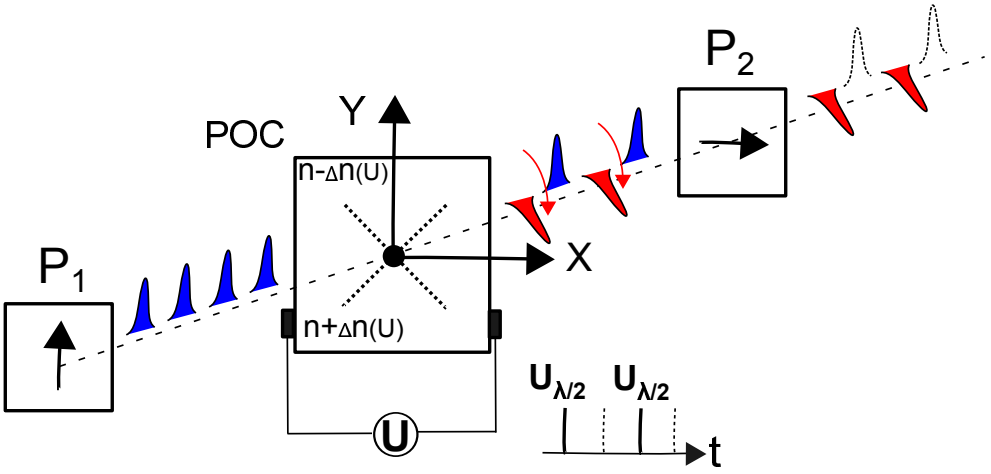

Figure 2.4: Pulse Picker based on the electro-optical Pockels effect operation scheme. The initial train of the pulses is vertically polarized with a help of polarizer P_1. POC is a transparent crystal which possesses linear electro-optical effect. If no voltage is applied to POC light passes via crystal with no changes in the polarization. Such light is blocked completely by a polarizer P_2, with axis turned over 90^o angle with respect to the one of P_1. Application of the voltage U induces birefringence in POC. If value of the voltage is high enough $U_{\lambda/2}$ birefrince results in rotation of the polarization plane on 90^0. Such pulses can pass through P_2 . Adjusting the repetition rate of the voltage pulses one may achieve arbitrary sequences of the pulses at the output.

and the crystal becomes birefringent. The main axis of the electrically induced birefringence is at 45^o with respect to the incoming polarization. It means that light will split in the crystal into two beams with mutually orthogonal polarizations (along the main axis and perpendicular to it). The difference in refractive indexes for the beams propagate along the main axes is proportional to the electric field E: A Pulse Picker (PP) is used to pick out single optical pulses of picosecond or femtosecond duration from a sequence of pulses. Operation of the pulse picker is based on the linear electrooptic effect (Pockels effect). An electro-optical non-centrosymetric uniaxial crystal POC (e.g. potassium-dideuterium phosphate (KDP)), is placed between two polarizers P_1 and P_2 with the axes oriented at 90^o angle to each other (see Fig. 2.4). Linearly polarized light passes through the first polarizer. By applying a high voltage U ($\sim$ 10 kV) pulse to the electro-optical crystal, birefringence is induced. The crystal becomes birefringent. The main axis of the electrically induced birefringence is at 45^o with respect to the incoming polarization. It means that light will split in the crystal into two beams with mutually orthogonal polarizations (along the main axis and perpendicular to it). The difference in refractive indexes for the beams propagate along the main axes is proportional to the electric field E:

$$\Delta n = AE \tag{2.4}$$

Here A is electro-optical coefficient of the material. During the propagation in the electro-optical media the waves acquire a phase difference:

$$\delta = \frac{4\pi}{\lambda}\frac{l}{d}AU \tag{2.5}$$

Here λ is the wavelength of the incident light, l and d are the length and the thickness of the crystal, respectively. U is the applied voltage. When the phase difference reaches $\lambda/2$, the polarization is rotated by 90^o and linearly polarized light freely passes through the second polarizer. The intensity of light after the second polarizer is given by:

$$I = I_0 \sin^2\left(\frac{\pi}{2}\frac{U}{U_{\frac{\lambda}{2}}}\right) \tag{2.6}$$

Here $U_{\frac{\lambda}{2}}$ is the amplitude of the voltage which induces $\lambda/2$ phase difference. When no voltage is applied, the polarization does not rotate and the second polarizer does not pass any light.

Using the Pulse Picker syncronized with the built-in laser trigger trg the pump repetition rate can be easily reduced. If one wants to see pump-induced effects, there is no need to decrease the repetition rate of the probe. Due to its low fluence the probe pulse will hardly perturb the studied system. Thus the repetition rate of the probe pulses can be left high (i.e. 1 kHz). Instead we trigger the camera at the repetition rate of the pump. The exposition time has to be smaller than $\leq \frac{1}{f}$ (f is the repetition rate of the laser system). To synchronize the camera with the pumping event, we employed an electrical delay generator DG, synchronized with the pulse picker PP. It provides an electronic delay Δt_1 to the CCD camera so that the recorded image originates from the chosen pump.

Interestingly, with the help of such a synchronization scheme, it is possible to measure magnetization dynamics with subpicosecond resolution up to seconds. To do so, one needs to introduce an extra delay:

$$\Delta t = n \cdot \frac{1}{f} \qquad n = 1, 2, \ldots \tag{2.7}$$

This is equivalent to the measurements with the help of the next coming probe pulses. In this way we measured milliseconds laser-induced dynamics of magnetic domains in $DyFeO_3$ (Fig. 2.5).

If one wants to use the set-up in a single shot mode, the mechanical shutter (SH), triggered by the DG with an appropriate delay Δt_2 has to be included. The delay generator has an in-built option for an externally triggered single-shot mode. In this mode the delay generator is normally in the standby mode. This mode lasts up to the moment when the external trigger from the pulse picker is coming. In response to the external trigger the DG produces an electrical pulse to trigger the camera and the shutter. Once this is done, the procedure of the reinitialization can be performed with no presence of the pump pulse. The single-shot mode of the delay generator can

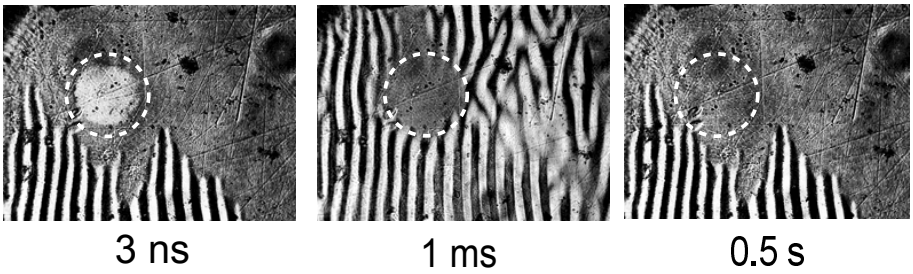

Figure 2.5: Magnetization dynamics, induced by a fs laser pulse in the vicinity of the Morin temperature. The white dashed line shows the area exposed to the optical pumpinig.

be easily controlled with the help of an external computer (PC) via an in-built GPIB interface.

References

[1] T. Satoh, Y. Terui, R. Moriya, B. A. Ivanov, K. Ando, E. Saitoh, T. Shimura, and K. Kuroda, "Directional control of spin-wave emission by spatially shaped light," *Nat Photon*, vol. 6, pp. 662–666, Oct. 2012.

[2] R. V. Mikhaylovskiy, E. Hendry, V. V. Kruglyak, R. V. Pisarev, T. Rasing, and A. V. Kimel, "Terahertz emission spectroscopy of laser-induced spin dynamics in $TmFeO_3$ and $ErFeO_3$ orthoferrites," *Phys. Rev. B*, vol. 90, p. 184405, Nov 2014.

[3] Y. Tokunaga, S. Iguchi, T. Arima, and Y. Tokura, "Magnetic-field-induced ferroelectric state in $DyFeO_3$," *Phys. Rev. Lett.*, vol. 101, p. 097205, Aug 2008.

[4] A. Kimel, A. Kirilyuk, P. Usachev, R. Pisarev, A. Balbashov, and T. Rasing, "Ultrafast non-thermal control of magnetization by instantaneous photomagnetic pulses," *Nature*, vol. 435, no. 7042, pp. 655–657, 2005.

[5] R. Iida, T. Satoh, T. Shimura, K. Kuroda, B. A. Ivanov, Y. Tokunaga, and Y. Tokura, "Spectral dependence of photoinduced spin precession in $DyFeO_3$," *Phys. Rev. B*, vol. 84, p. 064402, Aug. 2011.

[6] C. D. Stanciu, F. Hansteen, A. V. Kimel, A. Kirilyuk, A. Tsukamoto, A. Itoh, and T. Rasing, "All-optical magnetic recording with circularly polarized light," *Phys. Rev. Lett.*, vol. 99, p. 047601, Jul 2007.

Chapter 3

Laser excitation of lattice-driven anharmonic magnetization dynamics in dielectric $FeBO_3$

Here we suggest a fundamentally novel approach to steer the magnetization using optically generated sound wave which is strongly coupled to the spins in the medium. Unlike pure spin resonances, this coupled quasi-acoustic mode has a much higher Q-factor and thus opens intriguing opportunities for highly efficient coherent control of magnetism.

We demonstrate the advantages of this scenario, triggering a standing acoustic wave in the antiferromagnetic dielectric $FeBO_3$ by a fs laser pulse. Due to a strong magneto-elastic coupling, this excitation leads to coherent oscillations of the magnetic anisotropy followed by spins. This mode is characterized by a large amplitude and a very small damping and the efficiency of the excitation is high enough to push the spin dynamics into an anharmonic regime.[1]

[1]The chapter is adapted from: D. Afanasiev, I. Razdolski, K. M. Skibinsky, D. Bolotin, S. V. Yagupov, M. B. Strugatsky, A. Kirilyuk, T. Rasing, and A. V. Kimel,"Laser excitation of lattice-driven anharmonic magnetization dynamics in dielectric $FeBO_3$," Phys. Rev. Lett., vol. 112, p. 147403, Apr 2014.

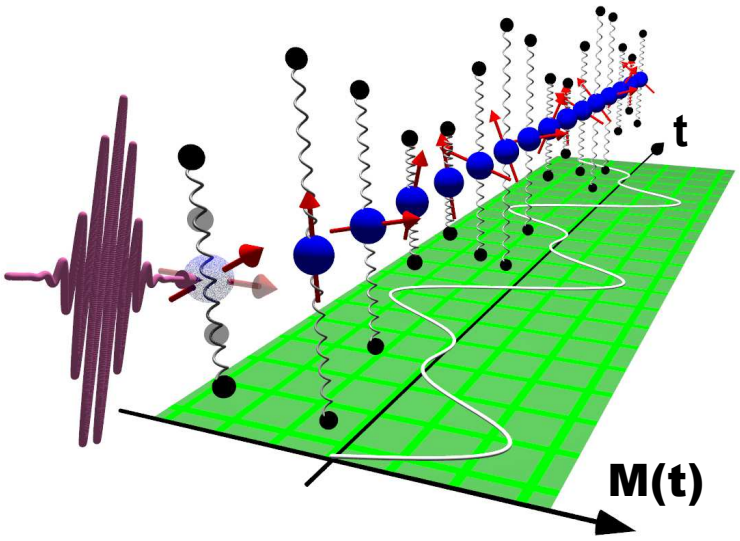

Figure 3.1: Artistic representation of the laser-induced lattice-driven magnetization dynamics

3.1 Coherent dynamics of magnetization launched via a light-induced acoustic perturbation

Efficient control of spin dynamics by femtosecond (fs) laser pulses is a heavily debated topic in modern science [1] which is relevant for future magnetic recording [2], spintronics [3], and the recently emerged area of magnonics [4]. Fundamentally, such an optical control of spins is counter-intuitive since the action of the electric field of light on elementary electric dipoles, which is the strongest perturbation in light-matter interaction, conserves the spin of the electron [2]. Nevertheless, it has been shown that excitation of metals or semiconductors with the help of a fs laser pulse can lead to a collapse of the magnetic order [5, 6] or even magnetization reversal [7]. A crucial role in these phenomena is played by the free electron gas. The fs laser pulse heats the free electrons creating a strongly non-equilibrium electron distribution which eventually promotes the demagnetization and remagnetization of the metallic magnet [8]. Unfortunately, such a mechanism of all-optical demagnetization can hardly be realized in dielectric magnetic media where no free electrons are present. This obstacle motivated an intense search for alternative ways to excite spin dynamics in magnetic dielectrics by means of light. Several mechanisms based on Impulsive Stimulated Raman Scattering by magnons [9], photo-induced magnetic anisotropy [10] and resonant THz pumping [11] have been successfully demonstrated during the last decades. Nevertheless, in all these approaches the amplitude of the excited spin dynamics was so small that the dynamics did not even enter an anharmonic regime. In general the

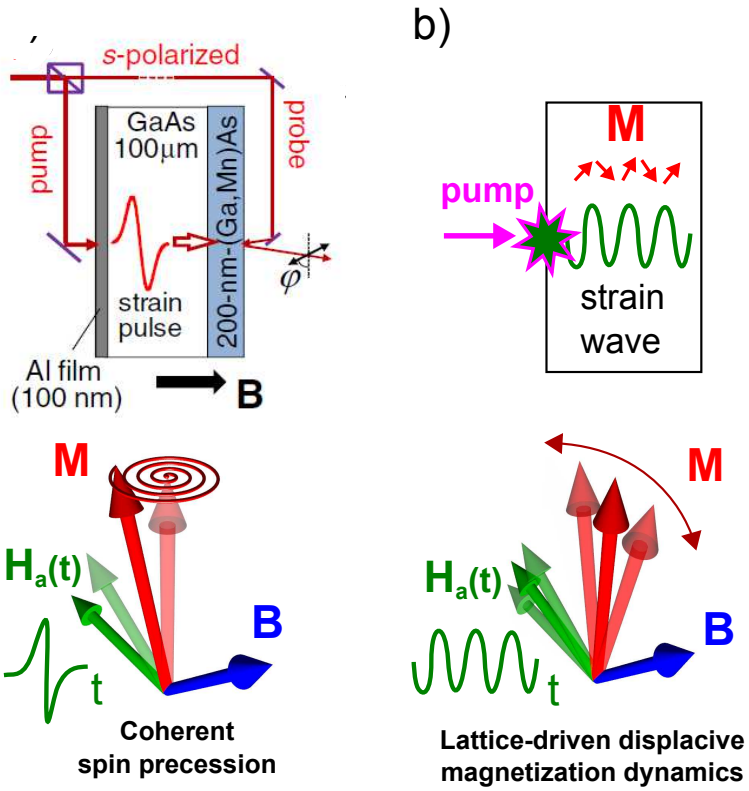

Figure 3.2: Schematic of pump-probe experiments with strain pulses on the semiconductor (Ga,Mn)As [12]. (b) Illustration of impulsive mechanism of ferromagnetic precession excitation

magnetization deviations from the equilibrium were about 1^o.

Recently, an alternative way to control spins by light via coherent phonon excitation was demonstrated in metals [13, 14], metallic surfaces [15] and semiconductors [12]. The magnetization deviations here are stronger and reach values up to 10^o. Inspired by this success a scenario of laser-induced acoustically mediated magnetization reversal was suggested theoretically [16]. All these articles reveal the potential of the coupled magneto-acoustic excitations for optical control of magnetism. Even more intriguing is the use of such techniques in the vicinity of reorientation phase transitions [17] where the magnetic anisotropy value crosses zero value and the magnetization orientation is undefined and thus might be controlled by an external laser-induced strain pulse.

The main idea in these works is to inject an ultrashort high-amplitude wavepacket of mechanical strain into a ferromagnetic layer. Such strain pulse impulsively impacts the magneto-crystalline anisotropy. In such way the equilibrium spin orientation

changes instantaneously, i.e. much faster than the period of the spin precession. As a result the spin precession is launched around the initial equilibrium. Experimentally such an acoustic excitation is a bipolar acoustic pulse, generated via ultrafast optical heating [18]. The obtained strains have large amplitudes up to 10^{-3}. They can be easily guided over distances up to 100 μm. To generate, such a strain a thin film of silver or cobalt ($\sim$100 nm) is sputtered on the surface of the magnetically ordered material. The absorption of the visible light in the skin layer of the metal results in thermal expansion, which induces mechanical strain. This strain propagates to the magnetic layer and excites the spin precession. However, in order to effectively perturb the spins, the magnetic material has to possess a strong coupling between the mechanical strain and the magnetization. To satisfy this requirement, diluted magnetic semiconductors (Ga,Mn)As or thin metallic films (Ni, Terfenol-D, Galfenol) which possess strong magnetostrictive properties are utilized. It is striking that for all these experiments the materials were ferromagnetic. However, the value of the magneto-elastic coupling in ferromagnets is, in principle, smaller by nature than in antiferromagnets [19]. Thus the large potential of antiferromagnets has remained unexplored.

The aforementioned mechanism has an impulsive action on the magnetic system, similarly to effects caused by the Impulsive Stimulated Raman Scattering mechanism. However, the presence of mechanical strain as mediator between the magnetization and optical excitation paves the way to manipulate the magnetization displacively. Alternatively, a single acoustic phonon mode can be excited impulsively by a laser pulse. Being coupled to the magnetization it can drive the magnetization. If the frequency of the acoustic mode is lower than that of spin oscillations, the spins will follow the lattice quasistatically. Typical lifetimes of phonon modes can be up to μs [20]. This is much longer than the coherence lifetime of ferromagnetic precession which is usually in the range of 1 ps - 1 ns.

In order to launch such an excitation with light one needs to trigger an acoustic wave optically. Importantly, because the acoustic phonon dispersion is gapless, such a wave should have a non-zero k-vector in order to provide non-zero frequency modulation. It is difficult to trigger high k-vectors excitations with the help of a visible light wave, which has nearly zero k-vector. However, for particular situations, the coupling to acoustic phonons with non-zero frequency can be possible:

1. An inhomogeneous distribution of the intensity of light is a source of waves with non-zero k-vectors

2. An otherwise running wave can be confined as a result of resonance between sample faces or an artificially created surface pattern. Such a confined wave is a standing acoustic wave with non-zero frequency but zero wavevector [21–23].

Recently an effective way to excite magnetization dynamics via an optically generated surface acoustic wave in thin Ni films was reported [24]. The transient grating technique was employed to generate narrow-band, widely tunable, in-plane surface elastic waves which displacively drive the magnetization in nickel films. For this experiment an interference of two pump pulses is employed to create the spatial pattern

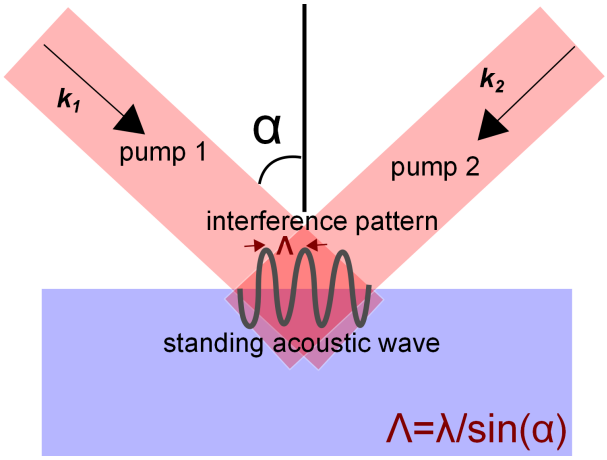

Figure 3.3: (a) Two spatially overlapping laser pulses produce a sinusoidal intensity grating with period Λ on the sample via the interference effect and launch standing in-plane Rayleigh surface acoustic wave which drives the magnetization.

of the surface acoustic wave. The wavelength of such an excitation can be controlled by tuning the spatial period of the interference pattern. This flexibility allowed to excite a broad spectrum of phonons where crossing of the acoustic and magnetic modes occurs and magneto-acoustic coupling is most effective (see Fig. 3.3).

In this Chapter we mostly concentrate on how a laser-induced acoustic standing wave can drive the magnetization dynamics. In order to excite the standing acoustic wave, the inhomogeneity due to the absorbed intensity has to be compared to the sample thickness. In such way absorption profile can create an exponentially decaying distribution of heat-induced lattice distortions and trigger a broad spectrum of acoustic waves. The further process of the establishment of the standing acoustic wave all along the sample thickness depends on the boundary conditions. Moreover, even in absolutely transparent media, laser generation of sound waves is possible. The process is called Impulsive Stimulated Brillouin Scattering. In this case light induces sound through photoelastic modulation of the refractive index.

Here we report on the optical excitation of the lattice-driven magnetization dynamics in iron borate $FeBO_3$. This oxide combines weak ferromagnetism and strong magneto-elastic coupling with high transparency in the visible spectral range. These features allow one to optically monitor the dynamics of the magnetic and elastic oscillations. All these features make it a perfect candidate for the ultrafast pump-probe measurements.

3.2 Magnetic properties of antiferromagnetic $FeBO_3$

Single crystals of $FeBO_3$ have the space group D^6_{3d}. At room temperature it is an antiferromagnet with Neel temperature $T_N = 348$ K [25]. Its unit cell contains two iron

ions Fe^{3+}, the spins of which (S_1, S_2) couple antiferromagnetically. Each iron ion has an octahedral environment of anions formed by the $(BO_3)^{3+}$ complexes. The interion distances for (Fe-O) and (Fe-Fe) are equal to 2.028 $\mathring{A}$ and 3.601 $\mathring{A}$, respectively. The (O-Fe-O) bond angles are equal to 91.82° and 88.18° [26]. Therefore, the iron environment by the six oxygen ions is almost cubic (see Fig. 3.4).

The magnetizations of the magnetic sublattices can be introduced as $\mathbf{M}_1 = \frac{1}{2}n \cdot S_1$ and $\mathbf{M}_2 = \frac{1}{2} \cdot nS_2$ (here n is concentration of the iron ions), $|\mathbf{M}_1| = |\mathbf{M}_2| = \mathrm{M_0}$. The value of $\mathrm{M_0}$ at 0 K is about 520 G [26]. The magnetizations of the two antiferromagnetically coupled sublattices $\mathbf{M}_1$, $\mathbf{M}_2$ lie in the plane perpendicular to the 3_zcrystallographic axis. The Dzyaloshinskii-Moria interaction leads to a canting of the magnetizations over a small angle $\sim 0.7^o$, resulting in a net magnetic moment $\mathrm{M}=|\mathbf{M}_1 + \mathbf{M}_2| \approx 9$ emu/cm^3 also perpendicular to the 3_z axis.

In order to describe the equilibrium and dynamical properties of the magnetic subsystem, an expansion of the thermodynamical potential which contains the invariants under the magnetic symmetry group of $FeBO_3$ is used. Here we use expansion in terms of normalized vectors $\mathbf{l}$ and $\mathbf{m}$. Taking into account invariants up to the second order, one obtains [27]:

$$\Phi_{\mathrm{M}}^{(2)} = \frac{1}{2}\mathcal{J}m^2 + \frac{1}{2}al_z^2 + \frac{1}{2}cm_z^2 + D_z\left(l_x m_y - l_y m_x\right) \tag{3.1}$$

Here $\mathcal{J}$ is the coefficient representing the strength of the homogeneous exchange interaction, a and c define the strength of the single-ion anisotropy. It is convenient to introduce the Dzyaloshinskii vector $\mathbf{D}$ oriented solely along the z-axis, so that $\mathbf{D}=(0, 0, D_z)$. Recently the sign of the Dzyaloshinskii vector was determined for the case of $FeBO_3$ [28].

With minimization of the thermodynamical potential given by Eq. (3.1) one can represent $\mathbf{m}$ as a function of $\mathbf{l}$:

$$\mathbf{m} = \frac{1}{\mathcal{J}}\left[\mathbf{D}, \mathbf{l}\right] \tag{3.2}$$

It is seen that the weak ferromagnetic moment is proportional to the in-plane component of the antiferromagnetic vector. When $\mathbf{l}$ is oriented along the 3_z axis, the magnetic moment does not appear and the magnetizations of the sublattices are perfectly antiparallel. This situation can be observed in hematite and dysprosium orthoferrite at low temperature. A temperature increase leads to a reorientation of the antiferromagnetic vector into the plane perpendicular to the 3_z axis. The reorientation is accompanied by an emergence of the magnetization $\mathbf{M}$. Such a spin-reorientation and induction of a magnetization is called the Morin transition.

It is convenient to express the coefficients in the thermodynamical potential as:

$$\mathcal{J} = 4\mathrm{H_{ex}M_0}, \qquad a = 2\mathrm{H_0M_0}, \qquad D_z = 2\mathrm{H_DM_0} \tag{3.3}$$

Here $\mathrm{H_{ex}}$, $\mathrm{H_o}$, $\mathrm{H_D}$ are effective fields of the exchange, uniaxial out-of-plane anisotropy and the Dzyaloshinskii interaction, respectively (see Table 3.1).

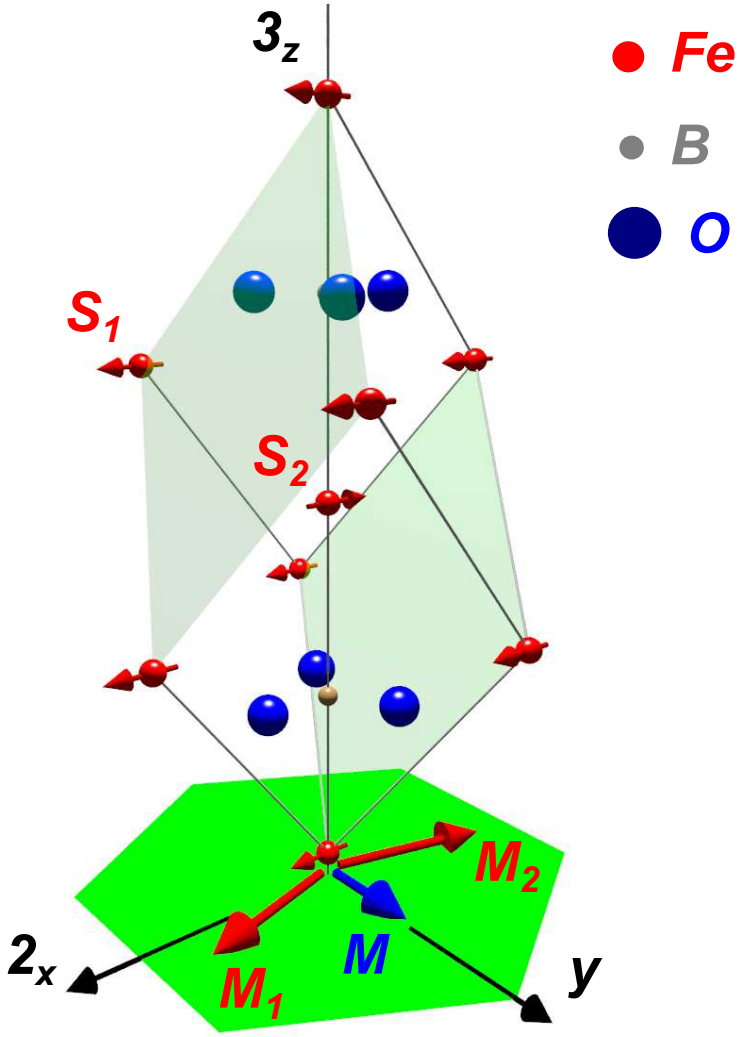

Figure 3.4: Elementary cell of $FeBO_3$. In the chosen Cartesian system of coordinates x, y, z: $x \parallel 2_y$, $y \parallel m$, $z \parallel 3_z$. The schematics of the orientations of the vectors $\mathbf{M}_1$, $\mathbf{M}_2$ and $\mathbf{M}$ in $FeBO_3$ slab are indicated.

H_{ex}, kOe	H_o, kOe	H_D, kOe
$3{\cdot}10^3$	3	100

Table 3.1: Effective magnetic fields of $FeBO_3$. The data are taken from [29].

In order to define the orientation of $\mathbf{l}$ and $\mathbf{m}$ in the sample plane, one needs to account for the in-plane magnetic anisotropy, leading to high-order terms in the free energy expansion. These terms up to the 6^{th} order are:

$$\Phi_{\mathrm{M}}^{(4,6)} = \frac{1}{2i} b \left[l_+^3 - l_-^3 \right] l_z + \frac{1}{2} f \left[l_+^3 + l_-^3 \right] m_z + \frac{1}{2} g \left[l_+^6 + l_-^6 \right] \tag{3.4}$$

Here $l_\pm = l_x \pm i l_y$ and d, f are phenomenological parameters that characterize the three-fold remnants of a cubic anisotropy in crystals of trigonal symmetry, e is a parameter which characterizes the hexagonal in-plane magnetic anisotropy.

In order to define the magnetic ground state of the crystal, it is convenient to introduce spherical coordinates:

$$\mathbf{l} = \begin{cases} l_x = \sin\theta\cos\phi, \\ l_y = \sin\theta\sin\phi, \\ l_z = \cos\theta. \end{cases} \tag{3.5}$$

Here ϕ is an in-plane angle which vector $\mathbf{l}$ makes with the 2_x symmetry axis, θ is an angle which vector $\mathbf{l}$ makes with the 3_z symmetry axis. In this coordinate system the total free energy is given by the expression:

$$\begin{aligned} \Phi_{\mathrm{M}} = & \frac{1}{2}\mathcal{J}m^2 + \frac{1}{2}a\cos^2\theta + \frac{1}{2}bm_z^2 + D_z\sin\theta\left(m_y\cos\phi - m_x\sin\phi\right) + \\ & d\cos\theta\sin^3\theta\sin 3\phi + fm_z\sin^3\theta\cos 3\phi + e\sin^6\theta\cos 6\phi \end{aligned} \tag{3.6}$$

This potential has a minimum when:

$$\mathbf{m} = \begin{cases} m_x = \frac{D_z}{\mathcal{J}} sin\theta\sin\phi, \\ m_y = -\frac{D_z}{\mathcal{J}} sin\theta\cos\phi, \\ m_z = -\frac{f}{\mathcal{J}}\cos\theta. \end{cases} \tag{3.7}$$

One can assume that $\theta = \pi/2 + \delta$, where $\delta \ll 1$. Then equation (3.6) can be rewritten as:

$$\Phi_{\mathrm{M}} = \frac{1}{2}a^*\delta^2 - d\delta\sin 3\phi + e\cos 6\phi \tag{3.8}$$

Here $a^* = a + \frac{D^2}{E}$. So, it becomes clear that a rotation of the vector $\mathbf{l}$ in the basal plane leads to a variation of the angle ϕ. After minimizing of Eq. (3.8) with respect to the angle δ one gets:

$$\delta = \frac{d}{a^*}\sin 3\phi \tag{3.9}$$

Substitution of (3.9) in the energy expression shows that the energy of the in-plane anisotropy is given by:

$$\Phi_{\mathrm{M}}^{(4,6)} = \left(e + \frac{d^2}{4a^*}\right)\cos 6\phi = e^* \cos 6\phi \tag{3.10}$$

Here e^* is the effective parameter of the in-plane hexagonal anisotropy. For the case $a^*<0$:

1. $e^*<0$, $\phi = \frac{\phi}{3}n$, $\theta = \frac{\pi}{2}$
2. $\phi = \frac{\phi}{6}(2n+1)$, $\theta = \frac{\pi}{2} + (-1)^n \frac{d}{a^*}$

In the first case the vector **l** is oriented along one of the 2_x axes and **m** lies in the plane perpendicular to the axis at a small angle. In the second case **m** is oriented along the 2_x, while **l** acquires a small angle with the basal plane. It is common to introduce a field of the in-plane hexagonal anisotropy H_a as:

$$H_a = \frac{6e^*}{M_0}$$

The temperature dependence of H_a was measured in [30] and shows that the second case appears only for very low temperatures (<5 K). If this happens, the magnetization gets oriented along one of the 2_x axis. The value of H_a is extremely small with respect to H_o. At room temperature H_a=0.26 Oe [31].

Due to the extremely low value of the intrinsic in-plane magnetic anisotropy iron borate is almost isotropic in the easy-plane. It makes the in-plane magnetic structure very susceptible to external perturbations, including stress [32, 33] and optical excitation [34, 35].

3.3 Elastic properties of antiferromagnetic $FeBO_3$

The elastic dynamics of a mechanical body is described with the help of the following equation [36]:

$$\rho \frac{\partial^2 u_i}{\partial t^2} = \frac{\partial \sigma_{ij}}{\partial x_j} \tag{3.11}$$

Here ρ is the density, u_i characterizes the displacement along the i axis, σ_{ij} is a component of the mechanical stress tensor.

The stress tensor is defined by the elastic energy Φ_{E} of the body:

$$\sigma_{ij} = \frac{1}{2}\frac{\partial \Phi_{\mathrm{E}}}{\partial u_{ij}} \tag{3.12}$$

The symmetric infinitesimal strain tensor u_{ij} is defined as:

$$u_{ij} = \frac{1}{2}\left(\frac{\partial u_i}{\partial x_j} + \frac{\partial u_j}{\partial x_i}\right) \tag{3.13}$$

C_{ij},	C_{11}	C_{12}	C_{13}	C_{14}	C_{33}	C_{44}	C_{66}
10^{11} erg/cm^3	44.5	14.5	14.0	2.0	30.5	9.5	15

Table 3.2: The elastic constants of the $FeBO_3$. The data are taken from Ref. [37].

The potential Φ_{E} is defined by the symmetry of the material and in general has the form:

$$\Phi_{\mathrm{E}} = \frac{1}{2} C_{ijkl} u_{ij} u_{kl} \tag{3.14}$$

Making use of the symmetry of $FeBO_3$ (point group $\overline{3}m$), the elastic energy of $FeBO_3$ is written as [33]:

$$\begin{aligned}\Phi_{\mathrm{E}} = {} & \frac{1}{2} C_{11} \left(u_{xx}^2 + u_{yy}^2\right) + 2C_{66} u_{xy}^2 + C_{12} u_{xx} u_{yy} + 2C_{44} \left(u_{xz}^2 + u_{yz}^2\right) \\ & + C_{13} \left(u_{xx} + u_{yy}\right) u_{zz} + \frac{1}{2} C_{33} u_{zz}^2 + 2C_{14} \left(u_{xx} u_{yz} - u_{yy} u_{yz} + 2u_{xy} u_{xz}\right)\end{aligned} \tag{3.15}$$

Here the numbers denote pairs of the coordinates according to the following rule: $1 \to xx, 2 \to yy, 3 \to zz, 4 \to xz, 5 \to yz, 6 \to xy$.

The values of the elastic constant are given in Table 3.2 .

Because of the high symmetry of $FeBO_3$ in the basal plane the components xz and yz are equivalent. For this reason C_{15}=C_{14} and C_{55}=C_{44}.

It is easy to show that the plane wave of the transverse sound which propagates along the z direction can be described by the equations:

$$\frac{\partial^2 u_x}{\partial t^2} = \frac{C_{44}}{\rho} \cdot \frac{\partial^2 u_x}{\partial z^2} \tag{3.16}$$

$$\frac{\partial^2 u_y}{\partial t^2} = \frac{C_{44}}{\rho} \cdot \frac{\partial^2 u_y}{\partial z^2} \tag{3.17}$$

The density of $FeBO_3$ is 4.28 g/cm^3 [37]. One can see that the propagation speed of such wave is $\vartheta_t = \sqrt{\frac{C_{44}}{\rho}}$=4.71 km/s.

The longitudinal sound wave propagating along the z direction satisfies the equation:

$$\frac{\partial^2 u_z}{\partial t^2} = \frac{C_{33}}{\rho} \cdot \frac{\partial^2 u_z}{\partial z^2} \tag{3.18}$$

The propagation speed of the longitudinal sound is $\vartheta_l = \sqrt{\frac{C_{33}}{\rho}}$=8.44 km/s.

3.4 Magneto-elastic properties of antiferromagnetic $FeBO_3$

One of the most prominent manifestations of the interaction of magnetic and elastic subsystems is the so-called magneto-elastic gap in the spin-wave spectrum of antiferromagnets .

It was found that the value of the frequency of the ferromagnetic resonance in such antiferromagnetic materials as α-Fe_2O_3, MnF_2, Cr_2O_3, cannot be explained only by the magnetic anisotropy and strength of the external magnetic field. Instead, the frequency of the ferromagnetic resonance is given by two contributions:

$$\mathrm{f}^2 = \mathrm{f}_\mathrm{M}^2 + \mathrm{f}_\mathrm{ME}^2, \tag{3.19}$$

Here $\mathrm{f_M}$ is a merged contribution from the field and the anisotropy and $\mathrm{f_{ME}}$ is a result of the magneto-elastic gap. The basic explanation of the term states that it appears due to a spontaneous magnetostrictive deformations which create an effective field for the spins.

However, this manifestation turned out to be only the short wavelength part of the more general and fundamental interaction between the magnetic and elastic subsystems in magnets. For a broad range of k-vectors, elementary excitations of the magnetic system (magnons) and the elastic system (phonons) are coupled, so they no longer exist separately. Such waves are called magnetoelastic waves (see Fig. 3.5). It makes sense to distinguish two types of the magneto-elastic coupling. In ferrimagnets, such as YIG, exhibiting a spin wave dispersion proportional to $\sim k^2$, one observes a crossing of the uncoupled dispersions. In such case the magneto-elastic interaction then generates quasiphonon and quasimagnon branches (Fig. 3.5a). The crossover of this type does occur only if the sound velocity exceeds the magnon group velocity for a sufficient range of k-vectors.

In ferromagnets, dipole-dipole interaction energies dominate the magnetoelastic energy. In antiferromagnets their contribution is suppressed, bringing the magnetoelastic energy to the leading order. Especially this becomes evident in spin-orientation phase transitions where the magnetic anisotropy is reduced. However, here it is necessary to distinguish between antiferromagnets with anisotropies of easy-plane and easy-axis types. In antiferromagnets with easy-plane anisotropy, the spin-wave dispersion is linear $\sim k$. As a result, the magnon branch intersects with that of the phonons only in the vicinity of $k = 0$. It means that the magneto-elastic coupling is strong only for long-wave length excitations.

Iron borate is an easy-plane antiferromagnet with the Neel temperature above the Debye temperature $\mathrm{T_N} < \mathrm{T_D}$ and for this reason relates to the family called "high temperature antiferromagnets". The speed of the spin waves is higher than the speed of sound and the branches of pure elastic and magnetic waves do not intersect (Fig. 3.5b).

A general expression for the energy of the magneto-elastic coupling for an antiferromagnet can be written as:

$$\Phi_\mathrm{ME} = \frac{1}{2} B_{ijkl}\, l_i\, l_j\, u_{ij}, \tag{3.20}$$

where B_{ijkl} is a component of a phenomenological 4^{th} rank magneto-elastic tensor. The magneto-elastic energy of $FeBO_3$ is given by the expression [33]:

$$\begin{aligned}\Phi_{\mathrm{ME}} = {} & B_{11}\left(l_x^2 u_{xx} + l_y^2 u_{yy}\right) + B_{12}\left(l_x^2 u_{yy} + l_y^2 u_{xx}\right) + B_{66} l_x l_y u_{xy} + \\ & + 2B_{14}\left[2 l_x l_y u_{xz} + \left(l_x^2 - l_y^2\right) u_{yz}\right] + 2B_{41}\left[l_y l_z \left(u_{xx} - u_{yy}\right) + 2 l_x l_z u_{xy}\right] + \\ & + B_{44}\left(l_x l_z u_{xz} + l_y l_z u_{yz} + B_{13}(l_x^2 + l_y^2)\right) u_{zz} + B_{31} l_z^2 \left(u_{xx} + u_{yy}\right) + B_{33} l_z^2 u_{zz}\end{aligned} \tag{3.21}$$

In order to solve the problem of coupled magnetic and elastic oscillations, one needs to solve the coupled Landau-Lifshitz and acoustic wave equations. In these equations the effective magnetic field acting on the magnetization $\mathbf{M}$ is $\mathbf{H}_{eff} = -\frac{\delta \Phi}{\delta \mathbf{M}}$ and the strain tensor $\sigma_{ij} = \frac{1}{2}\frac{\partial \Phi}{\partial u_{ij}}$ where:

$$\Phi = \Phi_{\mathrm{M}} + \Phi_{\mathrm{E}} + \Phi_{\mathrm{ME}} \tag{3.22}$$

It is seen that both equations are coupled via derivatives of the energy Φ.
The strength of the magneto-elastic coupling is characterized by ξ_{me}:

$$\xi_{me} = \left|\frac{\Delta \mathrm{C}}{\mathrm{C}}\right| = \frac{\mathrm{f_{ME}}}{\mathrm{f}} \tag{3.23}$$

Here, ΔC is magnetoelastic contribution to the effective elastic modulus. This value defines how much the phonon spectrum of the magnet is affected by the magneto-elastic coupling. It is clear that this value of the coupling between magnon and phonon modes can be affected by an external magnetic field. This field can shift the dispersion curve of the magnons. For this reason ΔC is a function of the external field.

The highest coupling in "high temperature" antiferromagnets such as $FeBO_3$ occurs in the long-wavelength band of the spectrum, where the magneto-elastic gap appears. This makes such magnets especially interesting for optical pump-probe experiments, where the long-wavelength branch of the spectra is usually affected by the pumping light. Moreover, iron borate has an extremely large value of the magnetoelastic contribution ΔC to the effective elastic modulus [38] $\mathrm{C_{eff}} = \mathrm{C} + \Delta\mathrm{C}$, which in zero magnetic field could reach values up to $|\Delta \mathrm{C}/\mathrm{C}| = 0.8$.

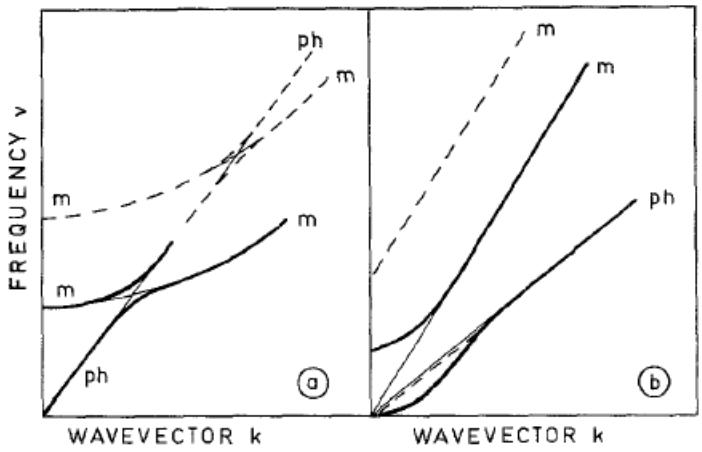

Figure 3.5: Schematic dispersion curves for magnons (m) and phonons (ph) in ferromagnetic like YIG ($T_N < T_D$) (a) and a weak ferromagnet like $FeBO_3$ ($T_N < T_D$) (b). Thin lines: no magneto-elastic interaction. Solid lines: with magneto-elastic interaction in a small magnetic field. Dashed line: elevated field. The picture is taken from Ref. [29]

3.5 Optical and magneto-optical properties of $FeBO_3$

Iron borate is a transparent (green) room-temperature weak antiferromagnet (T_N = 348 K). It is one of the few magnets possessing finite spontaneous magnetization at room temperature and being transparent in the visible spectral range. A large Faraday rotation (300 deg/cm, at λ=800 nm) in combination with high transparency in the visible and near infrared spectral ranges makes this material an excellent candidate for magneto-optical studies and applications [39].

The green color of $FeBO_3$ is unusual for ferric ions in an oxygen lattice. This suggests that the crystal field at the Fe^{3+} ions is significantly modified by the boron ions [25].

Under normal ambient conditions, $FeBO_3$ is an insulator with a fundamental absorption edge at 2.9 eV. The absorption spectra consists of two broad bands (see Fig. 3.6). The band edge originates from electric dipole allowed charge transfer transitions either from the oxigen ligands to the d-levels of Fe^{3+} or between two Fe^{3+} ions with antiparallel spins [40]. Two broad bands in the visible range near 0.9 μm and 0.62 μm with relatively small absorption are also present. They originate from the parity forbidden $d-d$ transitions inside the Fe^{3+} multiplet. Due to the crystal field this prohibition becomes partially lifted. In particular, the crystal-field transitions ${}^6A_1 \rightarrow {}^4T_{1g}$ and ${}^6A_1 \rightarrow {}^4T_{2g}$ of Fe^{3+} from high- ($S = \frac{5}{2}$) to low-spin ($S = \frac{3}{2}$) configurations are partially allowed [41].

Iron borate is an optically uniaxial crystal with the refractive indexes n_x=n_y=2.16 and n_z=2.02 at the wavelength of λ=632.8 nm [25]. Since n_z<n_x,n_y $FeBO_3$ demon-

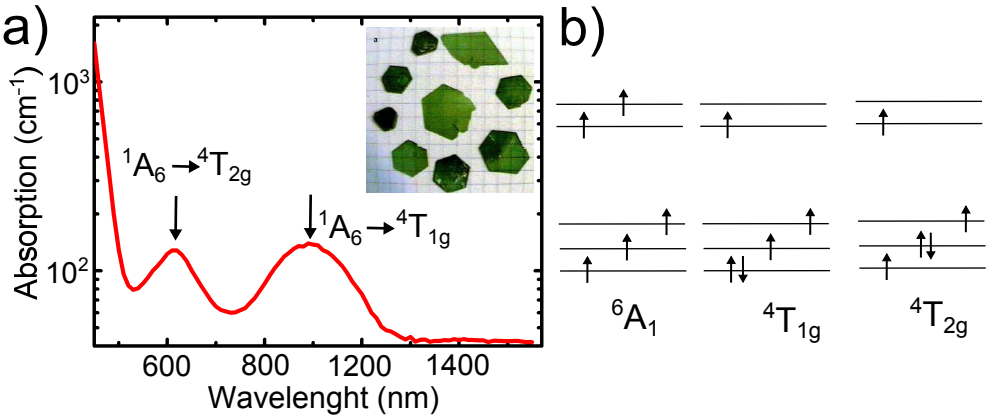

Figure 3.6: (a) A typical optical absorption spectrum of the studied $FeBO_3$ samples. The studied samples are shown on the inset. Several electronic configuration for the d^5 ion in the octahedral crystal field

strates negative optical birefringence. In order to avoid issues caused by the birefringence in the experiments, platelets cut perpendicular to the [001]-axis which is the direction of the optical axis, are used.

Unfortunately, the Faraday effect cannot be observed with light propagating along the optical axis because the magnetization lies in the plane of the platelet. In order to be sensitive to the in-plane magnetization one needs to tilt the sample over a finite angle with respect to the incident beam. In this case the rotation of the polarization of light caused by the Faraday effect is strongly affected by the crystallographic birefringence. The interplay between these two effects leads to drastic changes in the resulting rotation of the polarization plane, depending on sample thickness and angle between the wave vector and the $z-$axis [42]. To maximize the Faraday rotation for a given crystal thickness one needs to adjust the angle of incidence.

3.6 Pump-probe experimental set-up

Here we studied a series of iron borate single crystals with thicknesses from 4 μm to 40 μm. The crystals were grown with the help of the solution in a melt method [43]. All crystals were cut, such that normal to the sample coincides with the 3_z symmetry axis, so the sample surface is the (001) plane.

Experimentally, the possibility to trigger the lattice-driven magnetization dynamics by single light pulse in $FeBO_3$ was studied employing a typical optical pump-probe technique with a mechanical delay line in the geometry shown in Fig. 3.7. For the experiments we employed an amplified Ti:sapphire laser system producing 200 fs pump pulses at a central photon energy of 1.55 eV at a repetition rate of 1 kHz. The laser-induced magnetization dynamics was monitored with a delayed probe pulse measuring the pump-induced Faraday rotation $\theta_F = \chi \cdot (\mathbf{M}, \mathbf{e_k})$. Here χ is the magneto-optical

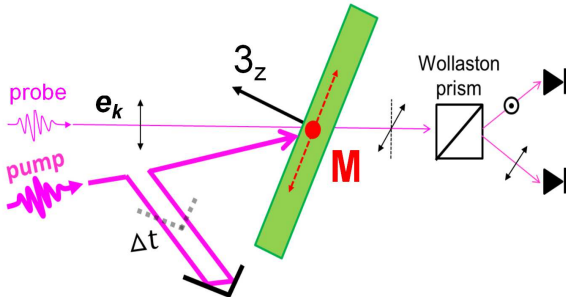

Figure 3.7: Experimental geometry of the optical pump-probe setup employed to excite lattice-driven magnetization dynamics in $FeBO_3$

(MO) susceptibility and $\mathbf{e_k}$ is the unit vector in the direction of the light propagation. The intensity ratio between the pump and probe pulses was about 50. Both beams were focused on the sample to a spot diameter of about 200 μm for the pump and 60 μm for the probe.

The pump-induced magnetization dynamics is expected to be strongly elliptical with the main axis oriented in the sample plane. This is because of the weak in plane magnetic anisotropy and a decrease of the net magnetization value, which accompanies an inclination of the magnetization from the basal plane. Thus, in order to maximize the value of the Faraday rotation and to study its dynamics, all the samples were tilted over a small angle ($\leq 20^o$) from the normal incidence.

The measurements were performed in two geometries (see Fig. 3.8). In the first case the projection of the magnetization on the incidence angle is absent and can appear only after excitation of the in-plane magnetization dynamics (Fig. 3.8a). For this reason the Faraday rotation is absent for fields more than 15 Oe, see Fig. 3.8b. The Faraday rotation from the second geometry shows typical hysteresis loop (Fig. 3.8d) and is used to calibrate the in-plane magnetization dynamics.

The difference between the angles of incidence for the pump and the probe was set to about 20^o. In order to avoid an influence of possible artifacts of non-magnetic origin we measured the polarization rotation θ at two polarities of the external magnetic field. The Faraday rotation then was calculated as the difference of θ_F between two opposite fields: $\theta_F = \frac{1}{2}[\theta(H_+) - \theta(H_-)]$. In the measurements a saturating magnetic field > 15 Oe was applied in the sample plane ($\mathbf{H} \perp \mathbf{e_k}$). Because of the weak in-plane anisotropy, the magnetization got oriented nearly along the external field, which was confirmed by static MO measurements (Fig. 3.8b). Most of the measurements were done at room temperature.

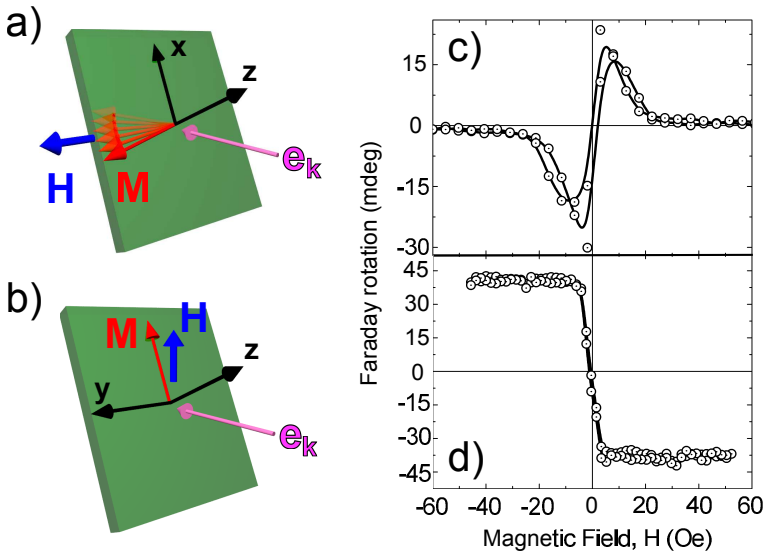

Figure 3.8: (a) The geometry used to measure in-plane magnetization dynamics. (b) The field dependence of the Faraday rotation measured for the field, applied in the sample plane. (c) The geometry used to calibrate in-plane magnetization dynamics. (d) The field dependence of the Faraday rotation measured in the orthogonal geometry.

3.7 Optical excitation of spins dynamics in $FeBO_3$

We could not observe any laser-induced dynamics of the signal in the experiments with the probe incident normal to the sample ($\mathbf{e_k} \parallel 3_z$). Nevertheless, rotating the sample around **H**, such that the wave-vector of the probe $\mathbf{e_k}$ and the 3_z axis are no longer collinear, allows to detect the in-plane component of the magnetization. In our case it was set to 17^0 in order to maximize the ratio between the Faraday rotation and the birefringence [42]). The experiment reveals that ultrafast laser excitation can effectively excite oscillations of the magneto-optical signal (see Fig. 3.9). It is possible to separate two oscillations which arise on different timescales and demonstrate different behavior with respect to the polarization of the pump light.

Initially, high-frequency strongly damped oscillations (the damping ratio is 0.16) with frequencies around 10 GHz appear on a timescale $\leq$ 1.5 ns - (1). Interestingly, the dynamics at longer time delays (2) reveals signs of an additional low frequency oscillation. The last, contrary to fast precession demonstrates no pump polarization dependence.

3.7.1 Ferromagnetic spin precession

In order to reveal the origin of the high-frequency mode we applied an external magnetic field in the sample plane. The field dependence of the frequency is shown in Fig. 3.10b and demonstrates a dependence, which is typical for the ferromagnetic res-

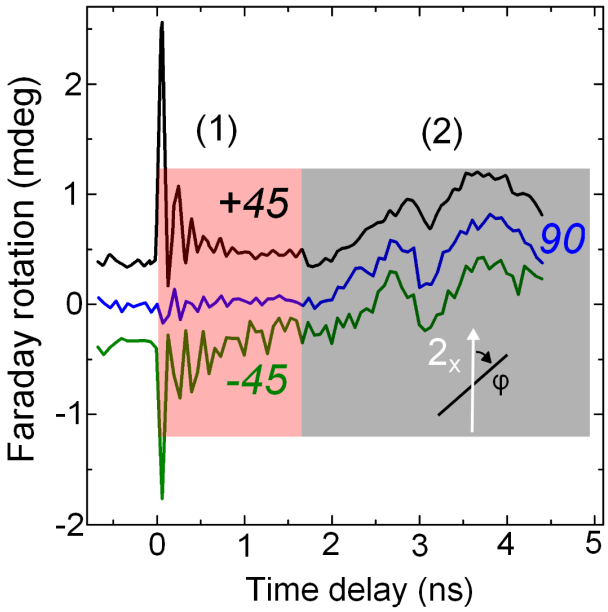

Figure 3.9: The Faraday rotation as a function of the pump-probe delay for three different linear pump polarizations. The colored rectangles depict the timescales where different magnetic processes occur.

onance in easy plane weak ferromagnets [30]: $f_{FMR} = \gamma\sqrt{H\,(H + H_D) + H_{ME}^2}$. This spin resonance is associated with a spin motion in the (001) plane such that small oscillations of **M** in the (010) plane appear, while **L** oscillates in the basal plane.

Fitting the frequency dependence one can subtract the frequency of the magneto-elastic gap and the Dzyaloshinskii field:

$$f_{ME} = \gamma H_{ME} = 2.8 \text{ GHz} \qquad H_D = 6 \cdot 10^4 \text{Oe} \tag{3.24}$$

Here we introduce the value of the effective magneto-elastic field H_{ME}.

The optical excitation of the quasiferromagnetic (FMR) mode in $FeBO_3$ via the Inverse Coutton-Mouton Effect (ICME) was reported earlier, see Ref. [44]. The ICME can be interpreted as an instantaneous light-induced magnetic anisotropy axis [45]. The direction of this axis is defined by the light polarization. If such axis is parallel or orthogonal to the initial spins directions (the $y-$axis), the effect is zero. If not, the light induces a torque which effectively launches the spin precession.

To explain the ICME one should define terms in the free energy which depend on both the electric field of the linearly polarized light and the antiferromagnetic vector:

$$\Phi_{lm} = \mathcal{A} L_x L_y \cdot \mathcal{E}_x \mathcal{E}_y^*$$

Here $\mathcal{A}$ is a phenomenological parameter. $\mathcal{E}_x$ and $\mathcal{E}_y$ are the $x-$and the $y-$components of the electric field of the pump, respectively. In a perfect agreement with the data presented in Ref. [44], the phase and the amplitude of the oscillations are sensitive to the linear pump polarization (Fig. 3.10c). The amplitude of the spin precession decreases as the field increases, being inversely proportional to the frequency of the FMR precession as predicted for the inertia-driven mechanism of excitation of spin resonances [45].

3.7.2 Lattice-driven magnetization dynamics

The measurements for longer time delays up to 24 ns show that the pump pulse excites low-frequency nearly damping-free (damping ratio $\leq$0.01) oscillations. The phase of the photo-induced oscillations is sensitive to the direction of the applied field and experiences a π-shift when sign of the external field changes (Fig. 3.12).

Figure 3.13a shows the low frequency oscillations in various external magnetic fields. It is remarkable that relatively small fields suppress the oscillations dramatically. A Fourier analysis of the spectra of the oscillations demonstrates both first f and second $2f$ harmonics of the magnetic excitation, with frequencies of 0.51 ± 0.05 and 1.01 ± 0.05 GHz, respectively. Both frequencies are hardly sensitive to the value of the external magnetic field (Fig. 3.13b). This is in contrast to the behavior expected for the homogeneous magnetization precession around an effective magnetic field $\mathbf{H_{eff}}$ in $FeBO_3$ (see Fig. 3.13c). Moreover, the observed frequencies are much lower than the frequencies of the ferromagnetic resonance in $FeBO_3$ ($f << f_{FMR}$). Hence, the observed magnetization oscillations cannot be due to a precession of the magnetization around its equilibrium orientation and can only be explained in terms of the oscillations of the equilibrium orientation itself. These oscillations are, in fact,

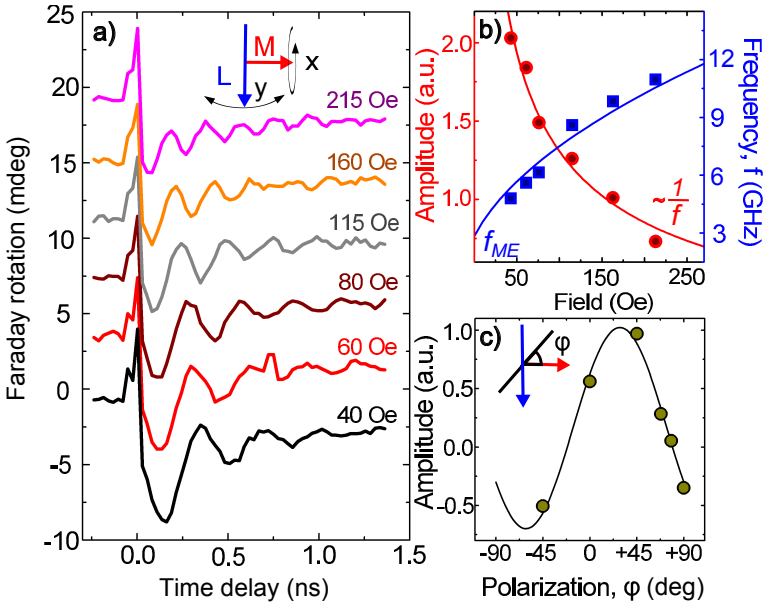

Figure 3.10: Optically excited FMR resonance. (a) Probe polarization rotation vs. the time delay between linearly polarized pump and probe pulses for different values of applied magnetic field on the timescale $\leq$1.5 ns. (b) Amplitude and frequency of the optically excited FMR resonance as a function of the external field with the fit functions. (c) The polarization dependence of the optically excited FMR as a function of incident pump beam polarization

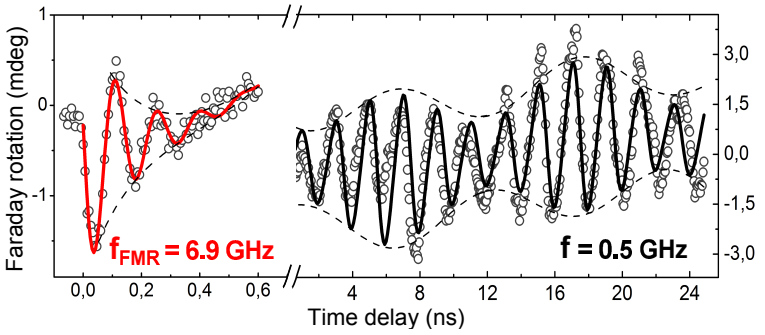

Figure 3.11: Femtosecond laser excitation of short-living high frequency FMR mode at f_{FMR}=6.9 GHz. Femtosecond laser excitation of long-living lattice-driven magnetic mode at f=0.5 GHz, obtained with the help of the Faraday effect in the external magnetic field of 40 Oe with a pump fluence of 38 mJ/cm^2 for the sample thickness 9 μm .

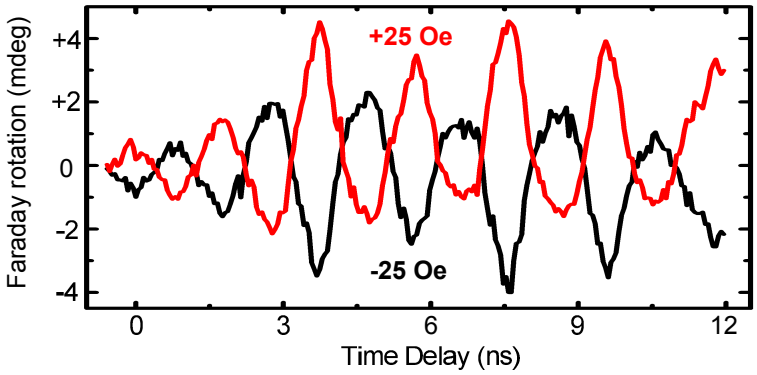

Figure 3.12: The excitation of the pump-induced oscillation for two opposite fields applied in the sample plane. The field value is 25 Oe.

oscillations of the effective magnetic field defined by the $\mathbf{H_{eff}}$. Because of the relation f << f_{FMR} the magnetization tracks the new equilibrium quasi-statically and oscillations are not accompanied with ferromagnetic precession. Since $\mathbf{H_{eff}} = \mathbf{H_a} + \mathbf{H} + \ldots$, it is natural to conclude that the oscillations of $\mathbf{H_{eff}}$ are, in fact, due to oscillations of the laser-induced contribution to the anisotropy field $\delta\mathbf{H_a}$. These oscillations are presumably triggered via the aforementioned lattice-driven effect (Fig. 3.2b).

To verify this hypothesis we performed the measurements on samples of different thicknesses. Note, that the frequency of the FMR is expected to be thickness independent. Fig. 3.14a shows that the thickness d strongly influences the frequency of the oscillations, while the maximum deviation of the spins in the oscillations in all the samples are comparable, being in the range of 5-7^o.

The thickness dependence of the lowest frequency f in the spectrum of the oscillations can be well described by f= $\vartheta_l/2d$, with $\vartheta_l = 8.7 \pm 0.1$ km/s (Fig. 3.14b). This value is in a very good agreement with the speed of the longitudinal sound wave propagating along the 3_z axis [37]. It suggests that the observed oscillations of the magnetic anisotropy are due to a coupling between the magnetic subsystem and a longitudinal sound wave, impulsively excited by the laser. After the excitation such a wave is spatially confined by the sample surfaces. The boundary conditions given by the free surfaces lead, similarly to Ref. [22], to a formation of a standing wave oscillating at the frequency f and described by the strain tensor component $s_{zz}=\frac{\partial u}{\partial z}$. Here $u(z)$ is a mechanical displacement of the atoms along $z \parallel 3_z$:

$$s_{zz} = s^0_{zz}(l) \sin(2\pi \mathrm{f} t) \sin\left(\frac{\pi l}{2d} \cdot z\right)$$

Here $l = 1, 2, 3 \ldots$ is the number of the acoustic overtone. Such a standing strain wave results in periodic sample deformations along the $z-$axis leading, in particular, to a modulation of the thickness d with a frequency f:

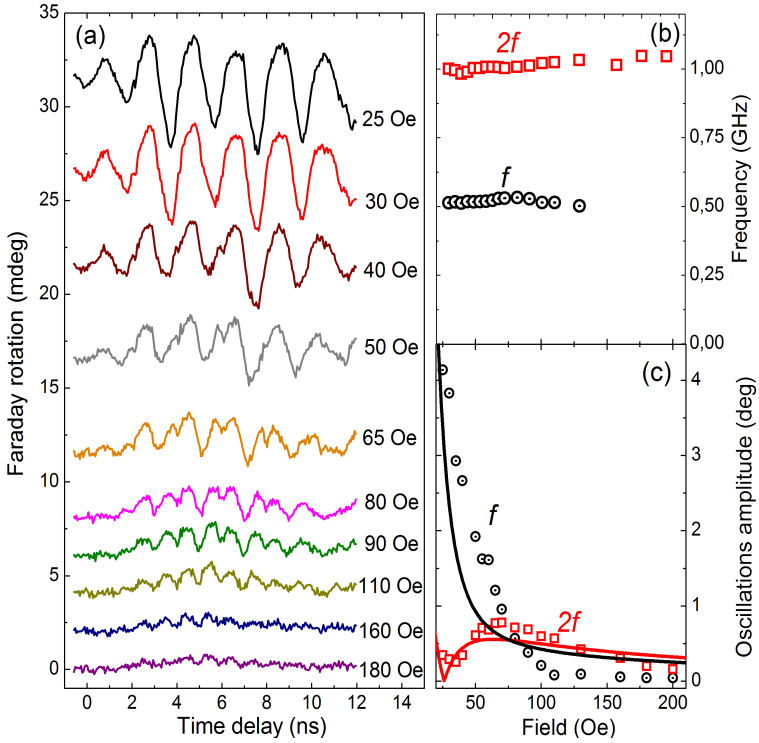

Figure 3.13: Time-resolved MO response to a pump pulse in $FeBO_3$, measured for different magnetic fields. (a) Probe polarization rotation *vs*. the time delay between linearly polarized pump and probe pulses for different values of the applied magnetic field. (b) Field dependence of the frequencies of two harmonics. (c) Experimental data (points) and theoretical fit based on the constructed theory (solid lines) of the amplitudes of the 1st and the 2nd harmonics of the spin oscillations as a function of magnetic field. Fit parameters are G_4=4.3·10^7 erg/cm^3, G_6=5.7·10^4 erg/cm^3 and the laser-induced strain amplitude is s^0_{zz}=3.3·10^{-4}. Sample thickness is 9 μm. Pump fluence is 38 mJ/cm^2.

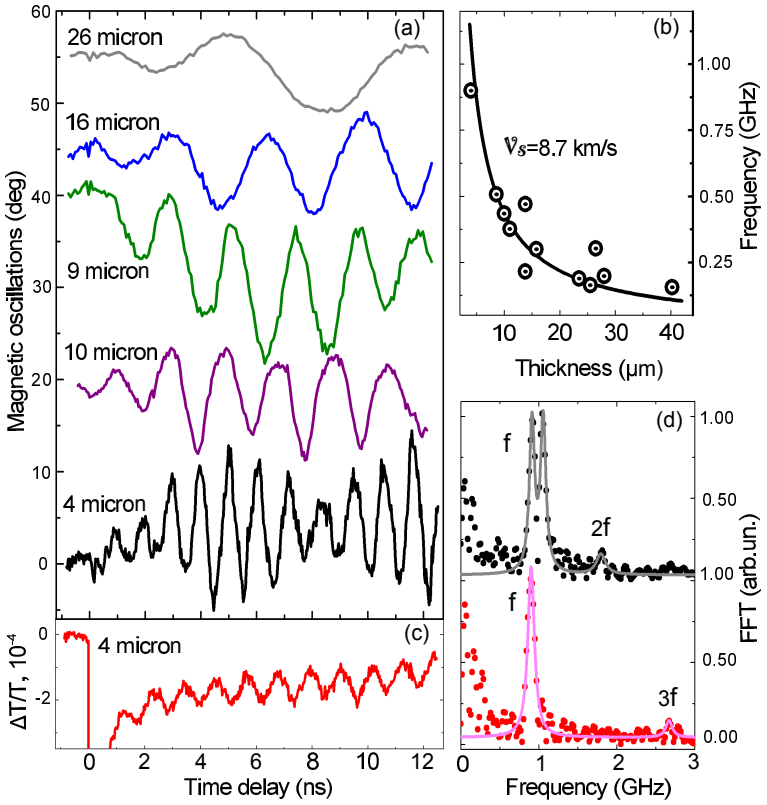

Figure 3.14: Pump-induced dynamics in $FeBO_3$, measured for different samples thicknesses. (a) Magnetization oscillations *vs.* the time delay between linearly polarized pump and probe pulses for samples with different thickness. (b) Lowest frequency in the spectrum *vs.* sample thickness: dots are experimental data, thick line is hyperbolic fit f= $\vartheta_l/2d$. (c) Differential transmission signal for the sample with thickness 4 μm. (e) Normalized FFT spectra of the Faraday rotation (black) and the differential transmission (red) for 4 μm thick sample. Solid lines are lorentzian fits of the observed peaks. External field is 25 Oe. Pump fluence is 38 mJ/cm^2. The origin of the splitting of the f-line in the FFT spectrum for the Faraday rotation could be a nonlinearity of the magneto-acoustic interaction and an inhomogeneity of the sample thickness over the probed area.

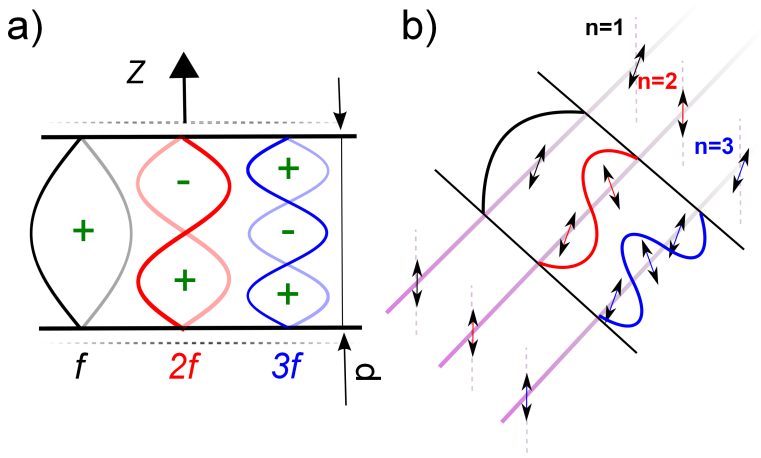

Figure 3.15: (a) The schematics of standing sound waves up to 3^{rd} harmonics along the sample thickness. (b) The propagation of the probe beam along the sample thickness showing that cumulative effect from even harmonics on its polarization is zero

$$d = d_0 + \int_0^{d_0} s_{zz} dz = d_0 + s_{zz}^0 (l) \frac{2d_0}{\pi l} \left(1 - \cos \frac{\pi}{2} l\right) \sin (2\pi f t)$$

This thickness oscillations causes density variations along the $z-$axis and, in accordance with the Clausius-Mosotti, relations results in a change of the refractive index [46]:

$$\frac{N\alpha}{V} = \frac{n^2 - 1}{n^2 + 2}$$

Here N is the number of atoms, α is the polarizability of the medium, V is the sample volume. The transmission coefficient T at normal incidence is:

$$\mathrm{T} = \frac{4n}{(n+1)^2} \tag{3.25}$$

So, a periodic modulation of the optical density leads to an oscillatory behaviour in the differential transmission $\Delta \mathrm{T}/\mathrm{T} \sim 10^{-4}$ (Fig. 3.14c) and roughly corresponds to a mechanical strain $s_{zz}^0 \sim 10^{-4}$. The frequencies of the oscillations in the differential transmission signal and the Faraday rotation are the same (Fig. 3.14c). However, unlike the Faraday rotation, the amplitude and spectrum of the oscillations observed in the transmittance do not depend on the magnetic field. This indicates that acoustic phonons play the master role and are not affected by the spin magnetization, while the spin oscillations are driven by the lattice vibration.

To reveal the nature of the anharmonicity of the dynamics visible in the measurements for different bias fields, we performed measurements for different pump

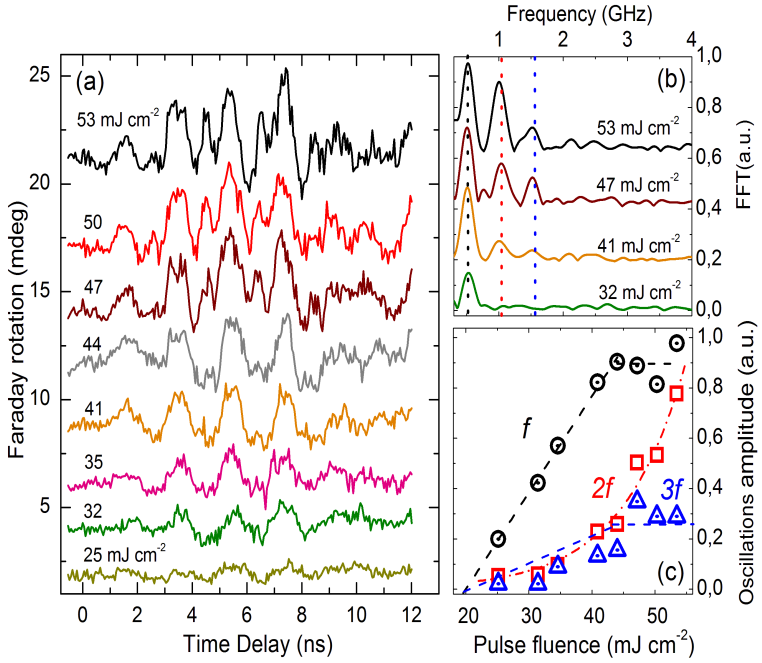

Figure 3.16: Laser-induced dynamics of the MO response in $FeBO_3$ measured for different pump fluences. (a) Probe polarization rotation *vs*. the time delay between linearly polarized pump and probe pulses for different values of pump fluence. (b) FFT spectrum for different pump fluences. (c) Pump fluence dependence of the observed harmonics. The dashed lines are guides to the eye. External magnetic field is 100 Oe. Sample thickness is 9 μm.

fluences. Figure 3.16b shows that the oscillations spectrum contains at least three harmonics effectively generated above the fluence threshold of20 mJ/cm^2. Note, that the measured signal is proportional to the integral magnetization over the sample thickness. Hence, in the assumption of a linear relationship between the strain and the magnetization ($s_{zz} \sim M_y$) [19], the odd harmonics can originate from the overtones of the acoustic standing wave ($l = 2, 3, \dots$). However, the even harmonics must have a different origin, because their integral effect over an integer number of periods is zero [22]. Figure 3.15 demonstrates the averaging of the Faraday rotation for even harmonics. Experimentally, for none of our measurements we observed even harmonics in the transmittance, while signals at even harmonics were visible in the Faraday rotation (Fig. 3.14d).

Indeed, Fig. 3.16c reveals nearly similar intensity dependencies for the 1st and 3rd harmonics that are clearly distinct from that of the 2nd harmonic. Until the saturation near 44 mJ/cm^2, the 1st and 3rd harmonics have a nearly linear fluence dependence while the 2nd demonstrates a quadratic behaviour. This implies that the second harmonic arises from a non-linear coupling between the magnetization and the sound. The different nature of the 1st and 2nd harmonics is also confirmed by their

significantly different behavior in the external field (Fig. 3.13c). In agreement with this, our experiments show no 2^{nd} harmonic in the differential transmission signal (see Fig. 3.14d).

3.8 Mechanism of coupling of light to lattice vibrations

We note that for $FeBO_3$ absorption of light at the pump wavelength (800 nm) is very low, less than 80 cm^{-1}. It corresponds to the absorption length 125 μm and indicates that the excitation by the pump is rather homogeneous across the sample thickness. Hence, it is reasonable to consider non-dissipative mechanisms of the strain generation. Consider the coordinate system with the $x-$ and $y-$axes in the plane of the sample whereas the $z-$axis is aligned along the 3_z-axis of the crystal. For the light incident close to the sample normal, the electric field is given by a superposition of x- and y-components:

$$\boldsymbol{\mathcal{E}} = \mathcal{E}_x \mathbf{e}_x + \mathcal{E}_y \mathbf{e}_y, \tag{3.26}$$

where $\mathbf{e}_x$ and $\mathbf{e}_y$ are unit vectors parallel to the x- and y-axes, respectively. The mechanical strain along the z- axis can be generated by an electric field in a centrosymmetric crystal by means of an electrostriction-like effect [46]:

$$s_{zz}(\mathrm{f}) = \zeta_{zzxx}\mathcal{E}_x(\omega_1)\mathcal{E}_x^*(\omega_2) + \zeta_{zzyy}\mathcal{E}_y(\omega_1)\mathcal{E}_y^*(\omega_2) + c.c., \tag{3.27}$$

here ζ_{zzxx}, ζ_{zzyy} are components of the electrostriction tensor ζ_{ijkl} (for the space group of $FeBO_3$ ζ_{zzxx}=ζ_{zzyy}) and ω_1 , ω_2 are the frequencies of the optical waves exciting the strain, so that f=(ω_1-ω_2)/2π. It is seen that, the light-sound coupling does not depend on the orientation of the linear polarization of light. This is also confirmed experimentally (see Fig. 3.17). An ultrafast laser pulse being short in the time domain (Δt=200 fs) is spectrally broad with a bandwidth $\sim$5 THz and simultaneously provides electric fields with the frequencies ω_1 and ω_2. Microscopically, such a non-dissipative mechanism can be explained in terms of Impulsive Stimulated Brillouin or Raman Scattering [47, 48].

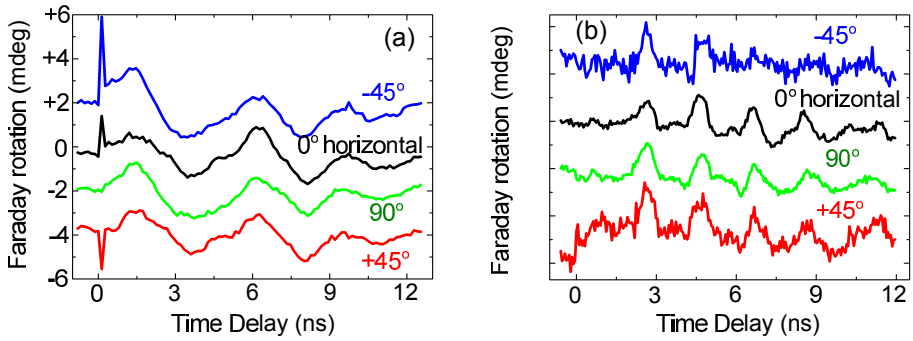

Figure 3.17: The excitation of pump-induced oscillations for different linear pump (a) and probe (b) polarizations, showing that the observed signal is not sensitive for either of them.

3.9 Theoretical description of the lattice-driven magnetization dynamics

In the space group D^6_{3d}, a longitudinal sound wave, propagating along the 3_z axis, cannot change the symmetry and the direction of the magneto-crystalline anisotropy in the basal plane but can trigger oscillations of its value [33] (see Fig. 3.18a). This may happen due to strain-induced changes in the dipole-dipole and the single-ion magnetic interactions [49]. If the easy axis does not coincide with the external field, such oscillations will lead to oscillations of the equilibrium orientation, which is determined by the competition of the magneto-crystalline easy-axis and the external magnetic field. An increase of the magnetic field leads to a suppression of the magnetic oscillations (Fig. 3.13a).

In the absence of an external magnetic field, the magnetization is oriented along one of the six directions corresponding to the minimum of the energy of the magneto-crystalline profile. If an external magnetic field is applied along one of those direction, oscillations of the strength of the magnetic anisotropy cannot trigger magnetization dynamics. To confirm this we performed measurements applying a permanent external field for different directions in the sample plane. Note that the obtained data is modulated by the sensitivity of the Faraday rotation to the magnetization components, so that magnetization components perpendicular to the incident probe beam are not visible. The results are demonstrated in Fig. 3.19. It is seen that the amplitude of the oscillation changes sign crossing the 2_x axis. The period of the angular dependence is close to 60^o. This is in accordance with the suggested mechanism.

To obtain a better insight in to the problem, we provide a phenomenological analysis of it. Symmetry invariants present in Φ_{ME} do not describe the experimentally observed coupling between longitudinal sound propagating along the 3_z axis and the magnetization in the basal plane. The coupling emerges if one accounts for magneto-elastic symmetry invariants which contain both the longitudinal strain component u_{zz} and components of the vector $\mathbf{l}$. As it is seen from Eq. (3.8), the parameters b and g determine the strength of the in-plane anisotropy $\mathrm{H_a}$. Thus, one can phenomeno-

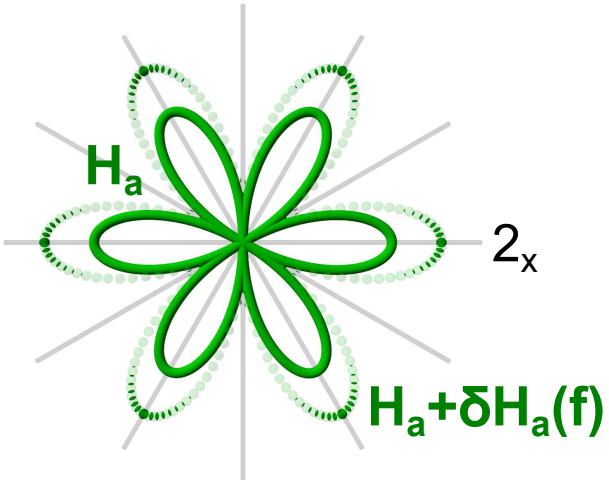

Figure 3.18: Strain-induced variations δH_a of the strength of the six-fold magneto-crystalline anisotropy field H_a at the frequency f.

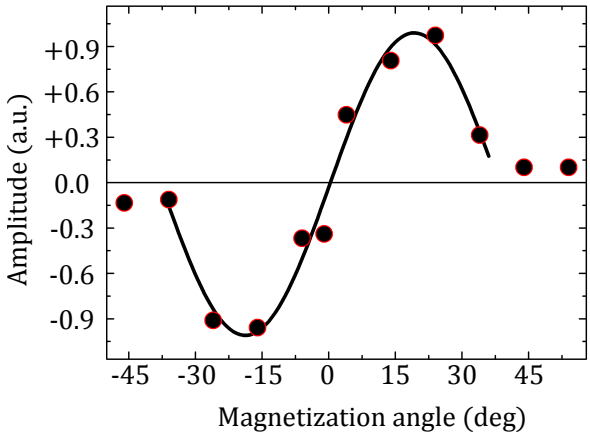

Figure 3.19: The amplitude of the spin precession as function of the angle between the magnetization and the 2_x symmetry axis.

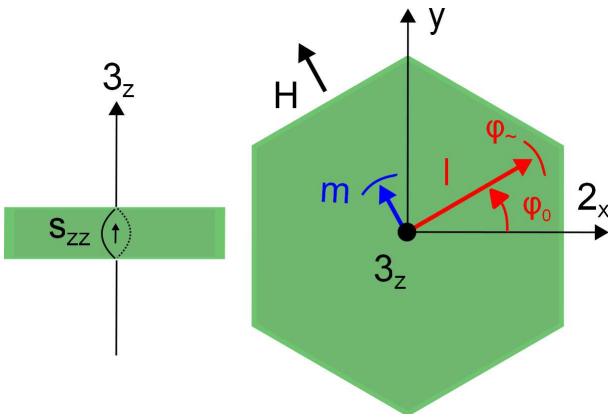

Figure 3.20: Model of the pump-induced magnetization dynamics ϕ in terms of **m** and **l** vectors driven by the standing longitudinal acoustic wave s_{zz}. The initial orientation of the antiferromagnetic vectro ϕ_0 is given by the external magnetic field **H**.

logically introduce new strain-dependent energy invariants as those which lead to a renormalization of the in-plane anisotropy strength:

$$b_{eff} = b + \delta b\,(\epsilon_{ij}) \qquad g_{eff} = g + \delta g\,(\epsilon_{ij}) \tag{3.28}$$

Here ϵ_{ij} is a strain tensor: $\epsilon_{ij} = \epsilon^0_{ij} + s_{ij}$ consisting of a static magnetostrictive ϵ^0_{ij} and a dynamical part s_{ij}. In the linear approximation only terms proportional to ϵ_{zz} and $\epsilon_{xx} + \epsilon_{yy}$ satisfy the symmetry operations of the $FeBO_3$ space group and can contribute to Φ_{ME}. Our experiment shows that the magnetic oscillations are caused by ϵ_{zz}. The dynamical strain-induced contributions to the effective constants of the in-plane anisotropy can be written as: $\delta b = G_4 \cdot \epsilon_{zz}$ and $\delta g = G_6 \cdot \epsilon_{zz}$.

$$\Phi^{+}_{\mathrm{ME}} = \frac{1}{2i} G_4 \left[l^3_+ - l^3_-\right] l_z \epsilon_{zz} + \frac{1}{2} G_6 \left[l^6_+ + l^6_-\right] \epsilon_{zz} \tag{3.29}$$

Such terms modulate the value of the effective anisotropy constant e^* responsible for the strength of the in-plane anisotropy. Such laser-induced dynamical strain acts like a driving force for the magnetization dynamics. Values of the static magnetostrictive deformations can be found, minimizing the free energy Φ with respect to ϵ_{ij}, which gives $\epsilon^0_{ij} \sim B/C \cong 10^{-5}$. Renormalization of the energy invariants should not change the order of the cubic and the hexagonal anisotropies. Hence, one can find that the relations for determination of parameters G_4 and G_6 are $G_4\epsilon^0_{zz} \sim 10^3$ erg/cm^3 (see Ref. 5, 6) and $G_6\epsilon^0_{zz} \sim h \sim 1$ erg/cm^3 (see Ref. 7). Assuming that G_4 and G_6 do not depend on the frequency of the strain, one finds the upper bounds for the values $G_4 \leq 10^8$ erg/cm^3, $G_6 \leq 10^5$ erg/cm^3.

To describe the low frequency magnetization dynamics ($f << f_{\mathrm{FMR}}$) driven by acoustic vibrations it is reasonable to assume that the magnetic oscillations follow

the acoustic ones in a quasi-equilibrium fashion. Thus the description of the magnetization dynamics can be done for the static equilibrium. Let the angle $\phi_\sim$ describe the in-plane rotation of the vector $\mathbf{l}$ from the initial orientation. In this case, by minimizing the free energy $\Phi + \Phi^{+}_{\mathrm{ME}}$ with respect to $\mathbf{l}$ the angle $\phi_\sim$ is obtained as a function of the laser-induced strain:

$$\phi_\sim = \frac{\left[\left(\frac{3bG_4}{a'} + 6G_6\right) e_{zz} + \frac{3G_4^2}{2a'} e_{zz}^2\right] \sin 6\phi_0}{2M_0\left(H_{me} + \frac{D}{E}H\right) - 36\left(g + G_6 u^0_{zz}\right)\cos 6\phi_0 - 36G_6 e_{zz}\cos 6\phi_0} \tag{3.30}$$

Here $\mathrm{H_{ME}}$ is the expression for the magnetoelastic field in terms of magnetic and elastic parameters:

$$\mathrm{H_{ME}} = \frac{4C_{66}B_{14}^2 - 4C_{14}B_{14}B_{66} + C_{44}B_{66}^2}{2M_0\left(C_{44}C_{66} - C_{14}^2\right)}, \tag{3.31}$$

ϕ_o is the angle between the initial orientation of $\mathbf{l}$ and the $x-$axis, mostly defined by the external field, see Fig. 3.20.

Note, that from Eq. (3.30) it is clearly seen that the magnetization dynamics cannot be triggered by an acoustic vibration which propagate in the z-direction if the magnetization is oriented such that $\phi_0{=}n\cdot\frac{\pi}{6}$, $n\in\mathbb{Z}$. Expansion of Eq. (3.30) and limiting to the first two terms gives:

$$\begin{aligned}
&\phi = \frac{\left(Le_{zz} + Ke_{zz}^2\right)\sin 6\phi_0}{T - V\cos 6\phi_0 - 36G_6 e_{zz}\cos 6\phi_0} = \\
&\frac{\left(Le_{zz} + Ke_{zz}^2\right)\sin 6\phi_0}{T - V\cos 6\phi_0}\left(1 - \frac{36G_6 e_{zz}\cos 6\phi_0}{T - V\cos 6\phi_0}\right)^{-1} \approx \\
&\approx \frac{L\sin 6\phi_0}{T - V\cos 6\phi_0} e_{zz} + \left[\frac{K\sin 6\phi_0}{T - V\cos 6\phi_0} + \frac{18LG_6\sin 12\phi_0}{\left(T - V\cos 6\phi_0\right)^2}\right] e_{zz}^2 + O\left(e_{zz}^3\right)
\end{aligned} \tag{3.32}$$

Here the following relations are used:
$L = \frac{3bG_4}{a'} + 6G_6$, $K = \frac{3G_4^2}{2a'}$, $T(H) = 2M_0\left(\frac{H_D}{2H_e x}H + H_{ME}\right)$, $V = 36(g + G_6 u^0_{zz})$.

Equation (3.32) explains the appearance of the even harmonics in the magnetization dynamics via the non-linear interaction $\sim e_{zz}^2$ between the laser-induced longitudinal sound wave and the in-plane magnetization. Further expansion of Eq. (3.30), in principle, can explain the appearance of the higher harmonics including those observed in the experiment. The third harmonic, however, can also originate from the sound overtones. This is not accounted for by the suggested theory.

Using this theoretical framework and the field dependence of the observed 1st and 2nd harmonics of the magnetic excitations allowed us to estimate the phenomenological parameters ($G_4 \sim 10^7$ erg/cm^3 , $G_6 \sim 10^5$ erg/cm^3) and the laser-induced strain amplitude ($s^0_{zz} \sim 10^{-4}$). The fit of the experimental data with these parameters describes the experiment very well (see Fig. 3.13). Note that static magnetostrictive deformations [50] ϵ^0_{zz} in $FeBO_3$ are about 10^{-5} and thus $s_{zz} >> \epsilon^0_{zz}$. Such an inequality is, in fact, the reason for the strongly anharmonic behavior of the acoustically-driven oscillations of the magnetization.

3.10 Conclusions

We showed a novel scenario to trigger a magnetic mode using optically generated standing sound waves. This mode is characterized by a large amplitude and a very small damping and the efficiency of the excitation is high enough to push the spin dynamics into an anharmonic regime. Despite the relatively low frequencies of the observed lattice-driven magnetic mode in $FeBO_3$, such excitation can be effectively used for the coherent control of magnetization [51, 52], because the expected lifetimes of such coupled modes can last up to microseconds [20, 53, 54]. Also we would like to note that the observed amplitudes of the lattice-mediated oscillations of the spins are as large as 5^o. This is only a factor of two smaller than those required for the novel mechanism of magnetic switching, theoretically suggested in Ref. [16]. Our work, however, reveals that achieving higher magnetization deviation amplitudes is hampered by the anharmonicity of the magneto-acoustic excitation.

References

[1] A. Kirilyuk, A. V. Kimel, and T. Rasing, "Ultrafast optical manipulation of magnetic order," *Rev. Mod. Phys.*, vol. 82, pp. 2731–2784, Sep 2010.

[2] J. Stöhr and H. C. Siegmann, "Magnetism," *Solid-State Sciences. Springer, Berlin, Heidelberg*, p. 5, 2006.

[3] I. Žutić, J. Fabian, and S. Das Sarma, "Spintronics: Fundamentals and applications," *Rev. Mod. Phys.*, vol. 76, pp. 323–410, Apr 2004.

[4] V. V. Kruglyak, S. O. Demokritov, and D. Grundler, "Magnonics," *Journal of Physics D: Applied Physics*, vol. 43, no. 26, p. 260301, 2010.

[5] E. Beaurepaire, J.-C. Merle, A. Daunois, and J.-Y. Bigot, "Ultrafast spin dynamics in ferromagnetic Nickel," *Phys. Rev. Lett.*, vol. 76, pp. 4250–4253, May 1996.

[6] J. Wang, C. Sun, J. Kono, A. Oiwa, H. Munekata, L. Cywiński, and L. J. Sham, "Ultrafast quenching of ferromagnetism in inmnas induced by intense laser irradiation," *Phys. Rev. Lett.*, vol. 95, p. 167401, Oct 2005.

[7] C. D. Stanciu, F. Hansteen, A. V. Kimel, A. Kirilyuk, A. Tsukamoto, A. Itoh, and T. Rasing, "All-optical magnetic recording with circularly polarized light," *Phys. Rev. Lett.*, vol. 99, p. 047601, Jul 2007.

[8] K. Vahaplar, A. M. Kalashnikova, A. V. Kimel, D. Hinzke, U. Nowak, R. Chantrell, A. Tsukamoto, A. Itoh, A. Kirilyuk, and T. Rasing, "Ultrafast path for optical magnetization reversal via a strongly nonequilibrium state," *Phys. Rev. Lett.*, vol. 103, p. 117201, Sep 2009.

[9] A. V. Kimel, A. Kirilyuk, P. A. Usachev, R. V. Pisarev, A. M. Balbashov, and T. Rasing, "Ultrafast non-thermal control of magnetization by instantaneous photomagnetic pulses," *Nature*, vol. 435, pp. 655–657, June 2005.

[10] F. Hansteen, A. Kimel, A. Kirilyuk, and T. Rasing, "Femtosecond photomagnetic switching of spins in ferrimagnetic garnet films," *Phys. Rev. Lett.*, vol. 95, p. 047402, Jul 2005.

[11] T. Kampfrath, A. Sell, G. Klatt, A. Pashkin, S. Mahrlein, T. Dekorsy, M. Wolf, M. Fiebig, A. Leitenstorfer, and R. Huber, "Coherent terahertz control of antiferromagnetic spin waves," *Nat Photon*, vol. 5, pp. 31–34, Jan. 2011.

[12] A. V. Scherbakov, A. S. Salasyuk, A. V. Akimov, X. Liu, M. Bombeck, C. Brüggemann, D. R. Yakovlev, V. F. Sapega, J. K. Furdyna, and M. Bayer, "Coherent magnetization precession in ferromagnetic (Ga,Mn)As induced by picosecond acoustic pulses," *Phys. Rev. Lett.*, vol. 105, p. 117204, Sep 2010.

[13] J.-W. Kim, M. Vomir, and J.-Y. Bigot, "Ultrafast magnetoacoustics in nickel films," *Phys. Rev. Lett.*, vol. 109, p. 166601, Oct 2012.

[14] J. V. Jger, A. V. Scherbakov, T. L. Linnik, D. R. Yakovlev, M. Wang, P. Wadley, V. Holy, S. A. Cavill, A. V. Akimov, A. W. Rushforth, and M. Bayer, "Picosecond inverse magnetostriction in galfenol thin films," *Applied Physics Letters*, vol. 103, no. 3, pp. –, 2013.

[15] A. Melnikov, I. Radu, U. Bovensiepen, O. Krupin, K. Starke, E. Matthias, and M. Wolf, "Coherent optical phonons and parametrically coupled magnons induced by femtosecond laser excitation of the Gd(0001) surface," *Phys. Rev. Lett.*, vol. 91, p. 227403, Nov 2003.

[16] O. Kovalenko, T. Pezeril, and V. V. Temnov, "New concept for magnetization switching by ultrafast acoustic pulses," *Phys. Rev. Lett.*, vol. 110, p. 266602, Jun 2013.

[17] L. Tsymbal, "Features of acoustic properties of $ErFe0_3$ in second-order phase transitions," *Zh. Eksp. Teor. Fiz*, vol. 102, p. 974, 1992.

[18] H. T. Grahn, H. J. Maris, and J. Tauc, "Picosecond ultrasonics," *IEEE Journal of Quantum Electronics*, vol. 25, pp. 2562–2569, 1989.

[19] E. A. Turov and V. G. Shavrov, "Broken symmetry and magnetoacoustic effects in ferroand antiferromagnetics," *Soviet Physics Uspekhi*, vol. 26, no. 7, p. 593, 1983.

[20] B. Y. Kotyuzhanskii, L. Prozorova, and L. Svistov, "Relaxation of magnetoelastic waves in antiferromagnetic $FeBO_3$," *Zh. Eksp. Teor. Fiz*, vol. 84, pp. 1574–1579, 1983.

[21] M. Bombeck, A. S. Salasyuk, B. A. Glavin, A. V. Scherbakov, C. Brüggemann, D. R. Yakovlev, V. F. Sapega, X. Liu, J. K. Furdyna, A. V. Akimov, and M. Bayer, "Excitation of spin waves in ferromagnetic (Ga,Mn)As layers by picosecond strain pulses," *Phys. Rev. B*, vol. 85, p. 195324, May 2012.

[22] F. Hudert, A. Bruchhausen, D. Issenmann, O. Schecker, R. Waitz, A. Erbe, E. Scheer, T. Dekorsy, A. Mlayah, and J.-R. Huntzinger, "Confined longitudinal acoustic phonon modes in free-standing Si membranes coherently excited by femtosecond laser pulses," *Phys. Rev. B*, vol. 79, p. 201307, May 2009.

[23] S. Ge, X. Liu, X. Qiao, Q. Wang, Z. Xu, J. Qiu, P.-H. Tan, J. Zhao, and D. Sun, "Coherent longitudinal acoustic phonon approaching THz frequency in multilayer molybdenum disulphide," *Sci. Rep.*, vol. 4, pp. –, July 2014.

[24] J. Januonis, C. L. Chang, P. H. M. van Loosdrecht, and R. I. Tobey, "Frequency tunable surface magneto elastic waves," *Applied Physics Letters*, vol. 106, no. 18, pp. –, 2015.

[25] A. Kurtzig, R. Wolfe, R. LeCraw, and J. Nielsen, "Magneto-optical properties of green room temperature ferromagnet: $FeBO_3$," *Applied Physics Letters*, vol. 14, no. 11, pp. 350–352, 1969.

[26] R. Diehl, "Crystal structure refinement of ferric borate, $FeBO_3$," *Solid state communications*, vol. 17, no. 6, pp. 743–745, 1975.

[27] E. A. Turov, A. Tybulewicz, and S. Chomet, *Physical properties of magnetically ordered crystals*. Academic Press, 1965.

[28] V. E. Dmitrienko, E. N. Ovchinnikova, S. P. Collins, G. Nisbet, G. Beutier, Y. O. Kvashnin, V. V. Mazurenko, A. I. Lichtenstein, and M. I. Katsnelson, "Measuring the dzyaloshinskii-moriya interaction in a weak ferromagnet," *Nat Phys*, vol. 10, pp. 202–206, Mar. 2014.

[29] W. Wettling, W. Jantz, and H. Dtsch, "Magnetically tunable sound velocity in iron borate," *Applied physics*, vol. 23, no. 2, pp. 195–198, 1980.

[30] V. Doroshev, I. Krygin, S. Lukin, A. Molchanov, A. Prokhorov, V. Rudenko, and V. Seleznev, "Basal magnetic anisotropy of a weak ferromagnetic $FeBO_3$ crystal," *ZhETF Pisma Redaktsiiu*, vol. 29, p. 286, 1979.

[31] M. Seavey, "Observation of light-induced anisotropy in ferric borate by acoustic resonance," *Solid State Communications*, vol. 12, no. 1, pp. 49 – 52, 1973.

[32] B. Sokolov, "Effect of nonuniform mechanical stresses on the domain structure of iron borate," *Physics of the Solid State*, vol. 47, no. 9, pp. 1707–1713, 2005.

[33] M. Strugatsky and K. Skibinsky, "Hydrostatic pressure and hexagonal magnetic anisotropy of hematite," *Physics of the Solid State*, vol. 51, no. 6, pp. 1172–1175, 2009.

[34] D. E. Lacklison, J. Chadwick, and J. L. Page, "Photomagnetic effect in ferric borate," *Journal of Physics D: Applied Physics*, vol. 5, no. 4, p. 810, 1972.

[35] M. Borovets, A. Garmonov, S. Rudov, and Y. M. Fedorov, "Photomagnetization of iron borate," *JETP Lett*, vol. 50, no. 10, 1989.

[36] W. P. Mason, *Physical acoustics*. Elsevier Science, 2013.

[37] W. Jantz, W. Wettling, and J. R. Sandercock, "Determination of magnetic and elastic properties of $FeBO_3$ by light scattering," *Journal of Physics C: Solid State Physics*, vol. 9, no. 11, p. 2229, 1976.

[38] M. Strugatsky and K. Skibinsky, "Theory of birefringence of sound in easy-plane rhombohedral antiferromagnets with inclusion of hexagonal anisotropy and mechanical stresses," *Physics of the Solid State*, vol. 52, no. 6, pp. 1204–1209, 2010.

[39] W. Wettling, W. Jantz, and C. E. Patton, "Light scattering study of phonons parametrically excited in the weak ferromagnet $FeBO_3$," *Journal of Applied Physics*, vol. 50, no. B3, pp. 2030–2032, 1979.

[40] B. Andlauer, J. Schneider, and W. Wettling, "Optical and magneto-optical properties of *yig* and $FeBO_3$," *Applied physics*, vol. 10, no. 3, pp. 189–201, 1976.

[41] S. Ovchinnikov and V. Zabluda, "The energy band structure and optical spectra of $FeBO_3$ calculated with allowance for strong electron correlations," *Journal of Experimental and Theoretical Physics*, vol. 98, no. 1, pp. 135–143, 2004.

[42] A. J. Kurtzig, "Faraday rotation in birefringent crystals," *Journal of Applied Physics*, vol. 42, no. 9, pp. 3494–3498, 1971.

[43] M. Strugatsky, S. Yagupov, and A. Y. Khrenov, "FeBO3:Ni monocrystals: photoinduced magnetic effects and synthesis," in *Fifth International Conference on Correlation Optics*, pp. 365–367, International Society for Optics and Photonics, 2002.

[44] A. M. Kalashnikova, A. V. Kimel, R. V. Pisarev, V. N. Gridnev, A. Kirilyuk, and T. Rasing, "Impulsive generation of coherent magnons by linearly polarized light in the easy-plane antiferromagnet $FeBO_3$," *Phys. Rev. Lett.*, vol. 99, p. 167205, Oct 2007.

[45] B. A. Ivanov, "Spin dynamics of antiferromagnets under action of femtosecond laser pulses," *Low Temperature Physics*, vol. 40, no. 2, pp. 91–105, 2014.

[46] Y. Shen, "Electrostriction, optical kerr effect and self-focusing of laser beams," *Physics Letters*, vol. 20, no. 4, pp. 378 – 380, 1966.

[47] Y.-X. Yan and K. A. Nelson, "Impulsive stimulated light scattering. i. general theory," *The Journal of Chemical Physics*, vol. 87, no. 11, pp. 6240–6256, 1987.

[48] A. Kobyakov, M. Sauer, and D. Chowdhury, "Stimulated brillouin scattering in optical fibers," *Adv. Opt. Photon.*, vol. 2, pp. 1–59, Mar 2010.

[49] D. Sander, "The correlation between mechanical stress and magnetic anisotropy in ultrathin films," *Reports on Progress in Physics*, vol. 62, no. 5, p. 809, 1999.

[50] Y. N. Mitsay, K. Skibinsky, M. Strugatsky, A. Korolyuk, V. Tarakanov, and V. Khizhnyi, "Gakel-turov oscillations in iron borate," *Journal of magnetism and magnetic materials*, vol. 219, no. 3, pp. 340–348, 2000.

[51] E. Carpene, C. Piovera, C. Dallera, E. Mancini, and E. Puppin, "All-optical subnanosecond coherent spin switching in thin ferromagnetic layers," *Phys. Rev. B*, vol. 84, p. 134425, Oct 2011.

[52] E. Rozkotova, P. Nemec, N. Tesarova, P. Maly, V. Novak, K. Olejnik, M. Cukr, and T. Jungwirth, "Coherent control of magnetization precession in ferromagnetic semiconductor $(ga, mn)as$," *Applied Physics Letters*, vol. 93, no. 23, pp. –, 2008.

[53] L. E. Svistov, V. L. Safonov, J. Low, and H. Benner, "Detection of uhf sound in the antiferromagnet $FeBO_3$ by a SQUID magnetometer," *Journal of Physics: Condensed Matter*, vol. 6, no. 39, p. 8051, 1994.

[54] V. Lutovinov, V. Preobrazhenskii, and S. Semin, "Damping of sound in antiferromagnets of the easy-plane type with a high Néel temperature," *Soviet Journal of Experimental and Theoretical Physics*, vol. 47, p. 609, 1978.

Chapter 4

Imaging and all-optical control of the ultrafast photo-Induced magnetization across the Morin transition in $DyFeO_3$

Magnetic phase transitions imply substantial changes of the magnetic structure. For this reason one can expect magnetization dynamics emerging during magnetic phase transformations to be essentially non-linear. Here we show that the excitation of antiferromagnetic iron oxide $DyFeO_3$ with a single 60 fs laser pulse triggers a transition across the Morin point by pushing the antiferromagnet from a collinear to a non-collinear spin state and inducing a net magnetization. Time-resolved imaging reveals that the pulse first excites antiferromagnetic spin precession. Upon the damping of the precession, the non-collinear spin state with net magnetization emerges. The direction of the photo-induced net magnetization is defined by the pump polarization and the direction of the antiferromagnetic vector in the initial collinear spin state.[1]

4.1 Introduction

Photoinduced phase transitions and their dynamics triggered by femtosecond laser pulses is a subject of intense and multidisciplinary research in contemporary science [1–4]. In magnetism this is an especially intriguing problem since understanding the kinetics of phase transitions is crucial for achieving the fastest possible magnetic recording and information processing.

[1]The chapter is adapted from: D. Afanasiev, B. Ivanov, A. Kirilyuk,T. Rasing, R.V. Pisarev and A. V. Kimel,"Imaging and All-Optical Control of the Photo-Induced Magnetization Across the Ultrafast Morin Transition in $DyFeO_3$" submitted

Up to date three main experimental approaches are being pursued to initiate ultrafast changes in the magnetic state of matter. In the first and the most frequently used one, femtosecond laser pulses destroy the spin order and quench the net magnetization in magnetic media, causing an order-disorder phase transition [5–7]. In the second, femtosecond laser pulses are employed to trigger the reorientation or even reversal of the net magnetization, promoting an order-order phase transition [8–11]. In the third the ultrafast laser excitation causes another type of order-order phase transition accompanied by the emergence a the net magnetization [12–16]. These processes are rather intriguing from a fundamental point of view, because ultrafast changes of the magnetic structure are linked to a transfer of momentum related to the initial phase. Identification of the channels of angular momentum transfer on ultrafast timescales may pave the way to novel ultrafast mechanisms of magnetization manipulation [17].

From the beginning of ultrafast magnetism, the ability to visualize magnetic dynamics in the laser excited area with femtosecond temporal resolution has been believed to be crucial for understanding the physics of the photo-induced processes. Studies of ultrafast demagnetization [18] , magnetization reorientation [10] and magnetization reversal [19], [20], [21] with both spatial and femtosecond temporal resolution allowed to substantially advance the understanding of the kinetics of the laser-induced magnetic changes. In particular, all-optical helicity dependent magnetization reversal via a strongly non-equilibrium state with no net magnetization as well as magnetization reorientation in a direction controlled by the polarization of light via low-amplitude spin precession, has thus been discovered. Visualization of the ultrafast dynamics of the emerging laser-induced magnetization as a magnetic phase transition is an intriguing phenomenon which has not been addressed until now.

In this Chapter, we address this issue by triggering a magnetic phase transition from a collinear to non-collinear antiferromagnetic state in $DyFeO_3$ with a 60 femtosecond polarized laser pulse and imaging the emerging photo-induced magnetization phase transition with femtosecond temporal resolution. It is shown that the emergence of the magnetization proceeds via a depletion of the collinear antiferromagnetic phase and that the initial orientation of its antiferromagnetic vector plays decisive role in defining the direction of the photo-induced magnetization. Despite the long emergence time of 20 ps, the direction of the photoinduced magnetization depends on both the direction of the external magnetic field and the polarization of the laser pulse so that for fields below 0.4 kOe a finite magnetization fraction can be aligned even against the external magnetic field.

4.2 The Morin transition

The Morin transition is a generic name for the spontaneous magnetic phase transition from the antiferromangnetic to the weak ferromagnetic state. It was first observed in hematite (α-Fe_2O_3) at 250 K [22]. Two other families of materials to demonstrate the Morin transition are orthochromites (e.g. $ErCrO_3$, $La_{0.9}Bi_{0.1}CrO_3$ [23]) and orthoferrites (e.g. $DyFeO_3$, $DyFe_{1-x}Co_xO_3$, $Ho_{0.5}Dy_{0.5}FeO_3$ and $YFe_{1-x}Mn_xO_3$). The Morin transition is a consequence of the spontaneous or field-induced spin-reorientation tran-

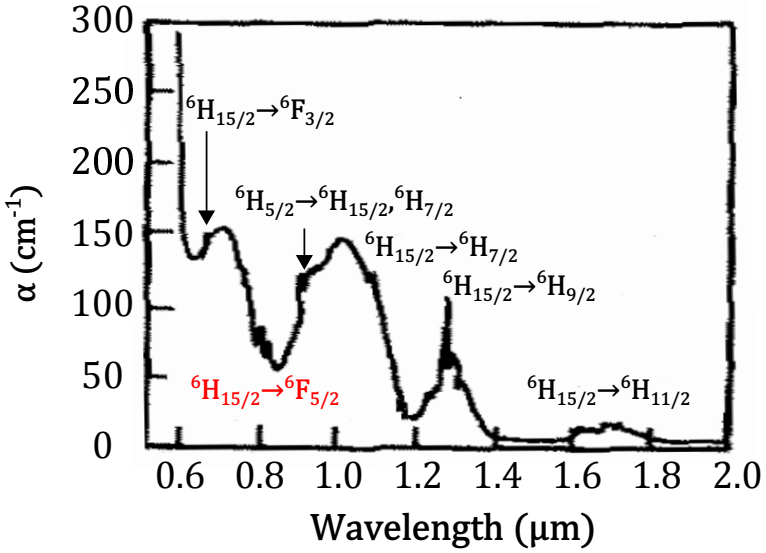

Figure 4.1: Absorption spectrum of $DyFeO_3$. Rare earth $4f - f$ transitions identified by ${}^{2S+1}L_J$ parent terms. The image is taken from Ref. [25]. A rare-earth transition at 0.8 μm, marked with red, reveals a absorption line which matches wavelength of the pump laser.

sition which is accompanied by a magnetic symmetry change from a magnetic configuration where the Dzyaloshinskii-Moria interaction is forbidden to one where it is permitted.

4.3 Crystallographic and Optical properties of $DyFeO_3$

For magneto-optical studies hematite, which is transparent for wavelengths only above 1.3 μm, is not convenient. The orthoferrites, highly transparent in the visible and near infrared, are much more convenient choice. Among them dysprosium orthoferrite is the only one undoped orthoferrite, which demonstrates the Morin transition.

The orthoferrites $RFeO_3$, where R is used to denote a rare-earth element, crystallize in an orthorhombically distorted perovskite structure with a space-group symmetry D_{2h}^{16}. All Fe^{3+} ions are crystallographically equivalent and have an octahedral oxygen environment. A change in R leads to a orthorhombic distortion, which almost does not affect the oxygen octahedron around the iron ions but tilts the octahedron axis off the z axis. Hence, it changes the Fe-O-Fe valence bond angle [24]. The mean values of the Fe-O and O-O interatomic distances are practically constant for the whole $RFeO_3$ rare-earth series and are 2.011 and 2.844 $\mathring{A}$, respectively. The deviation from the cubic symmetry grows as the R^{3+} ion radius decreases (a chemical compression), so that this deviation is minimal in $LaFeO_3$ and maximal in $LuFeO_3$.

As a consequence, the optical spectrum of $DyFeO_3$ as well as other orthoferrites is dominated by the interactions of the Fe^{3+} ion with its octahedral environment. Two

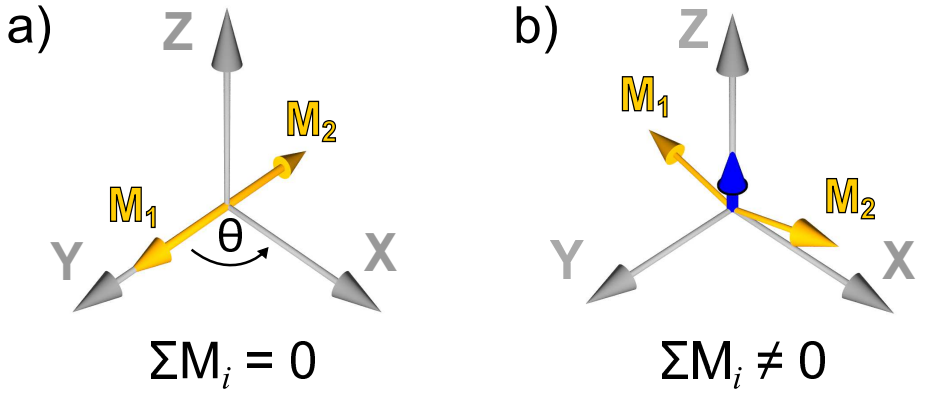

Figure 4.2: (a) Magnetic ground state of $DyFeO_3$ in the low-temperature phase ($T<T_M$) Γ_1. (b) Magnetic ground state of $DyFeO_3$ in the high-temperature phase ($T>T_M$) Γ_4.

broad bands in the visible spectral range for wavelengths near 1.0 μm and 0.7 μm are clearly seen in Figure 4.1a. They originate from the parity forbidden $d-d$ transitions inside the Fe^{3+} multiplet. Due to the crystal field this prohibition becomes partially lifted. In particular, the crystal-field transitions ${}^6A_1 \rightarrow {}^4T_1$ and ${}^6A_1 \rightarrow {}^4T_2$ of Fe^{3+} from high-spin ($S = 5/2$) to low-spin ($S = 3/2$) configurations become allowed. The most striking feature of the spectrum is the strong absorption at wavelengths below 600 nm. Fe^{3+} ion normally does not show such strong absorption in the visible spectral range and it is generally believed that charge-transfer transitions between iron and ligand ions are responsible for this intense absorption. These transitions are allowed in the electric-dipole approximation and for this reasons very intense and result in high absorption.

The rare-earth ions contribute to the optical spectrum as a series of sharp absorption peaks which appear on top of the $d-d$ bands. These peaks originate from the transitions inside of the Dy^{3+} ground multiplet between states with different full quantum number J [25]. The Dy^{3+} ions have 9 electrons (odd ion) in the outer shell and for this reason they are Kramers ions. This means that according to the Kramers theorem, splitting of the multiplets is not complete even in a crystal field of the lowest symmetry. Thus, the ground state is a degenerate doublet. The degeneracy can be lifted only by applying a magnetic field which breaks time-reversal symmetry. However, the doublets of Dy^{3+} in $DyFeO_3$ appear to be splitted by the exchange field of Fe^{3+}. Interestingly, the wavelength of 800 nm of the amplified Ti:Sapphire laser system, commonly used in ultrafast experiment, perfectly matches the absorption line ${}^6H_{15/2} \rightarrow {}^6F_{5/2}$ [26].

4.4 The spin-reorientation Morin transition in $DyFeO_3$

The magnetic subsystem of $DyFeO_3$ above 4 K and below the Neel point ($T_N = 645$ K) consists of antiferromagnetically coupled Fe^{3+} sublattices and paramagnetic Dy^{3+}

ions partly magnetized in the exchange field of the iron ions [27]. The Dy^{3+} spins order only at temperatures below 4 K. Contrary to other orthoferrites, where at low temperatures the spins of iron are oriented along the x axis, the spins in $DyFeO_3$ favor to be oriented along the y axis. In the vicinity of the Morin temperature ($T_M \cong 40K$) the Fe^{3+} spins reorient from the low-temperature antiferromagnetic Γ_1 configuration, with magnetic moments along the y axis, to the high-temperature Γ_4 phase with magnetic moments along the x axis [28–30] (see Fig. 4.2). This transition is accompanied by a magnetic symmetry change $mmm \rightarrow \underline{mm}m$. The Dzyaloshinskii-Moria interaction is forbidden by symmetry for spins directed along the y axis. As a result the antiferromagnetic vector in this phase $\mathbf{L}=\mathbf{M}_1\text{-}\mathbf{M}_2$ is aligned along the y axis and a net magnetization is absent: $\mathbf{M}=\mathbf{M}_1+\mathbf{M}_2=0$. The Γ_1 phase is characterized by two metastable states corresponding to two mutually antiparallel orientations of the antiferromagnetic vector $\mathbf{L}$. Without external stimuli the states are degenerate and the crystal splits in 180^o antiferromagnetic domains. Above T_M the spins are in the Γ_4 antiferromagnetic phase. The magnetic moments of the sublattices and the antiferromagnetic vector $\mathbf{L}$ get aligned along the x axis. Moreover, in this configuration the Dzyaloshinskii−Moriya interaction is not forbidden by symmetry and the spins of the two sublattices acquire a canting over an angle of about 0.5^o, giving rise to a small spontaneous magnetization $\mathbf{M}=\mathbf{M}_1 + \mathbf{M}_2 \neq 0$ along the z axis. Without application of any magnetic field the crystal splits into two types of domains with the magnetization parallel and antiparallel with respect to the z axis, respectively.

4.4.1 Thermodynamical potential

A phenomenological potential can be written to describe the Morin transition in $DyFeO_3$ [31]:

$$\Phi = \frac{1}{2}\mathcal{J}M^2 + D_y\left(L_xM_y - M_xL_y\right) + \Phi_a\left(\mathrm{T}\right) - \mathbf{M}\cdot\mathbf{H} \tag{4.1}$$

It is seen that the Dzyaloshinskii vector $\mathbf{D}=(0, D_y, 0)$ is oriented along the y axis. For this reason the net magnetization is zero in the state with spins oriented along the y direction. $\Phi_a\left(\mathrm{T}\right)$ is a temperature dependent anisotropy potential, which accounts for the spin-reorientation transition.

The expression for the uniaxial magnetic anisotropy Φ_a can be written as a power series of L_y^2:

$$\Phi_a\left(T\right) = \frac{1}{2}K_2\left(\mathrm{T}\right)L_y^2 + \frac{1}{4}K_4L_y^4, \tag{4.2}$$

where K_2 and K_4 are phenomenological parameters which describe the magnetic anisotropy. The positive sign of K_2 favors spins to be oriented along the $x-$axis. If K_2 is negative, the spins get oriented along the y direction. Thus a spontaneous spin-orientation transition can be described by a temperature dependent anisotropy $K_2(\mathrm{T})$. At the temperature T_M where K_2 changes sign the Morin transition occurs. The temperature evolution of the anisotropy parameter K_2 can be described in the simplest possible form as:

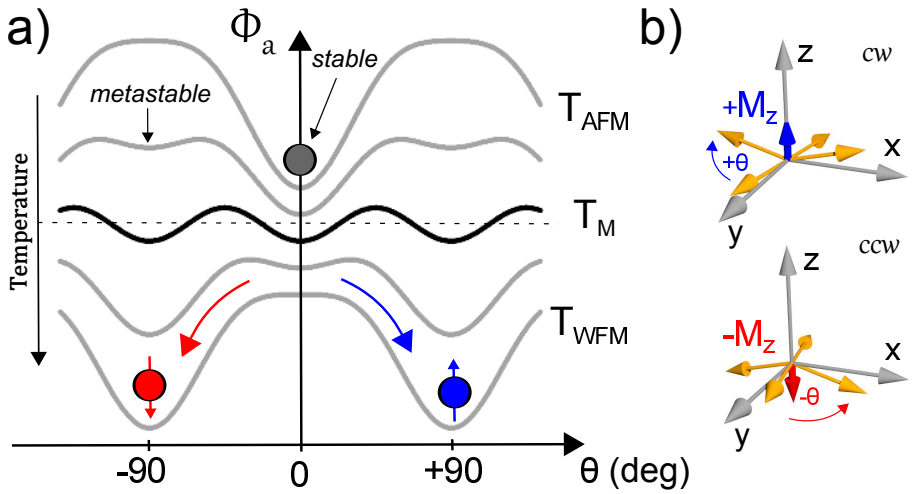

Figure 4.3: (a) Schematics showing evolution of the magnetic anisotropy profile in the vicinity of the spin-reorientational Morin transition. b) Sketch of the clockwise (*cw*) and counter clockwise (*ccw*) spin rotation leading to the net magnetization "up" and "down", respectively.

$$K_2(\mathrm{T}) = K_2(0) \cdot \left(1 - \frac{\mathrm{T}}{\mathrm{T_M}}\right), \tag{4.3}$$

where $K_2(0)$ is the anisotropy parameter at T=0 K.

To specify the crystallographic plane in which the spins rotate, higher orders of the antiferromagnetic vector L_y^2 have to be taken into account. The Morin transition can be fully parametrized with a single magnetic order parameter θ, which is the azimuthal angle between the spins and the y axis. The angle-dependent energy of the magnetic anisotropy can be rewritten in terms of θ:

$$\Phi_a(\theta) = k_2(T)\cos 2\theta + k_4 \cos 4\theta \tag{4.4}$$

The normalized anisotropy parameters k_2 and k_4 have the same sense as K_2 and K_4.

If k_4 <0, this describes a first-order phase transition. The temperature evolution of the anisotropic potential is shown in Figure 4.3a. The clockwise (*cw*) or counter clockwise (*ccw*) spin rotation results in the net magnetization emergence directed "up" or "down", respectively. The simultaneous presence of the stable and metastable states is typical for a first-order phase transition. This coexistence is also the reason for the temperature hysteresis.

4.4.2 Visual observation of the spontaneous Morin transition in z cut $DyFeO_3$

To study the Morin phase transition magneto-optically we have chosen a crystal cut perpendicularly to the z crystallographic axis ($z-DyFeO_3$). In this case the magnetization appears perpendicularly to the plane and thus it can be directly detected with the help of the Faraday rotation.

To visualize the transition we used linearly polarized light at the wavelength of 630 nm. The intensity contrast for magnetic structures was obtained with the help of nearly crossed polarizer and analyser.

At room temperature ferromagnetic domains can be easily visualized. The contrast between the magnetic domains with the opposite magnetizations is achieved due to contributions to the antisymmetric part of the dielectric permittivity proportional to the net magnetization M_z [32]. The sign of this contribution is defined by the sign of the weak magnetic moment. This leads to different magnetic circular birefringence in different domains so that the black and the white areas correspond to the domains in which the magnetization points "up" and "down", respectively. The domains have labyrinth like structure. Upon cooling the sample, the Morin transition was observed in the vicinity of 39 K. It was accompanied by an sudden disappearance of the labyrinth domain structure (see Fig. 4.4). Below T_M the spins get aligned along the y axis and the net magnetic moment disappears (Γ_1 phase). It is known that without external stimuli the states corresponding to the two mutually antiparallel orientations of the antiferromagnetic vector $\mathbf{L}$ in the Γ_1 phase are degenerate and the crystal splits into 180^o antiferromagnetic domains. A typical pattern of dark-grey and light-grey laminate structures which represents the 180^o antiferromagnetic domains is shown in Figure 4.4a. The contrast between the domains in dysprosium orthoferrite can be achieved due to contributions to the symmetric part of the dielectric permittivity tensor, proportional to the product of the antiferromagnetic vector and applied mechanical deformations via the so-called linear magneto-optical effect [33]. In our experiments the antiferromagnetic domains were visualized due to the stress applied in the [110] crystallographic direction.

Remarkably, despite what is commonly expected for first-order phase transitions, the Morin transition in $DyFeO_3$ does not show any pronounced temperature hysteresis. In Ref. [34] it has been suggested that the domain walls in the high (low) temperature phase play the role of the nuclei of the low (high) temperature phase. In this case the temperature hysteresis becomes very narrow. However, visualization of the phase transitions in our experiment does not confirm this mechanism. The hysteresis-free character of the transition can be explained by high sensitivity of the spin-reorientation transition to stress and magnetic field. These factors can lead to an easy nucleation of the metastable new magnetic phases as a result of fluctuations.

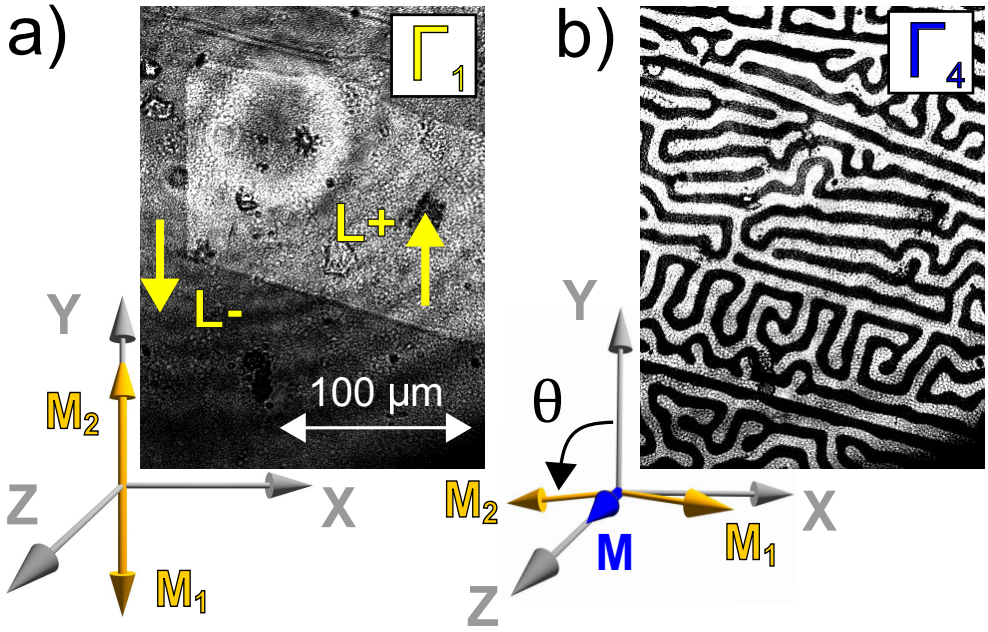

Figure 4.4: (a) Magneto-optical images of the antiferromagnetic domains in the low-temperature Γ_1 phase of $z-DyFeO_3$. The magnetic contrast represented by light-grey and dark-grey areas originating from antiferromagnetic domains with antiferromagnetic vector **L** oriented parallel (L+) or antiparallel (L-) with respect to the y axis.The bias temperature of the sample is 20 K. (b) Magneto-optical image of the magnetic domain pattern in the high-temperature Γ_4 phase. The magnetic contrast represented by black and white areas originating from areas with magnetizations parallel ($-M_z$) or antiparallel ($+M_z$) with respect to the z-axis. The bias temperature of the sample is 50 K.

4.5 Excitation and spatial-temporal imaging of the ultrafast photo-induced Morin transition

To study the dynamics of single pulse laser induced magnetization in $DyFeO_3$ across the Morin point we employed the technique of single shot imaging. The sample, initially set to the Γ_1 phase, was excited with the help of 60 fs pulse with the central wavelength of 800 nm. At the chosen wavelength the material is quite transparent having an absorption coefficient of 80 cm^{-1} [25]. The pump pulse is at the normal incidence and had a Gaussian spatial profile being focused into a spot with the full width half maximum of 40 μm. The magnetization dynamics was monitored with a help of much less intense linearly polarized and slightly broader temporally probe pulse at the wavelength of 630 nm. In order to minimize cumulative DC heating, we reduced the average power of the pump beam by decreasing the repetition rate down to 2 Hz. Although the repetition rate of the probe pulse was at 1 kHz, the CCD camera detecting the probe was synchronized with the pump. The exposition rate of the camera was set to 1 ms and thus guaranteed that the detected laser-induced changes are caused by a single pump pulse.

4.5.1 Photo-induced magnetization in the Γ_1 phase. The case $z-$cut $DyFeO_3$

The excitation of the $z-DyFeO_3$ crystal at T=20 K with a single pump pulse indeed initiates magnetic changes (Fig. 4.5). It is seen that pumping the dark-grey antiferromagnetic domains in which the vector $\mathbf{L}$ is parallel to the y axis produces a black domain while pumping the light-grey antiferromagnetic domain in which $\mathbf{L}$ is opposite, produces a white domain. Pumping such that the domain wall is in the middle of the spot produces two domains depending on the orientation of $\mathbf{L}$. The photo-induced domains are present up to 3 ns but disappear earlier than 1 ms after the excitation. The lifetime is likely defined by the cooling of the laser heated area. The color of the photo-induced domains does not depend on the orientation of the linear polarization of the probe, confirming that the contrast between the domains is due to the Faraday effect. It means that the photo-induced black and white areas must be assigned to domains with the photo-induced magnetization "up" and "down", respectively. The photo-induced domains disappear when the bias temperature of the sample crosses T_M. Hence, this experiment reveals that the photo-induced magnetization is indeed due to the crossing of the Morin transition and the direction of the photo-induced magnetization is defined by the orientation of the antiferromagnetic vector in the initial state.

We performed measurements of the photo-induced magnetization as a function of the incoming pump polarization. Figure 4.6a shows such a dependence. It is clearly seen that the linear pump polarization only slightly affects the photoinduced domains. Integration of the intensity detected by the camera in a 10×10 μm area gives a measure of the total magnetization in the spot. We plotted the result of the integration as a function of the angle between the linear polarization of the pump and the $y-$axis in Fig. 4.6b. The periodic dependence with two distinct periods equal to π and $\frac{\pi}{2}$ is noticeable. It is worth to note, that although the periodicity of the modulation is

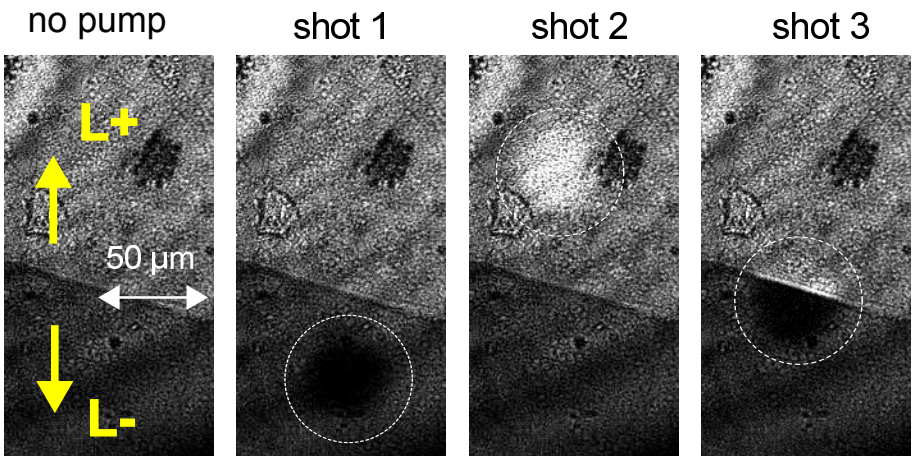

Figure 4.5: Images of the domains in $z-DyFeO_3$ taken 100 ps after excitation with a single 60 fs pump pulse. Areas imposed to the pulsed excitation are marked by a dashed line. "no pump" shows the image taken before the pump excited the sample and represents the local arrangement of the antiferromagnetic domains. "shot 1" forms a black domain having magnetization $-M_z$ in the dark-grey area. "shot 2" forms a white domain with the magnetization $+M_z$ in the light-grey area. "shot 3" affects both antiferromagnetic domains and induces a magnetization, the sign of which is defined by the direction of **L**.

present, the photoinduced magnetization does not change "color" during this cycle. The direction of the photoinduced magnetization remains insensitive to the helicity of circularly polarized pump pulse.

4.5.2 Temporal emergence of the photo-induced magnetization

To further understand the dynamics of the photo-induced magnetization we performed time-resolved measurements as a function of the pump-probe delay (see Fig. 4.7). Note that on top of the magneto-optical Faraday effect, which is linear with respect to the photo-induced magnetization, the images are affected by photo-induced and magnetization independent changes in the transmission of the sample [7]. The changes are especially intense in the first 20 ps. Nonetheless, the emergence and the growth of the induced magnetization and thus the high-temperature Γ_4 phase is clearly seen.

Taking a cross section along the spot diameter we obtained a two-dimensional picture showing the dynamics of the photo-induced magnetization across the laser excited area. Figure 4.8b demonstrates such dynamics for several pump fluences. It reveals two pump-induced effects. The pump pulse excites oscillations and generates magnetization. The color scheme represents the measured values of the magneto-optical signal. Regarding the Gaussian spatial distribution of the laser intensity (see inset in the left upper corner of Fig. 4.8), the obtained two-dimensional images, in fact, reveal how the dynamics depends on the fluence of the laser excitation. It is seen that the photo-induced magnetization emerges only in the areas where the fluence is

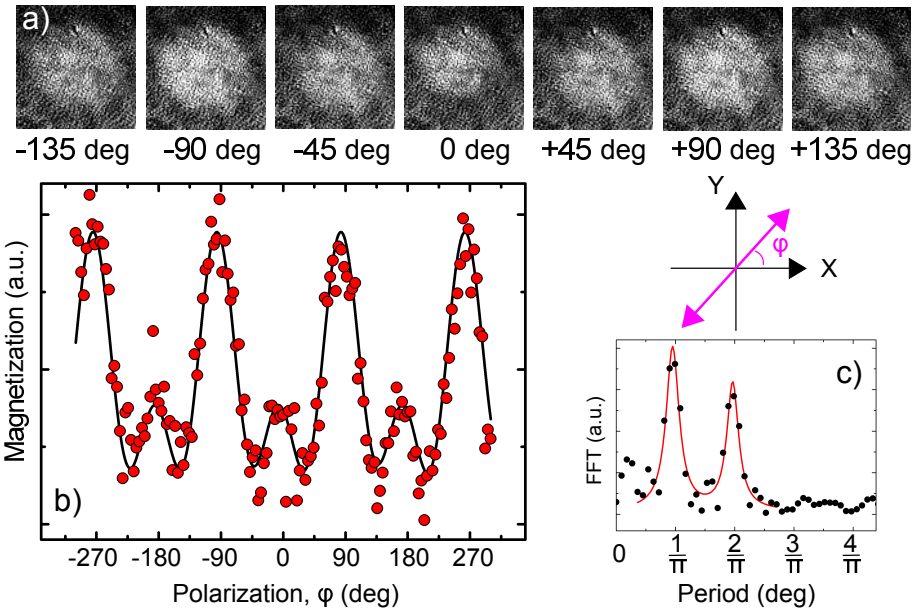

Figure 4.6: (a) Magneto-optical images of the photo-induced magnetization as a function of the incoming pump polarization. (b) Integrated intensity over the 10×10 rectangular in the center of the photo-induced domain plotted as a function of pump polarization orientation. (c) The Fourier transform of the polarization dependence shown in panel.

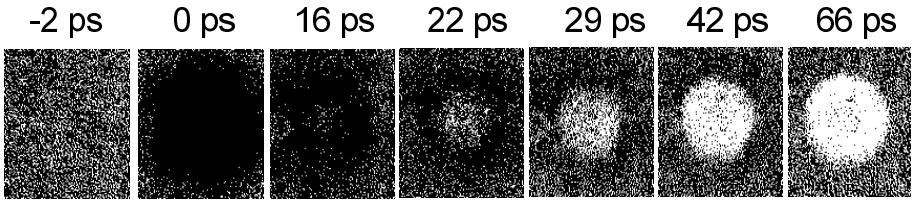

Figure 4.7: Time-resolved magneto-optical images of the photo-induced dynamics in $z-$cut of $DyFeO_3$. To emphasize the pump-induced effect, we subtracted from an original image, obtained at a given delay, the image of the same area at negative delay. The bias temperature is set to 20 K. The dynamics are recorded with no external field presence.

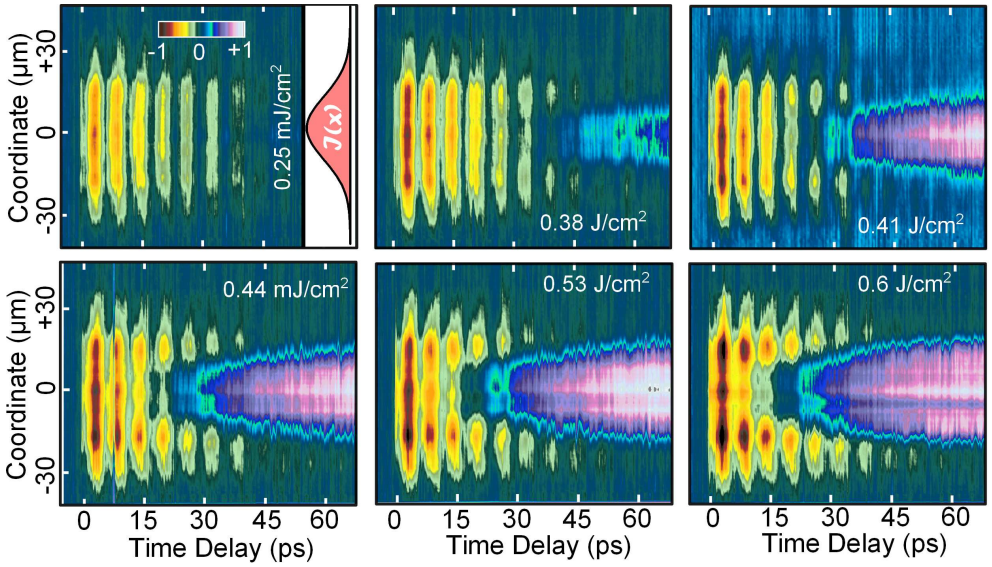

Figure 4.8: The spatially and temporally resolved emergence of the photo-induced magnetization along a 3 μm cross section for a set of the pump fluences. Each image is identified by the maximal fluence. The bias temperature is 23 K.

above 0.25 J/cm^2. The oscillations of the magnetization are seen across the whole photo-excited area.

To obtain quantitative results we analyzed the image obtained for the peak pump fluence equal to 0.6 J/cm^2. The time traces for each pixel were analyzed individually by performing a fitting procedure with the function $F(t)$:

$$F(t) = A + B\left(1 - \exp^{-\frac{t}{t_r}}\right) + C\exp^{-\frac{t}{t_l}}\sin\left(2\pi \mathrm{f_a} + \phi_0\right) \tag{4.5}$$

The fit parameters B and t_r represent the values of the photo-induced magnetization and characteristic rise time, respectively. of the oscillations. C, t_l, $\mathrm{f_a}$ are the amplitude, lifetime and initial phase of the oscillations. A reflects the value of the magnetization independent pump-induced changes to the optical transmission.

The fit function satisfactory describes the dynamics of the photo-induced magnetization (see Fig. 4.9a). The parameter t_r varies in the range from 20 ps to 60 ps depending on the laser fluence (Fig. 4.9b). The frequency of the oscillations $\mathrm{f_a}$ does not depend on the fluence, but the damping clearly does, being larger at higher fluences (Fig. 4.9b).

To interpret the observed oscillations we measured the dependence of their frequency as a function of the sample bias temperature. The value of $\mathrm{f_a}$ on approaching the Morin temperature decreases with a slope -2.3 GHz/K (see Fig. 4.9c). The rise of the bias temperature over the Morin point leads to a frequency increase. As a result, the temperature dependence of $\mathrm{f_a}$ shows a cusp at $\mathrm{T_M}$. It is known that the frequency

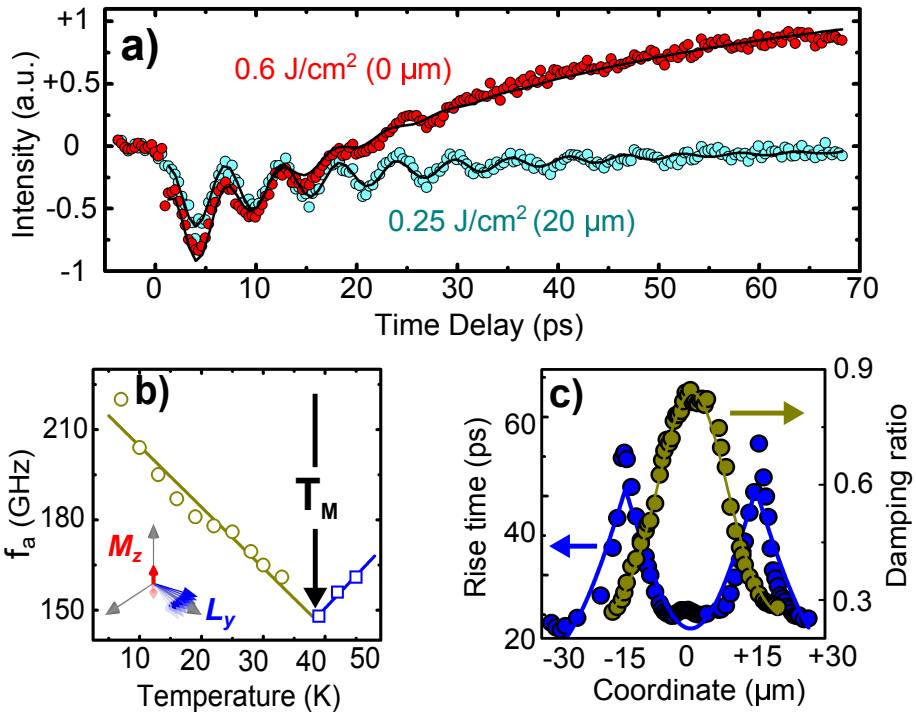

Figure 4.9: (a) The picoseconds dynamics of the photo-induced signal for two different pump fluences. (b) The spatial distribution of the AFM oscillations damping and the magnetization rise time within the photoinduced domain. (c) The temperature dependence of the photoinduced oscillation frequency. The sample temperature is 23 K. Inset demonstrates geometry of the spin precession in the Γ_1 phase.

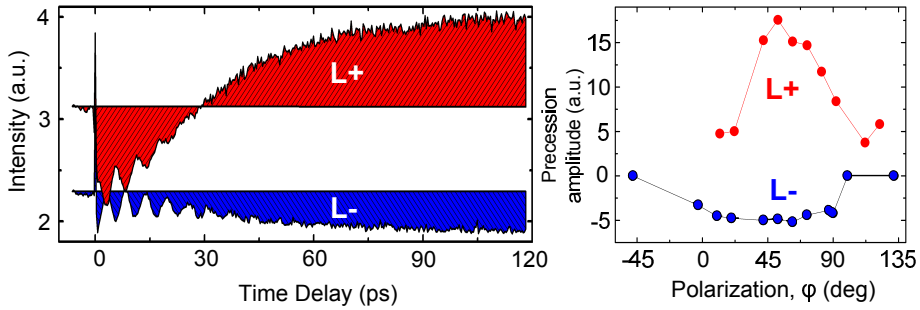

Figure 4.10: (a) The picoseconds dynamics of the photo-induced signal obtained for two antiferromagnetic domains with antiferromagnetic vector **L** oriented parallel (L+) or antiparallel (L-) with respect to the y axis. (b) Amplitude of the spin precession as a function of the pump polarization ϕ. The sample temperature is 23 K. Pump fluence is 0.44 J/cm^2.

of the antiferromagnetic resonance is given by:

$$\mathrm{f_a(T)} = \frac{\gamma}{2\pi} |L_y| \sqrt{\mathcal{J} |K_2\,(\mathrm{T})| + D_y^2} \tag{4.6}$$

Here γ is the gyromagnetic ratio. The exchange constants $\mathcal{J}$ and D_y only slightly vary within considered temperature range while K_2, being positive at T>$\mathrm{T_M}$, changes sign at $\mathrm{T_M}$. This breaks the monotonous temperature dependence of $\mathrm{f}_a\,(\mathrm{T})$ and leads to the cusp appearance. Thus the observed behavior closely follows the expected one for the frequency of the antiferromagnetic resonance in the the low temperature Γ_1 phase [35].This spin resonance is associated with spin oscillations in the (001)-plane such that the x component of the antiferromagnetic vector L_x and the z component of the magnetization M_z appear. For temperatures above $\mathrm{T_M}$ excitation of the oscillations is feasible still, however the emergence of the magnetization is not observed.

Although the damping ratio of the spin oscillations and the characteristic risetime of the photo-induced magnetization are functions heavily dependent of the intensity of the laser excitation, the product of these two quantities remains nearly constant. These observations point to the fact that the spin precession and the Morin transition are mutually correlated. One can conclude, that while the photo-induced exponentially growing magnetization is a measure of the high-temperature phase Γ_4, the amplitude of the oscillations can be a measure of the low temperature Γ_1 phase. From this it is clear why a faster exponential growth of the photo-induced magnetization must lead to a larger damping of the spin oscillations.

Note, that the phase of the oscillations is sensitive to the orientation of the antiferromagnetic vector and experiences a shift over 180^o upon crossing the border of the two antiferromagnetic domains (see Fig. 4.10). One can assume that the spin precession and the deterministic **L**-dependent photo-induced magnetization may correlate. Similarly to the magnetization, the oscillations amplitude is sensitive to the pump polarization. The dependence, however, is not that pronounced and the polarization dependent flip of the phase was not observed.

4.6 The importance of the pump polarization effect for the photo-induced magnetization

The polarization dependence performed on the $z-DyFeO_3$ does not allow to unambiguously establish the selection rules for the excitation of the magnetization dynamics. Although, the polarization dependence of the spin precession demonstrates a maximum in the vicinity of the pump polarization ϕ=45^o, the amplitude of the precession is never zero.

The absence of a clear polarization dependence can originate from the natural birefringence which is responsible for the transformation of the initial pump polarization all along the propagation path [36]. In the pump-probe experiments, the birefringence can influence both the pump and the probe. It does not allow to reveal the genuine polarization dependence of the pump on a polarization-sensitive effect. The birefringence destroys the linear dependence between the Faraday effect and the magnetization. As a result, it also seriously hampers an unambiguous correlation between the value of the Faraday rotation and the net magnetization. Such complications significantly complicate the study of the optical control of magnetism. The use of samples slabs cut along the optical axis [31] can help one to get rid of the effects of the birefringence and its associated problems.

4.6.1 Polarized light in birefringent media

It is known that in optically birefringent media the directions of the normal modes coincide with the birefringent axes. The propagation speed for each polarization is different. This means that the polarization of light which propagates not along these axes will transform all along the propagation path. It also means that only for the case of small birefringence or thin crystals it is possible to reveal the genuine polarization dependence of the mechanism responsible for the optical effect on the magnetization.

The measurements of the Faraday rotation in birefringent media may result in a nonlinear dependence between the magnetization in the media and the rotation of the probe polarization [37]. The regular way to overcome the natural birefringence in optical measurements is to set the polarization of the incident light along one of the principal crystallographic axes. If there was no Faraday rotation, the light would remain linearly polarized along the initial direction as it passed through the crystal. However, rotation of the incident polarization caused by the Faraday effect generates light polarization orthogonal to the incident one [38]. The birefringence, in turn, will phase shift this orthogonally polarized component with respect to the incident polarization, so that an elliptically polarized wave will further propagate in the medium (see Fig. 4.11). As a result, the polarization rotation at the exit of the sample can become even zero:

The Faraday rotation in birefringent media can be described by a simple equation [31]:

$$\tan 2\theta = \frac{2\gamma}{n_x^2 - n_y^2} \sin \frac{2\pi l}{\delta} \tag{4.7}$$

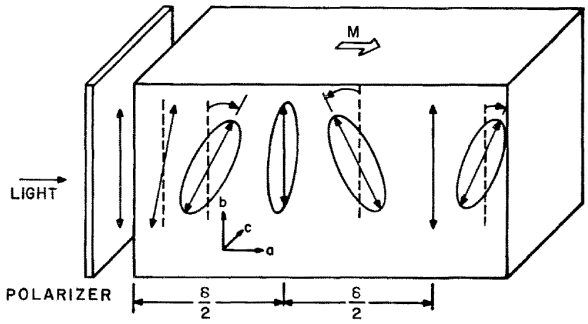

Figure 4.11: Faraday rotation of linearly polarized light in a magnetized birefringent media. Initial light polarization is chosen to be along one of the birefringent axes. The image is taken from Ref. [38].

Here $\delta = \frac{\lambda}{n_x - n_y}$ is the birefringent phase retardation and l is the crystal thickness. An efficient way to overcome the birefringence is to use crystals cut perpendicularly to the so-called optical axis. The optical axis (OA) is a special direction in a crystal in which beam of transmitted light experiences no birefringence. As a consequence, crystals cut along the OA direction preserve the initial polarization all along the propagation path.

4.6.2 The optical axis in the orthoferrites

It is know that orthoferrites are highly anisotropic biaxial media with high optical birefringence. The value of the birefringence in the near infrared spectral range is $\Delta n = n_x - n_y = (3-4) \cdot 10^{-2}$. The measurements show that the optical axis in the orthoferrites lies in the (100) crystallographic plane and for the wavelength of 630 nm makes an angle $\gamma \approx 52^o$ with the [001] crystallographic axis [31] (see Fig. 4.12a). In our measurements, using a crystal cut perpendicularly to the optical axis, we obtained a Faraday rotation of 700 mdeg/μm, which is in striking contrast to 130 mdeg/μm obtained on the $z-$cut slab.

We note that measurements performed on the z-cut sample do not allow to compare the photo-induced values of the magnetization with the static ones, because the birefringence destroys the simple linear relation between the magnetization and the Faraday rotation angle.

4.6.3 Stress-induced antiferromagnetic single domain state

It is known that $DyFeO_3$ possesses piezomagnetic properties [39]. By definition, application of a mechanical stress σ_{jk} in piezomagnetic crystals induces a small magnetic moment m_i^p in accordance with the equation:

$$m_i^p = \Lambda_{ijk}\sigma_{jk} \tag{4.8}$$

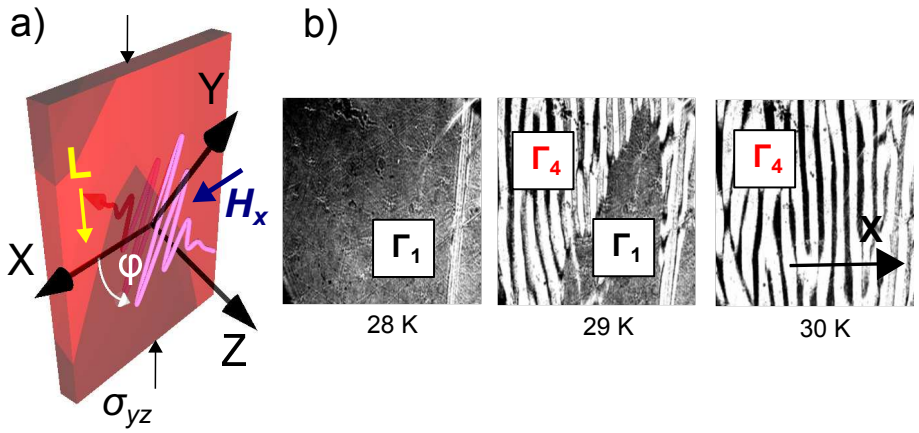

Figure 4.12: (a) Orientation of the crystallographic axis in $o-DyFeO_3$. (b) The magneto-optical photographs of the spontaneous Morin transition in $o-DyFeO_3$.

The axial piezomagnetic $c-$tensor Λ_{ijk} in the point group mmm has three non-zero components Λ_{xyz}, Λ_{yxz} and Λ_{zxy} [40]. The presence of a small piezomagnetic moment opens a way to affect the magnetic domain structure by an external magnetic field. The monodomain state can be induced by applying a field along one of the principal directions. In order not to interact with the photo-induced magnetization, the magnetic field has to be applied along the x or the y crystallographic directions. In our experiments the sample was glued to a holder such that due to the different coefficients of the thermal expansion of the holder and the sample, a cooling of the sample holder induces a stress σ_{yz} in the sample (100) plane and thus results in m_x^p. As a consequence, the direction of the antiferromagnetic vector can be controlled by applying a moderate bias magnetic field H_x [41].

The stress σ_{yz} does not contribute to the magneto-optical contrast of the antiferromagnetic domains. Thus antiferromagnetic domains remain invisible.

4.6.4 Visual observation of the spontaneous Morin transition in $o-DyFeO_3$

The static measurements show that the Morin transition emerges in the vicinity of the temperature T_M=29 K. This value is slightly lower than the one obtained for the $z-DyFeO_3$. Such a shift of T_M to lower values might originate from the holder-induced stress σ_{yz}. It is worth noting that in accordance with the data presented in Ref. [31], the domain structure in the magnetic Γ_4 phase is not labyrinth-like, but rather stripe-like, with the stripes normal along the $x-$direction (Fig. 4.12b).

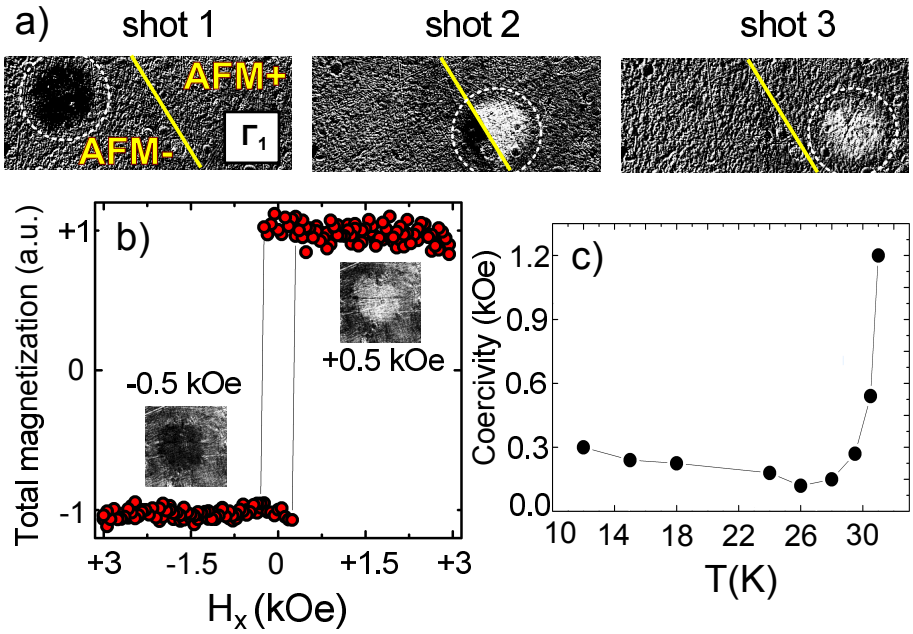

Figure 4.13: (a) Images of the photoinduced domains in $o-DyFeO_3$ taken 100 ps after excitation with a single 60 fs pump pulse. The grey color corresponds to the Γ_1 phase. Areas exposed to the pulsed excitation are marked by dashed lines. The solid line represents the border of two antiferromagnetic domains not visible optically. "shot 1" forms a black domain having magnetization $-M_z$. "shot 2" affects both antiferromagnetic domains and induces a magnetization, the sign of which is defined by the direction of **L**. "shot 3" forms a white domain with the magnetization $+M_z$. (b) Hysteresis-like dependence of the value of the photo-induced magnetization as a function of the external magnetic field H_x. Insets are magneto-optical images of the photo-induced magnetization 3 ns after the optical pumping event. (c) Coercivity of the field hysteresis of the antiferomagnetic domains as a function of the bias temperature.

4.6.5 Polarization dependence of the photo-induced spin precession and magnetization. The case of $DyFeO_3$ cut perpendicular to the optical axis.

Similarly to the case of $z-DyFeO_3$ the pump beam induces changes in the magneto-optical contrast in $o-DyFeO_3$. Despite the fact that the antiferromagnetic domains are not visible in the Γ_1 phase, the displacement of the pump beam within the field of view reveals a change of the pump-induced domains from "black" to "white" (Fig. 4.13a). Application of an external magnetic field H_x brings the sample in a monodomain antiferromagnetic state. The orientation of the vector **L** defines the direction of the photo-induced magnetization (Fig. 4.13b). Interestingly, the coercivity significantly rises up on approaching the Morin transition (Fig. 4.13d).

Figure 4.14a demonstrates magneto-optical images taken 2.6 ns after the pumping event for the two antiferromagnetic domains created by the application of H_x. The

intensity integral over the photo-induced domain represents the average direction of the net magnetization. Changing the polarization we reveal that the magnetization changes periodically with the period equal to 180^o (Fig. 4.14b). One can see that the polarization dependence shows a rather square-wave than harmonic dependence with flat saturation and sharp transition edges at 0^o and 90^o. Such an anharmonic waveform enables a control of the magnetization, varying the pump polarization only within 10^o. A reduction of the pump fluence leads to a less anharmonic polarization dependence (see inset Fig. 4.14b). The magnetization state demonstrates no difference for the left- and right-handed circular polarization. This is in contrast to what was demonstrated for the first-order phase transition in $HoFeO_3$ [9] and the second-order phase transition in $Sm_{0.5}Pr_{0.5}FeO_3$ [10].

The value of the Faraday rotation caused by the photo-induced magnetization can be roughly estimated from the measured changes in the magneto-optical contrast varying the analyzer angle. For a relatively long time delay, when photo-induced changes in transmission are in saturation, the magneto-optical signals $S^{\pm}$ obtained from the "white" and "black" pump-induced domains can be calculated as:

$$\begin{aligned} S^{+} &= I_0\,(1-\alpha)\cos^2\left(\theta+\theta_M^{+}\right) - S^{bg} \\ S^{-} &= I_0\,(1-\alpha)\cos^2\left(\theta-\theta_M^{-}\right) - S^{bg} \end{aligned} \tag{4.9}$$

Here θ is angle betwee the polarizer and the analyzer, $\theta_M^{\pm}$ is the Faraday rotation caused by the "up" and "down" oriented photo-magnetization, respectively, I_0 is the intensity of the incident probe light, α is saturation value of the differential transmission and $S^{bg} = I_0 \cos^2\theta$ is the value of the magneto-optical contrast measured at negative pump-probe delay. Fitting the Mallus law (Fig. 4.15a) to the observed dependencies, as shown in Fig. 4.15, gives values $\theta_M^{\pm}$=4.5±0.1^o and α = 0.11 - 0.17. The value of the static Faraday rotation in the Γ_4 phase is about 35^o. The photo-induced magnetization 3.4 ns after the pump excitation is about 13 % of the static magnetization.

In the same way as it was done in the case of the $z-$cut sample we performed time-resolved experiment for the angles $\pm 45^o$ between the pump polarization and the x-axis of the pump polarization (Fig. 4.16a). It is seen that the dynamics can be described with only two exponential contributions. One of these contributions has the time constant τ_1=60 ps and for the second one τ_2 >3.4 ns. To determine the timescale at which changes in transmission occur, we removed the analyzer from the probe path. In such a way we eliminate the contribution from the Faraday effect. Figure 4.16c clearly shows that for both pump polarizations, long-living transmission changes occur.A relaxation with a time constant close to τ_1 is also seen in the transmission. These traces point out that the time τ_1 is not due to magnetization dynamics.

It is quite counterintuitive that a 60 fs pump can affect the final magnetization, the formation of which takes two orders of magnitude longer time. To clarify the mechanism of the photo-induced magnetization emergence, we studied the dynamics in details. For this we performed the measurements of the spin-oscillations in the conventional pump-probe scheme. The pump repetition rate was increased up to 500 Hz in order to effectively employ the lock-in technique and balanced photodetector.

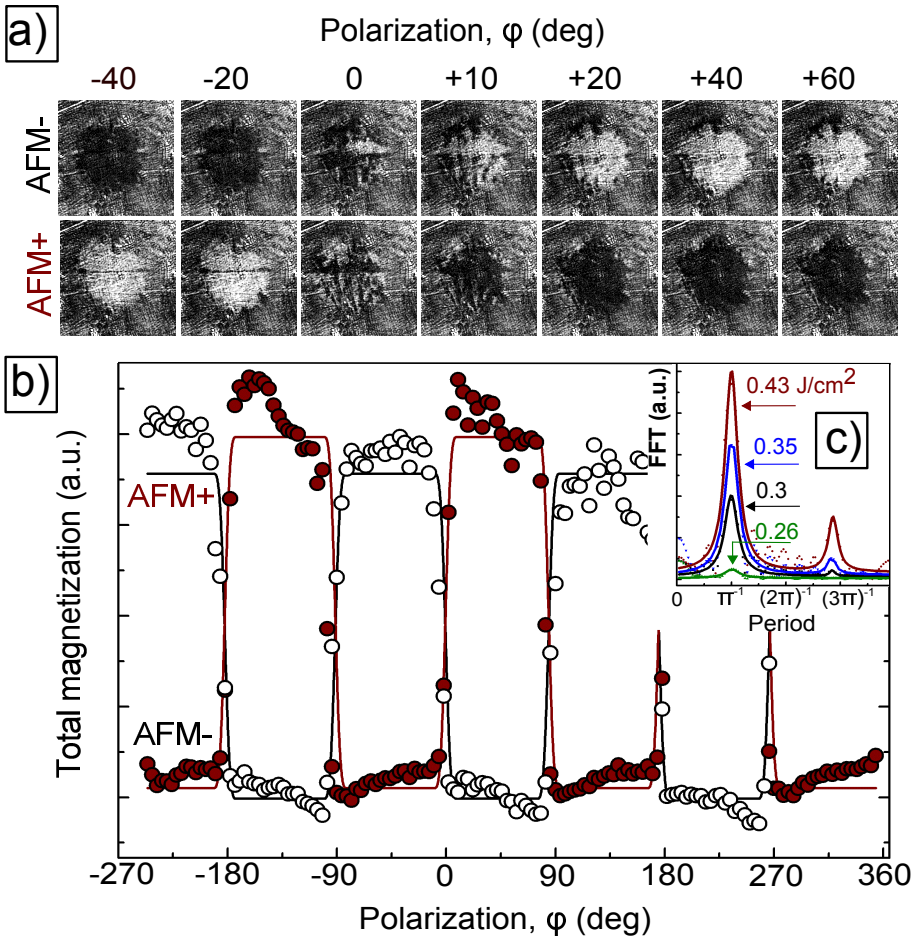

Figure 4.14: (a) Magneto-optical images of photo-induced magnetic domains in *o*-$DyFeO_3$ for different linear pump polarizations 2.6 ns after the pumping event. The measurements were done for different angles between the linear polarization of the pump and the x axis. (b) Signal integrated over the photo-induced magnetic domain representing the net photo-induced magnetization. Inset shows FFT transform of the polarization dependence and reveals the presence of anharmonicity in a form of higher harmonics.

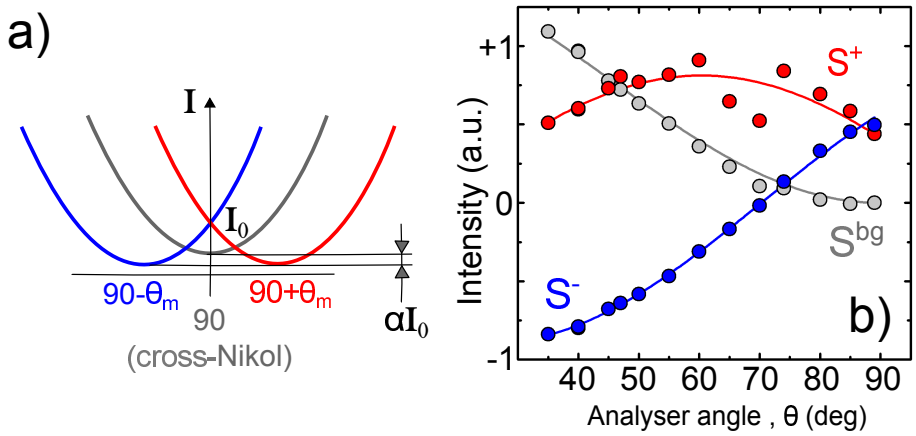

Figure 4.15: (a) Schematic representation of the Mallus law.The Faraday rotation θ_M results in change after the pump excitation, accompanied by an intensity change αI_0. (b) Experimental points and theoretical fit of the magneto-optical contrast due to the photoinduced magnetization $S^{\pm}$ and measurements of the Mallus law at negative pump-probe delay.

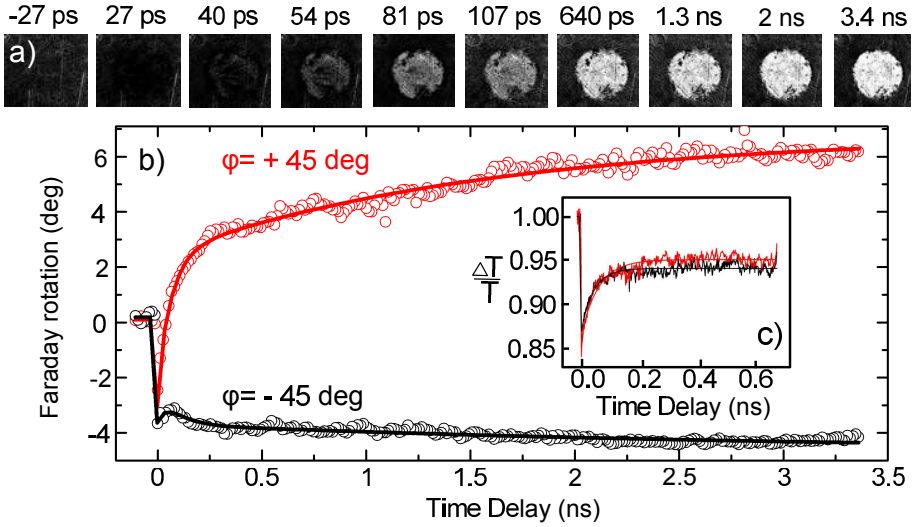

Figure 4.16: (a) Magneto-optical images showing the emergence of the photo-induced magnetization at different time delays. The pump polarization forms an angle of 45^o with the x axis. (b) The Faraday rotation integrated over the spot of the photo-induced magnetization for two orthogonal pump polarizations directed at angles $\pm 45^o$ with respect to the x-axis. (c) Pump-induced dynamics in the differential transmission.

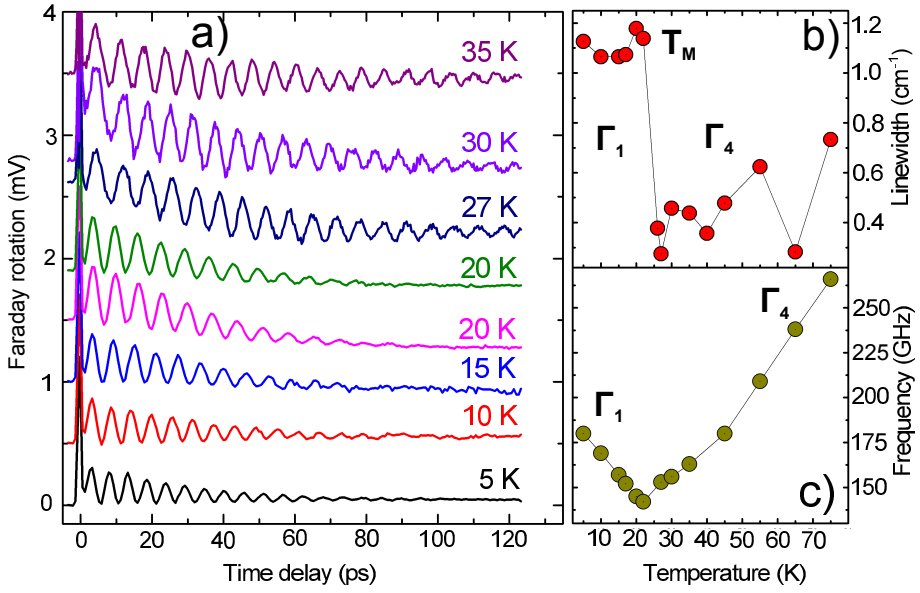

Figure 4.17: (a) Pump-probe traces of the Faraday rotation measured for different bias temperatures. Each trace is a difference between two measurements for two orthogonal pump polarizations. (b) Linewidth of the precession as a function of the bias temperature. The behavior is in good agreement with that reported in Ref. [35]. (c) Frequency of the oscillations for different bias temperatures. Pump polarization is $\pm 45^o$ with respect to the $x-$axis

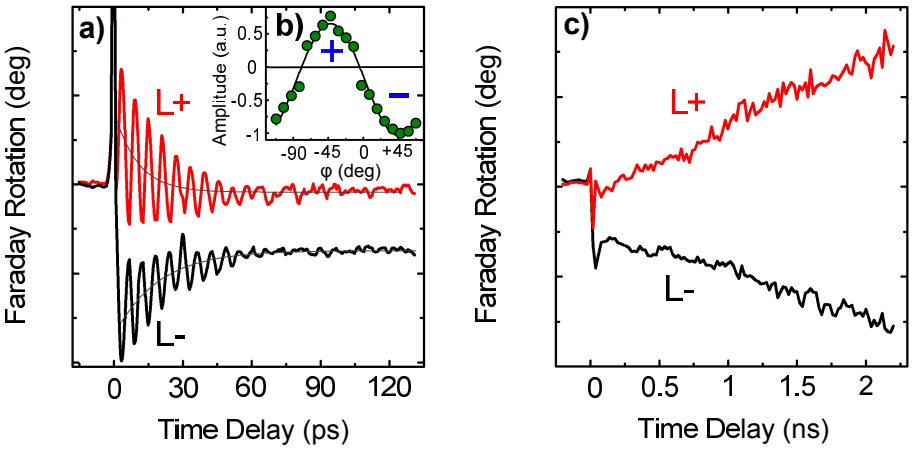

Figure 4.18: (a) Excitation of the antiferromagnetic precession in antiferromagnetic domains with opposite orientation of **L**. (b) Amplitude of the spin precession measured for different pump polarizations. (c) Pump-induced magnetization dynamics on a ns timescale. The sample is set to a bias temperature equal to 20 K.

Figure 4.17 shows that a linearly polarized pump excites spin oscillations in the whole range of bias temperatures. Similarly to the $z-$cut sample, the frequency of the oscillations is characterized by a softening as a function of temperature with a cusp at the Morin temperature. It is seen that the transition across the Morin point is accompanied by a sharp change in the oscillation lifetime while the frequency stays nearly the same. This striking feature was observed for the first time in Ref. [35]. The Ising axis of the Dy^{3+} ions is oriented at the angle of 30^o with respect to the y crystallographic direction. Because the spins of the iron ions are coupled to the spin of the rare-earths via the exchange interaction, these two systems can be considered as coupled oscillators. The coupling is stronger in the Γ_1 phase. In the Γ_4 phase the Fe^{3+} spins oscillate almost orthogonally with respect to the spins of Dy^{3+}. In this case the coupling is weaker and it result in a smaller damping of the antiferromagnetic resonance in the Γ_4 phase.

We performed the measurements for two antiferromagnetic domains, applying a moderate field along the x axis (Fig. 4.18a). It is clearly seen that the spin precession in both domains has opposite phase (π-shift). Interestingly, it is seen that the pump not only induces a precession around equilibrium but also instantaneously generates magnetization, similarly to data presented in Ref. [9]. Observation of this effect was complicated in the crossed Nicols imaging set-up. The excitation of the spin precession demonstrates no difference for left- and right-handed circularly polarized light. The amplitude and the phase of the spin precession are strongly sensitive to the orientation of a linearly polarized the pump pulse (Fig. 4.18b). It is remarkable that the phase of the photo-induced spin precession correlates with the direction of the photo-induced magnetization. The magnetization growth is not limited to picoseconds: a growth of the magnetic signal with no sign of saturation still is visible at 2.5 ns (see Fig. 4.18c).

$\mathrm{sign}(\mathcal{E}_x\mathcal{E}_y^*)$ / $\mathrm{sign}(L_y)$	+1	-1
+1	+1	−1
−1	−1	+1

Table 4.1: The photo-induced effects (magnetization and spin precession) as a function of the incoming pump polarization orientation and orientation of the **L** vector in antiferromagnetic domain. For the magnetization values ±1 correspond to $\pm M_z$. For the precession ±1 correspond the initial phase equal to 0 and π, respectively.

Table 4.1 summarizes how by changing the sign of L_y and $\mathcal{E}_x\mathcal{E}_y^*$, one can control the direction of the photo-induced magnetization and phase of the photo-induced spin oscillations.

4.7 Non-dissipative mechanism to excite the magnetization dynamics

An insight into the physics of light-matter interaction can be obtained using a phenomenology approach [42]. It is established experimentally that the magnetization dynamics is driven by linearly polarized light. Thus it is the symmetric part of the dielectric permittivity tensor ε that must contribute to the effect. According to the symmetry of the Γ_1 phase, all possible contributions to the symmetric part of the dielectric permittivity tensor ε_{ij}^s can be expressed as:

$$\varepsilon_{xy}^s = (\mathcal{A}L_x + \mathcal{B}M_z)\, L_y \tag{4.10}$$

Here $\mathcal{A}$ and $\mathcal{B}$ are phenomenological parameters. From this it can clearly be seen that the magnetism-related part of the energy of the light-matter interaction is sensitive exclusively to the linear pump polarization oriented in the (001) plane:

$$\Phi_{lm} = (\mathcal{A}L_x + \mathcal{B}M_z)\, L_y \cdot \mathcal{E}_x\mathcal{E}_y^* \tag{4.11}$$

Due to the presence of this term it can be shown that if a linearly polarized femtosecond pulse with $\mathcal{E}_x\mathcal{E}_y^* \neq 0$ propagates through a magnetic crystal it induces a net magnetization M_z:

$$\frac{\partial^2 M_z}{\partial \tau^2} + 2\lambda\frac{\partial M_z}{\partial \tau} + \omega_a^2 M_z = \begin{cases} (-\mathcal{A}D_y + \mathcal{B}K_2)\, L_y \cdot \mathcal{E}_x\mathcal{E}_y^* + \\ +\mathcal{A}\,|L_y| \cdot \frac{\partial(\mathcal{E}_x\mathcal{E}_y^*)}{\partial \tau} \end{cases} \tag{4.12}$$

Here $\tau = \gamma\,|L_y|\,t$ is the normalized time, γ is the gyromagnetic ratio, λ is a phenomenological damping parameter, $\omega_a = 2\pi \mathrm{f_a}$.

The first term in the right hand part of (4.12) possesses the same symmetry with respect to the antiferromagnetic vector and the pump polarization as the experimentally observed photo-induced magnetization (Table 4.1). This term is essential to

trigger the inertial spins dynamics [42], which can not only drive spin precession but even reorient the magnetization [9].

Indeed, integration of equation (4.12) from $-t$ to $+t$, so that $t \longrightarrow 0$ gives:

$$\frac{\partial M_z}{\partial \tau}|_{\tau=0} = \frac{(-\mathcal{A}D + \mathcal{B}K_2)\, L_y}{\omega_a} \cdot \mathcal{I}_0 \tag{4.13}$$

Here, $\mathcal{I}_0$ is the intensity of the incident light. Such dynamics is inertial and for this reason has to be described with a single sine function

The last term in Eq. (4.12) simply establishes initial deviation of L_x is sensitive only to the pump polarization:

$$\tfrac{\partial M_z}{\partial \tau}\,\big|_{\tau=0} = \mathcal{A}\,|L_y| \cdot \mathcal{E}_x \mathcal{E}_y^* \longrightarrow M_z|_{\tau=0} = \mathcal{A}\,|L_y| \cdot \mathcal{I}_0 \tag{4.14}$$

Her the product $\mathcal{E}_x \mathcal{E}_y^*$ exists only when the pump pulse is present in the media. Within this time it induces an instantaneous magnetization. As it is seen, this term does not depend on any parameters which characterizes the magnetic state. Such dynamics is gyroscopic and for this reason has to be described with a single cos function. Figure 4.18a shows that the experimentally observed dynamics is sine-like. It points to the fact that a contribution from the **L**-independent term of equation (4.12) is negligibly small.

The suggested mechanism clearly describes why the initial phase of the spin oscillations in Γ_1 is affected by a linear pump polarization and the orientation of the antiferromagnetic vector in the Γ_1 phase.

4.8 The mechanism of the ultrafast generation of a net magnetization across first-order the Morin transition.

To understand how a femtosecond laser pulse generates a Γ_4 domain with a defined magnetization, one needs to consider two individual effects which a laser pulse produces simultaneously. The first one the is laser-induced heating which leads to a repopulation of $4f$ levels of the Dy^{3+} ions. It can be effectively described as a time-dependent evolution of the magnetic anisotropy potential, Eq. (4.2). The second is a non-dissipative initial reorientation of the magnetization. Both these processes happen simultaneously in the time-domain. The interplay of these effects defines the observed magnetization dynamics.

Figure 4.19a gives the Short Time Fourier Transform (STFT) of the spin dynamics which reveals how the frequency of the antiferromagnetic oscillations depends on time for a low excitation fluence ($\sim$0.24 J/cm^2). At this fluence the transition across the Morin point is not observed. Note that the frequency of the spin precession f_a, determined by the curvature of the magnetic anisotropy potential at the bias temperature, has to experience a dynamical softening if the crystal approaches the Morin temperature. For higher fluences the transition is launched and the onset of the photoinduced magnetization is visible. Indeed, the softening of the frequency over the time is visible for 0.6 J/cm^2 (Fig. 4.19b).

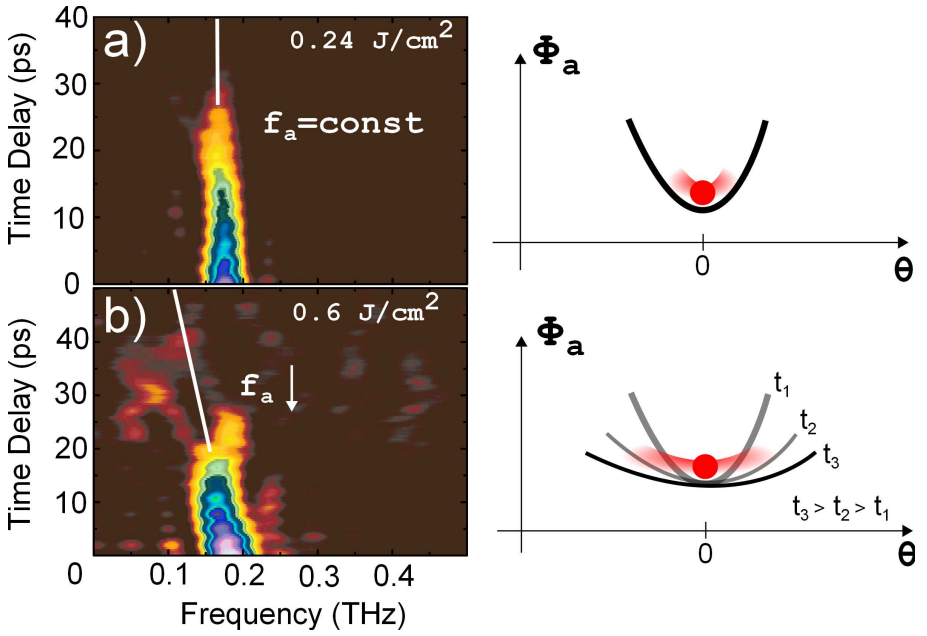

Figure 4.19: (a) Time-resolved Fourier transform of the time trace of the spin oscillations at a fluence when the Morin transition is not launched (0.24 J/cm^2). (b) Time-resolved Fourier transform of the time trace of the spin oscillations at a fluence when the Morin transition is launched (0.6 mJ/cm^2). The solid white line are guides to the eye to demonstrate the direction of the frequency evolution. The schematics from the right are illustrations of the oscillations at the bottom of the potential minimum and at a slowly varying potential when the curvature of the potential slowly changes and produces effectively a slowing down of the frequency.

The time evolution of the frequency of the oscillations reveals the evolution of the magnetic anisotropy potential (Fig. 4.19b). It is seen that the anisotropy change is not instantaneous.

Effectively the dynamics of the magnetic anisotropy potential can be described by a time-dependent anisotropy constant k_2:

$$k_2(t) = k_2(0) \cdot (1 - \xi t) \tag{4.15}$$

Here ξ is the temporal rate of the anisotropy constant change.

A nonlinear differential equation (4.16) with time-dependent anisotropy energy $\Phi_a(\theta, t)$, which describes dynamics of the angle θ, is:

$$\frac{\partial^2\theta}{\partial t^2} + 2\lambda\frac{\partial\theta}{\partial t} + \mathcal{J}\frac{\partial\Phi_a(\theta,t)}{\partial\theta} = 0 \tag{4.16}$$

The net magnetization can be found based on this equation via expression:

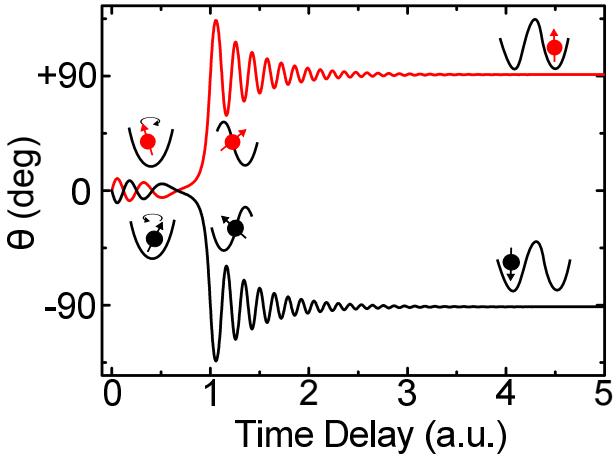

Figure 4.20: Modeling of the dynamics of the angle θ, whcih vector $\mathbf{L}$ forms with the $y-$axis across the first-order phase transition in the presence of an coherent spin precession, using Eq. (4.16). The dynamics is depicted for two values of the initial conditions $\pm\frac{\partial\theta}{\partial t}|_0$.

$$M_z = \frac{D}{\mathcal{J}}\sin\theta \tag{4.17}$$

The optomagnetic effects establish initial conditions for Eq. (4.16), based on the initial polarization and direction of the antiferromagnetic vector in the Γ_1 phase. This simple model allows to establish a correlation between the photo-induced magnetization and the precession phase. Figure 4.22 shows the results of such simulations. It is seen that the initial phase of the spin oscillations practically defines the direction of the photo-induced magnetization.

Although the suggested model qualitatively explains the phase of the oscillations, it is not clear how and why the initial phase of the oscillations defines the direction of the photo-induced magnetization in the metastable state. In a first-order phase transition (Fig. 4.21a) there is no route for a gradual transition between the Γ_1 (θ=0^o) and the Γ_4 phases (θ=90^o). This is in contrast to second-order phase transition (Fig. 4.21b). It is expected that a first-order phase transition in a given point of space has to happen on a timescale close to a quarter of the period of the antiferromagnetic precession, which is less than 2 ps. Thermodynamically stable minima are separated by a barrier. Hence it is expected that if the phase transition occurs, it should also be accompanied by large amplitude spin oscillations around the new equilibrium at the frequency of the spin resonance in the Γ_4 phase [43]. We failed to observe these oscillations experimentally. This finding reveals that the ultrafast kinetics of the phase transition cannot be fully explained thermodynamically.

It is well known, that in the kinetics of first-order phase transitions one can distinguish three consecutive steps [44]:

1. **Nucleation**. Initial stage of a first-order phase transition in which small nuclei

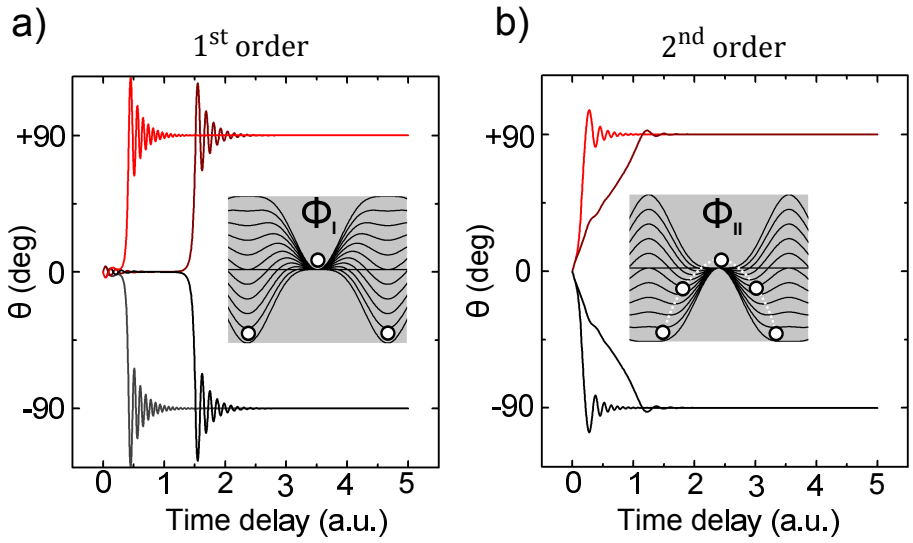

Figure 4.21: Modeling of coherent dynamics of the angle θ which vector **L** forms with the $y-$axis in time-dependent anisotropy potential which corresponds to (a) first-order phase transition. (b) second-order phase transition. Plots are typical for fast and relatively slow rate of the magnetic anisotropy change. Insets represent dynamics of the anisotropy potentials.

of the new phase are formed.

2. **Growth**. The process in which the nuclei grow to a macroscopic size. At the end of this phase the amount of the new phase is close to its final equilibrium value.

3. **Coarsening**. It is a very slow process by which the grown nuclei rearrange themselves and coagulate, gradually moving towards the equilibrium state predicted by equilibrium thermodynamics.

In the case of the Morin transition from the Γ_1 to the Γ_4 phase, nucleation results in the formation of nuclei with a net magnetization. If no external magnetic field is applied the nuclei with the magnetization "up" appear equally likely with the nuclei with the magnetization "down". The net photo-induced magnetization must be zero as the effect of light results in as many photo-induced areas with magnetization "up" as with "down".

A femtosecond laser pulse launches spin oscillations and creates supercritical nuclei of the new Γ_4 phase. The orientation of the magnetization is then predefined in accordance with Table 4.1. While the size of the nuclei grows in time (Fig. 4.22a), the spin oscillations experience a decay. As a result, for times longer than 20 ps the precession exist only in the areas free of any nuclei (Fig. 4.22b). The dynamics of the photo-induced magnetization demonstrates **L**-dependent growth without visible saturation even for timescales more than 2 ns (Fig. 4.22c).

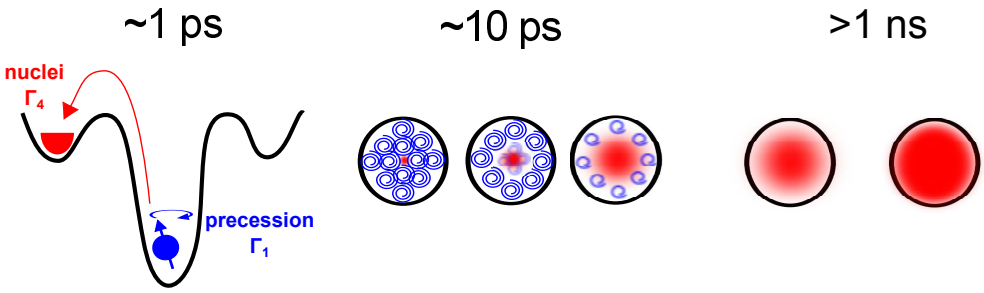

Figure 4.22: The possible scenario of the photo-induced Morin transition in $DyFeO_3$

4.9 Photo-induced magnetization in an external magnetic field

Finally it is interesting to study if light can orient the magnetization against an external magnetic field. We performed experiments in which the applied magnetic field has a component along the z-axis and thus effectively breaks the degeneracy between the two states of the magnetization in the Γ_4 phase. In particular, we canted the magnetic field in the sample plane over 15^0 angle and obtained projections of the field on all three crystallographic axes $\mathbf{H}$=(H_x,H_y,H_z). We found that if the field is less than H_z=0.4 kOe, the polarization can launch the ultrafast emergence of a photo-induced magnetization in the direction against the field. Such a photo-induced magnetization, however, will relax on a time scale of ns. A field above H_z=0.4 kOe overrides the photo-induced magnetization and orients the magnetization completely along the field direction.

Taking advantage of the imaging technique and using the fact that the intensity in the pump spot follows a Gaussian distribution, we revealed how the photo-induced magnetization depends on the pump fluence and external magnetic field. Figure 4.24a shows such a map of the photo-induced magnetization, taken 200 ps after the pumping event. The color code represents the fraction of the photo-induced magnetization which is sensitive to the polarization of the pump pulse.

The behavior of the polarization-dependent part of the photo-induced magnetization in the applied magnetic field can be nicely fitted by an exponential function (see Fig. 4.24b). This can be understood in the following way.

In an external field the free energy of a single cluster contains the Zeeman term, which represents the interaction of the cluster's magnetization with the external magnetic field. This energy is different for clusters with the magnetization along and against the direction of the external field. If a laser pulse creates clusters of the Γ_4 phase with a magnetization oriented oppositely with respect to the magnetic field, the field makes a growth of their size less favorable. One can assume that this process is described by the Boltzmann distribution:

$$\mathcal{P}_G \sim \exp\left[-\left(\Phi_0 - M_z \cdot H_z\right)/kT\right] \tag{4.18}$$

Here we introduce $\mathcal{P}_G$ as a probability of the cluster to grow in size and acquire the

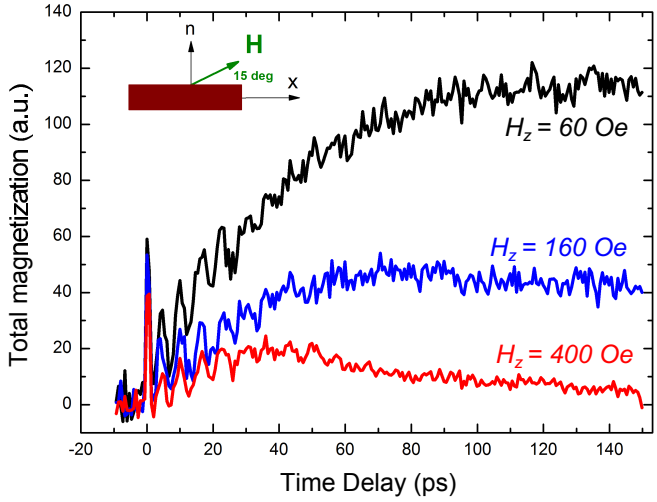

Figure 4.23: The picoseconds dynamics of the photo-induced signal plotted for different values of the external magnetic field having a projection in the direction of the photo-induced magnetization. Each trace is the difference for two orthogonal pump polarizations, oriented at the angle $\phi = \pm 45$ with respect to the x-axis. The sample temperature is 21 K.

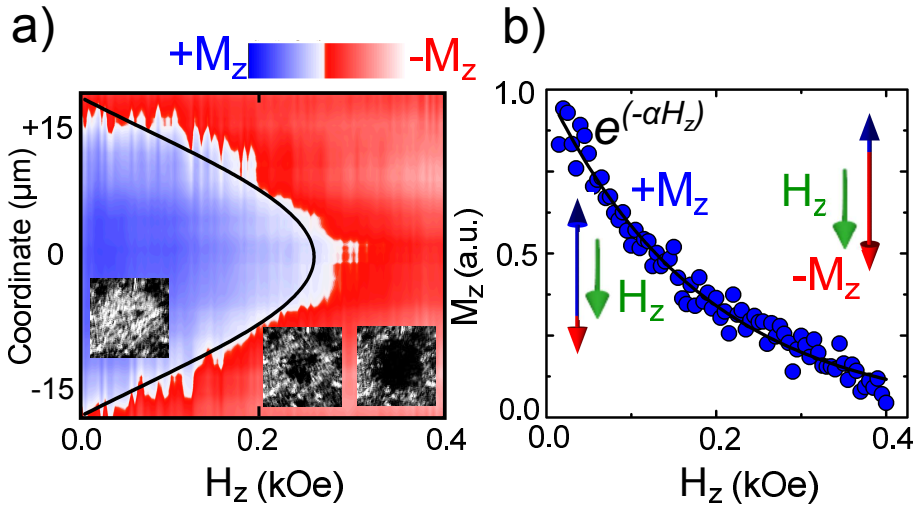

Figure 4.24: (a) A 3 μm cross-section of the photoinduced magnetization fraction oriented against the external magnetic field as function of it value. The magnetization snapshot is taken 200 ps after the pumping event. (b) The field dependence of the photo-induced magnetization fraction oriented against the external field direction. The solid line is an exponential fit of the dependence.

magnetization M_z, k is the Boltzmann constant and Φ_0 is field-independent energy. Such a distribution explains the exponential behaviour as observed in Fig. 4.24b.

4.10 Conclusions

To conclude, using time-resolved imaging we revealed the ultrafast laser-induced magnetization dynamics in antiferromagnetic $DyFeO_3$ in the vicinity of the Morin transition. We show that all-optical control of the photo-induced magnetization in antiferromagnets can be performed not only by changing the polarization of the light pulse but also by changing the direction of the antiferromagnetic vector. Hence, our study reveals a previously ignored degree of freedom for ultrafast optical control of magnetism. The physics reported here is also applicable to α-Fe_2O_3 which is one of the most widespread minerals having $T_M \approx 270$ K.

References

[1] M. Chollet, L. Guerin, N. Uchida, S. Fukaya, H. Shimoda, T. Ishikawa, K. Matsuda, T. Hasegawa, A. Ota, H. Yamochi, *et al.*, "Gigantic photoresponse in 1/4-filled-band organic salt (EDO-TTF) 2PF6," *Science*, vol. 307, no. 5706, pp. 86–89, 2005.

[2] A. Cavalleri, C. Tóth, C. W. Siders, J. A. Squier, F. Ráksi, P. Forget, and J. C. Kieffer, "Femtosecond structural dynamics in VO_2 during an ultrafast solid-solid phase transition," *Phys. Rev. Lett.*, vol. 87, p. 237401, Nov. 2001.

[3] P. Beaud, A. Caviezel, S. O. Mariager, L. Rettig, G. Ingold, C. Dornes, S.-W. Huang, J. A. Johnson, M. Radovic, T. Huber, T. Kubacka, A. Ferrer, H. T. Lemke, M. Chollet, D. Zhu, J. M. Glownia, M. Sikorski, A. Robert, H. Wadati, M. Nakamura, M. Kawasaki, Y. Tokura, S. L. Johnson, and U. Staub, "A time-dependent order parameter for ultrafast photoinduced phase transitions," *Nat. Mater.*, vol. 13, pp. 923–927, Oct. 2014.

[4] H. Ichikawa, S. Nozawa, T. Sato, A. Tomita, K. Ichiyanagi, M. Chollet, L. Guerin, N. Dean, A. Cavalleri, S.-i. Adachi, T.-h. Arima, H. Sawa, Y. Ogimoto, M. Nakamura, R. Tamaki, K. Miyano, and S.-y. Koshihara, "Transient photoinduced manganite," *Nat. Mater.*, vol. 10, pp. 101–105, Feb. 2011.

[5] E. Beaurepaire, J.-C. Merle, A. Daunois, and J.-Y. Bigot, "Ultrafast spin dynamics in ferromagnetic Nickel," *Phys. Rev. Lett.*, vol. 76, pp. 4250–4253, May 1996.

[6] E. Carpene, E. Mancini, C. Dallera, M. Brenna, E. Puppin, and S. De Silvestri, "Dynamics of electron-magnon interaction and ultrafast demagnetization in thin iron films," *Phys. Rev. B*, vol. 78, p. 174422, Nov. 2008.

[7] A. V. Kimel, R. V. Pisarev, J. Hohlfeld, and T. Rasing, "Ultrafast quenching of the antiferromagnetic order in $FeBO_3$: Direct optical probing of the phonon-magnon coupling," *Phys. Rev. Lett.*, vol. 89, p. 287401, Dec. 2002.

[8] A. V. Kimel, A. Kirilyuk, A. Tsvetkov, R. V. Pisarev, and T. Rasing, "Laser-induced ultrafast spin reorientation in the antiferromagnet $TmFeO_3$," *Nature*, vol. 429, pp. 850–853, June 2004.

[9] A. V. Kimel, B. A. Ivanov, R. V. Pisarev, P. A. Usachev, A. Kirilyuk, and T. Rasing, "Inertia-driven spin switching in antiferromagnets," *Nat Phys*, vol. 5, pp. 727–731, Oct. 2009.

[10] J. A. de Jong, I. Razdolski, A. M. Kalashnikova, R. V. Pisarev, A. M. Balbashov, A. Kirilyuk, T. Rasing, and A. V. Kimel, "Coherent control of the route of an ultrafast magnetic phase transition via low-amplitude spin precession," *Phys. Rev. Lett.*, vol. 108, p. 157601, Apr. 2012.

[11] L. Le Guyader, A. Kleibert, F. Nolting, L. Joly, P. M. Derlet, R. V. Pisarev, A. Kirilyuk, T. Rasing, and A. V. Kimel, "Dynamics of laser-induced spin reorientation in $Co/SmFeO_3$ heterostructure," *Phys. Rev. B*, vol. 87, p. 054437, Feb. 2013.

[12] K. Miyasaka, M. Nakamura, Y. Ogimoto, H. Tamaru, and K. Miyano, "Ultrafast photoinduced magnetic moment in a charge-orbital-ordered antiferromagnetic $Nd_{0.5}Sr_{0.5}MnO_3$ thin film," *Phys. Rev. B*, vol. 74, p. 012401, July 2006.

[13] M. Matsubara, Y. Okimoto, T. Ogasawara, Y. Tomioka, H. Okamoto, and Y. Tokura, "Ultrafast photoinduced insulator-ferromagnet transition in the perovskite manganite," *Phys. Rev. Lett.*, vol. 99, p. 207401, Nov. 2007.

[14] G. Ju, J. Hohlfeld, B. Bergman, R. J. M. van de Veerdonk, O. N. Mryasov, J.-Y. Kim, X. Wu, D. Weller, and B. Koopmans, "Ultrafast generation of ferromagnetic order via a laser-induced phase transformation in FeRh thin films," *Phys. Rev. Lett.*, vol. 93, p. 197403, Nov. 2004.

[15] B. Bergman, G. Ju, J. Hohlfeld, R. J. M. van de Veerdonk, J.-Y. Kim, X. Wu, D. Weller, and B. Koopmans, "Identifying growth mechanisms for laser-induced magnetization in FeRh," *Phys. Rev. B*, vol. 73, p. 060407, Feb. 2006.

[16] S. O. Mariager, F. Pressacco, G. Ingold, A. Caviezel, E. Möhr-Vorobeva, P. Beaud, S. L. Johnson, C. J. Milne, E. Mancini, S. Moyerman, E. E. Fullerton, R. Feidenhans'l, C. H. Back, and C. Quitmann, "Structural and magnetic dynamics of a laser induced phase transition in FeRh," *Phys. Rev. Lett.*, vol. 108, p. 087201, Feb. 2012.

[17] T. Li, A. Patz, L. Mouchliadis, J. Yan, T. A. Lograsso, I. E. Perakis, and J. Wang, "Femtosecond switching of magnetism via strongly correlated spin-charge quantum excitations," *Nature*, vol. 496, pp. 69–73, Apr. 2013.

[18] C. von Korff Schmising, B. Pfau, M. Schneider, M. Günther, C. M. Giovannella, J. Perron, B. Vodungbo, L. Müller, F. Capotondi, E. Pedersoli, N. Mahne, J. Lüning, and S. Eisebitt, "Imaging ultrafast demagnetization dynamics after a spatially localized optical excitation," *Phys. Rev. Lett.*, vol. 112, p. 217203, May 2014.

[19] K. Vahaplar, A. M. Kalashnikova, A. V. Kimel, D. Hinzke, U. Nowak, R. Chantrell, A. Tsukamoto, A. Itoh, A. Kirilyuk, and T. Rasing, "Ultrafast path for optical magnetization reversal via a strongly nonequilibrium state," *Phys. Rev. Lett.*, vol. 103, p. 117201, Sept. 2009.

[20] C. E. Graves, A. H. Reid, T. Wang, B. Wu, S. de Jong, K. Vahaplar, I. Radu, D. P. Bernstein, M. Messerschmidt, L. Mller, R. Coffee, M. Bionta, S. W. Epp, R. Hartmann, N. Kimmel, G. Hauser, A. Hartmann, P. Holl, H. Gorke, J. H. Mentink, A. Tsukamoto, A. Fognini, J. J. Turner, W. F. Schlotter, D. Rolles, H. Soltau, L. Strder, Y. Acremann, A. V. Kimel, A. Kirilyuk, T. Rasing, J. St hr, A. O. Scherz, and H. A. Drr, "Nanoscale spin reversal by non-local angular momentum transfer following ultrafast laser excitation in ferrimagnetic GdFeCo," *Nat. Mater.*, vol. 12, pp. 293–298, Apr. 2013.

[21] Y. Hashimoto, A. R. Khorsand, M. Savoini, B. Koene, D. Bossini, A. Tsukamoto, A. Itoh, Y. Ohtsuka, K. Aoshima, A. V. Kimel, A. Kirilyuk, and T. Rasing, "Ultrafast time-resolved magneto-optical imaging of all-optical switching in GdFeCo with femtosecond time-resolution and a μm spatial-resolution," *Rev. Sci. Instrum.*, vol. 85, no. 6, pp. –, 2014.

[22] F. J. Morin, "Magnetic susceptibility of αFe_2O_3 and αFe_2O_3 with added titanium," *Phys. Rev.*, vol. 78, pp. 819–820, Jun 1950.

[23] K. Iwahashi and S. Iida, "Induced parasitic ferromagnetism in $(La_{0.9},Bi_{0.1})CrO_3$," *J. Phys. Soc. Japan*, vol. Vol: 20, Aug. 1965.

[24] A. Gavriliuk, I. Troyan, R. Boehler, M. Eremets, I. Lyubutin, and N. Serebryanaya, "Electronic and structural transitions in $NdFeO_3$ orthoferrite under high pressures," *Journal of Experimental and Theoretical Physics Letters*, vol. 77, no. 11, pp. 619–624, 2003.

[25] D. L. Wood, J. P. Remeika, and E. D. Kolb, "Optical spectra orthoferrites," *J. Appl. Phys.*, vol. 41, no. 13, pp. 5315–5322, 1970.

[26] H. Schuchert, S. Hfner, and R. Faulhaber, "Optical investigation of $DyFeO_3$," *Zeitschrift fr Physik*, vol. 220, no. 3, pp. 273–279, 1969.

[27] A. Zvezdin and V. Matveev, "Theory of the magnetic properties of dysprosium orthoferrite," *ZhETF (Soviet Phys. JETP)*, vol. 77, pp. 1076–1086, 1979.

[28] A. Maziewski and R. Szymczak, "Visual observation of phase domains in dysprosium orthoferrite," *J. Phys. D: Appl. Phys.*, vol. 10, no. 4, p. L37, 1977.

[29] F. Hong, Z. Cheng, H. Zhao, H. Kimura, and X. Wang, "Continuously tunable magnetic phase transitions in the $DyMnFeO_3$ system," *Appl. Phys. Lett.*, vol. 99, no. 9, pp. –, 2011.

[30] W. Zhao, S. Cao, R. Huang, Y. Cao, K. Xu, B. Kang, J. Zhang, and W. Ren, "Spin reorientation transition in dysprosium-samarium orthoferrite single crystals," *Phys. Rev. B*, vol. 91, p. 104425, Mar. 2015.

[31] V. G. Baryakhtar, B. A. Ivanov, and M. V. Chetkin, "Dynamics of domain walls in weak ferromagnets," *Physics-Uspekhi*, vol. 28, no. 7, pp. 563–588, 1985.

[32] V. Zvezdin, A. K. Kotov, *Modern Magnetooptics and Magnetooptical Materials*. IOP, 1997.

[33] V. V. Eremenko, N. Kharchenko, Y. G. Litvinenko, and V. Naumenko, *Magneto-optics and Spectroscopy of Antiferromagnets*. Springer Science & Business Media, 2012.

[34] A. Zvezdin and S. Kalenkov, "Orthoferrite domain structure near reorientation temperature and its influence on phase transition," *Fiz. Tverd. Tela*, vol. 14, pp. 2835–2839, 1972.

[35] A. Balbashov, A. Volkov, S. Lebedev, A. Mukhin, and A. Prokhorov, "High frequency magnetic properties of dysprosium orthoferrite," *Zh. Eksp. Teor. Fiz*, vol. 88, pp. 974–987, 1985.

[36] R. Iida, T. Satoh, T. Shimura, K. Kuroda, B. A. Ivanov, Y. Tokunaga, and Y. Tokura, "Spectral dependence of photoinduced spin precession in $DyFeO_3$," *Phys. Rev. B*, vol. 84, p. 064402, Aug. 2011.

[37] S. Woodford, A. Bringer, and S. Bluegel, "Interpreting magnetization from faraday rotation in birefringent magnetic media," *Journal of Applied Physics*, vol. 101, no. 5, p. 053912, 2007.

[38] A. J. Kurtzig, "Faraday rotation in birefringent crystals," *Journal of Applied Physics*, vol. 42, no. 9, pp. 3494–3498, 1971.

[39] G. Gorodetsky, B. Sharon, and S. Shtrikman, "Magnetic properties of an antiferromagnetic orthoferrite," *Journal of Applied Physics*, vol. 39, no. 2, pp. 1371–1372, 1968.

[40] S. L. Gnatchenko, A. B. Chizhik, V. A. Bedarev, and N. F. Kharchenko, "Magnetization reversal of orthorhombic noncentroantisymmetric antiferromagnet $DyFeO_3$," *Low Temperature Physics*, vol. 21, pp. 736–743, Sept. 1995.

[41] J. Baruchel, M. Schlenker, and S. Palmer, "Neutron diffraction topographic investigations of \exotic" magnetic domains," *Nondestructive Testing and Evaluation*, vol. 5, no. 5-6, pp. 349–367, 1990.

[42] B. A. Ivanov, "Spin dynamics of antiferromagnets under action of femtosecond laser pulses (review article)," *Low Temperature Physics*, vol. 40, no. 2, pp. 91–105, 2014.

[43] E. Galkina, I. Mikhailov, and B. Ivanov, "Dynamic spin reorientation in orthoferrites irradiated by a laser pulse," *JETP Lett.*, vol. 93, no. 12, pp. 711–715, 2011.

[44] O. Penrose, "Kinetics of phase transitions," in *Stochastic Processes in Nonequilibrium Systems*, pp. 210–234, Springer, 1978.

Chapter 5

Laser-induced shift of the Morin point in antiferromagnetic $DyFeO_3$

Imaging the domain structure of antiferromagnetic $DyFeO_3$ reveals that intense laser excitation can control the temperature of the Morin transition from a collinear to a non-collinear spin state. Excitation of the antiferromagnet with femtosecond laser pulses with the central wavelength of 800 nm leads to a shift of the transition temperature over 1 K to higher values as if the light effectively cools the irradiated area down. It is suggested that the optical control of the Morin point can be a result of photo-ionization of Dy^{3+} ions.[1]

5.1 Introduction

Manipulation of magnetic order with the help of light is an exciting research subject with sometimes counter-intuitive results and an issue of intense debates in many areas of science, ranging from the physics of spintronics [1], magnonics [2], multiferroics [3] to organic chemistry [5]. The development of lasers which are able to generate sub-100 fs intense pulses has made optical control of magnetism especially appealing. In particular, it led to the seminal observation of subpicosecond demagnetization in ferromagnetic nickel by a 60-fs laser pulse [6] and triggered the field of ultrafast magnetism - a topic that has been continuously fueled by intriguing observations and caused no shortage of controversy in the scientific community [8]. Indeed the action of the electric field component of light on electronic charges, being the largest perturbation in the physics of light-matter interaction, conserves the spin of the electron and an efficient control of the magnetic properties of media with light is therefore counter-intuitive.

[1] The chapter is adapted from: D. Afanasiev, B. Ivanov, A. Kirilyuk,T. Rasing, R.V. Pisarev and A. V. Kimel,"Laser-induced shift of the Morin point in antiferromagnetic $DyFeO_3$" Opt. Express 23, 23978-23984 (2015).

Despite this fact, several effective mechanisms of such a control have been demonstrated up to date and antiferromagnetic rare-earth orthoferrites have played an important role in these studies. Due to a strong temperature-dependent magnetic anisotropy, many rare-earth orthoferrites posses temperature driven spin-reorientation phase transitions. Therefore, even laser-induced a heating is able to induce spin reorientation in these antiferromagnets [9, 10]. Rare-earth orthoferrites are also materials with a strong spin-orbit interaction in the excited state and optically induced population of the excited states can effectively change the spin-orbit interaction [11–13]. Such a photo-induced change of the spin-orbit interaction can lead to a modification of the magnetic anisotropy and thus it is equivalent to the action of an effective magnetic field experienced by the spins. Phenomenologically, the opto-magnetic fields can be described in terms of the Inverse Faraday and the Inverse Cotton-Mouton effects [14]. Recently, it was suggested that laser excitation of the charge-transfer transitions in the rare-earth orthoferrites can effectively lead to an optical modification of the spin-spin exchange interactions in these materials [15]. Phenomenologically this phenomenon can be seen as the inverse magnetorefractive effect [16, 17]. All these studies show that light can effectively manipulate spins, controlling spin-orbit and spin-spin interactions responsible for the very existence of spin order. Obviously, such a photo-induced change of the strength of the fundamental interactions should also affect the critical temperatures of the phase transitions in the orthoferrites. Despite a large number of publications on the spin dynamics induced in rare-earth orthoferrites by intense pulses in the visible and THz spectral range, an effect of such optical excitation on the critical temperatures of the orthoferrites has not been discussed until now. In the present manuscript we address this problem and report about the effect of intense laser radiation on the critical temperature of the spin reorientation phase transition in the antiferromagnetic dielectric $DyFeO_3$. It is argued that if an intense optical pumping ionizes Dy^{3+} ions, bringing them into the Dy^{4+} state, it should lead to a substantial change of the effective exchange interaction between the spins of the Dy and Fe ions. This will consequently affect the magnetic anisotropy experienced by the Fe-ions, change the temperature dependence of the magnetic anisotropy and thus shift the Morin point at which the spin reorientation occurs.

5.2 Experimental results

Phenomenologically, the Morin phase transition is explained as a result of the interplay between two contributions to the magnetic anisotropy experienced by the Fe^{3+} spins [19]. The first contribution in the vicinity of T_M almost does not depend on temperature. It originates from the spin-orbit interaction and the effect of the crystal lattice on the orbitals of the Fe^{3+} ions. The second contribution originates from the spin-spin exchange interaction between the $3d$-electrons of the Fe^{3+} and the $4f$-electrons of the Dy^{3+}-ions. This contribution is strongly temperature dependent, which is microscopically seen as a result of thermally induced repopulation of the $4f$ states of the Dy^{3+} ions.

The studied $DyFeO_3$ crystal was cut perpendicularly to the optical axis [4] and

had a thickness of 100 μm. Using the magneto-optical Faraday effect we visualized the magnetic domains in the $DyFeO_3$ crystal and studied how laser excitation, magnetic field and temperature affect the domain pattern. In our experiments we employed the technique of magneto-optical imaging with a possibility to excite the sample with a well defined sequence of ultrashort laser pulses. Each of the pulses had the duration of 60 fs.

We have found that a long-lived effect of optical excitation on the Morin point can be seen after the crystal is excited with about 10 ultrashort laser pulses. Each of these pulses had a fluence of about 20 μJ and a central wavelength of 800 nm. In order to characterize temperature proximity to the Morin point we introduce the value $\Delta T = T - T_M$. Figure 5.1 shows an image of the crystal taken at ΔT=-1 K after the illumination. It is seen that in the low temperature phase the excitation hardly contributes to the contrast. Upon an increase of the temperature the crystal undergoes the Morin transition from the collinear to non-collinear antiferromagnetic spin state. In the area irradiated by the laser pulses the Morin transition occurs at higher temperature than in the surroundings which were not affected by the ultrashort laser pulses. Note that, if the laser pulses would simply heat the area the Morin transition occur at a lower temperature.

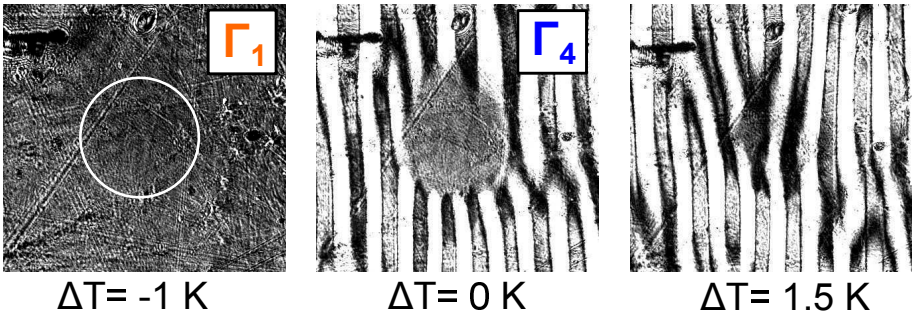

Figure 5.1: Magneto-optical images of the photo-excited $DyFeO_3$ single crystal at different temperatures. The area excited by a sequence of at least 10 ultrashort laser pulses is shown by a solid circle. In the low temperature phase ($\Delta T = T - T_M$=-1 K) one can hardly distinguish any contrast between the laser-excited and non-excited areas. A temperature increase reveals that in the area prepared by the laser-excitation the Morin transition occurs at higher temperatures.

It is known that for temperatures just below the Morin point, the transition from the Γ_1 to Γ_4 phase can be triggered by a moderate magnetic field $H > H_c$ applied along the $z-$crystallographic axis [19]. In order to trigger the field-induced Morin transition, we canted the magnetic field **H** in the sample plane (010) over 15 degrees such that the field aquired projections of the field on all three crystallographic axes. Figure 5.2 shows the images of the domain pattern obtained for the sample at a fixed temperature just below the Morin point ΔT=-5 K at different magnetic fields. These measurements clearly reveal that the irradiated area, compared to that part of the sample which was not excited by the laser light, experiences belated changes upon

the field increase.

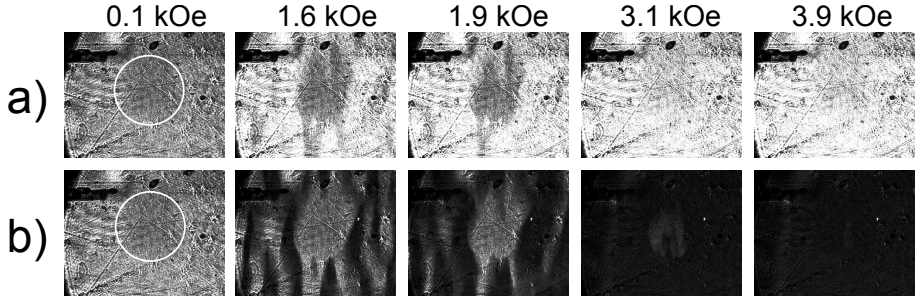

Figure 5.2: Magneto-optical images of the photoexcited $DyFeO_3$ single crystal obtained at different magnetic fields and at fixed temperature $\Delta T = T - T_M = -5$ K. Rows (a) and (b) correspond to the experiments performed in positive and negative magnetic field, respectively. Applying a positive field induces the Morin transition into a single domain state with the magnetization "up". Applying a negative magnetic field induces the Morin transition into a single domain state with the magnetization "down". The stripe domain pattern corresponds to the intermediate state, i.e. the state in which domains of two competing phases Γ_1 and Γ_4 coexist [26]. In the area excited by a sequence of the laser pulses, marked by the solid white line, the Morin transition occurs at higher fields.

To summarize the experimental observations we have studied the *H-T* phase diagram of the Morin transition. It was found that the diagram in the area which have been exposed to intense laser excitation is substantially shifted from the diagram of that part of the crystal which was not exposed to the laser light (Fig. 5.3). We could not reveal any dependence of the difference between the diagrams on the number of the laser pulses. Once the photo-excited state is formed the phase diagram does not change anymore.

All these experiments clearly reveal an effect of intense laser excitation on the Morin temperature in $DyFeO_3$ shifting the whole phase diagram to higher temperatures. We have not observed any correlation between the probability of the appearance of the area with a changed Morin temperature on the repetition rate of the exciting pulses. The lifetime of the photo-induced state exceeded 3 hours. We could not erase the photoinduced state even by heating the sample up to 150 K.

Finally, we have studied the laser-induced spin dynamics in the area prepared by excitation with at least 10 intense laser pulses. This area with the modified Morin point was excited with the help of a 60 fs pulse with a central wavelength 800 nm. The pump pulse exciting the sample at normal incidence had the Gaussian spatial profile. Similarly to the pulses we used to prepare the photo-induced state, the pump pulse was focused into a spot with the full width at half maximum of 40 μm. The following spin dynamics was monitored with the help of much less intense linearly polarized and temporally slightly broader probe pulses at the wavelength of 630 nm. Performing such experiments below the Morin point at T=33 K we have found that the pump pulse triggers the phase transition accompanied by oscillations of the magneto-optical signal as described in Chapter 4 (see Figure 5.4a). The oscillations of the magnetiza-

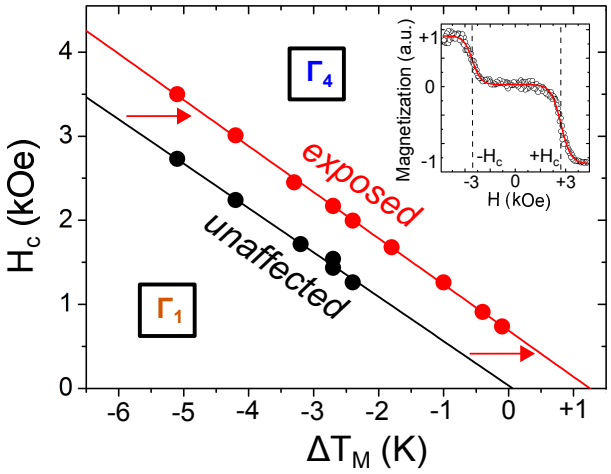

Figure 5.3: The phase diagram revealing the ratio of the critical magnetic field H and the critical temperature T at the Morin transition for the original $DyFeO_3$ and the crystal after the photoexcitation. It is seen that the Morin point in the photo-excited area is clearly shifted. The inset shows a typical dependence of the intensity on the CCD camera on the applied magnetic field and the way how the critical magnetic field was determined.

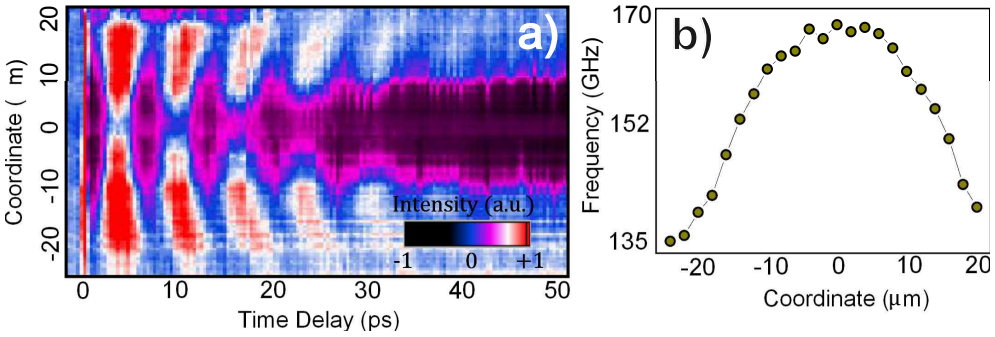

Figure 5.4: (a) The spatially and temporally resolved photo-induced magnetization dynamics in photoexcited $DyFeO_3$ along a 3 μm cross section. The pump-probe measurements are performed in the area preliminary exposed to the action of 10 pump pulses. The bias temperature is set to 33 K. (b) Spatial distribution of the frequency of the photo-induced oscillations.

tion are seen across the whole photo-excited area and their frequency approximately corresponds to the frequency of the antiferromagnetic resonance in the low temperature Γ_1 phase. It was found, that the frequency of the oscillations is not homogeneous across the photo-excited area and at the center of the spot the oscillations have a slightly higher frequency (Figure 5.4b). This observation is in perfect agreement with the statement that the photo-excitation of $DyFeO_3$ with intense laser pulses forms a new metastable state, with the Morin point shifted to higher temperatures.

5.3 Discussion

The Dy^{3+} ion contains 9 electrons on the outer $4f$ shell, thus being the Kramer's ion. The local symmetry the ion in $DyFeO_3$ is described by the point group C_S so that the original ground state multiplet ${}^6H_{15/2}$ (L=5, S=5/2, J=15/2), corresponding to that of the Dy^{3+} ion, splits and the lowest two doublets with a good accuracy are $|\pm\frac{15}{2}\rangle$ ($M_J = \pm 15/2$), $|\pm\frac{13}{2}\rangle$ ($M_J = \pm 13/2$) [22]. The energy separation between these two doublets is about E_1 =6.5 meV. Since the Dy^{3+} ions are located in non-centrosymmetric positions, otherwise forbidden optical transitions become allowed in electric dipole approximation, including the transition from ${}^6H_{15/2}$ to ${}^6F_{5/2}$ (L=3, S=5/2, J=5/2) around 1.5 eV, which perfectly matches the energy of the pumping photons.

Importantly, the light-induced shift of the Morin point was observed only under pumping by very intense laser pulses with fluence around 1 PW/cm^2. When dielectrics are excited by light with so large intensities, the multiphoton absorption, necessary to induce an interband transition, cannot be neglected [23]. Moreover, multiphoton process get significantly enhanced near optical resonances in the vicinity of real transitions, such as ${}^6H_{15/2} \rightarrow {}^6F_{5/2}$. Thus it is reasonable to assume that intense pumping of the Dy^{3+} ions in our experiments results in photo-ionization of the Dy^{3+} ions. In real crystals due to defects and impurities there is always a possibility that the excited electrons will be caught by deep and long-living states in the band gap. In this case the dysprosium ions are effectively brought to a long-living Dy^{4+} state. It is interesting to analyze how such an ionization of the dysprosium ions can affect the Morin point in $DyFeO_3$ crystals.

The Hamiltonian H^{df}_{exch} of the exchange interaction between the spin of the $3d$-electrons of the transition ions and the spins of $4f$-electrons of the rare-earth ions can be written as:

$$H^{df}_{exch} = -2\sum_{f,d} \mathcal{J} S_f S_d = -2\sum_{f,d} \mathcal{J}\frac{g_L - 1}{g_L} S_d \cdot g_L J_f \equiv \sum_f g_L \mu_B J_f \cdot H_{ex} \qquad (5.1)$$

Here $\mathcal{J}$ is the exchange integral of the d-f interaction and the summation is over all pairs of rare-earth f and transition ions d. We introduce the Lande factor g_L, determined by:

$$g_L = 1 + \frac{J(J+1) - L(L+1) + S(S+1)}{2J(J+1)} \qquad (5.2)$$

and the exchange field H_{ex} is introduced as:

$$H_{ex} = -2\sum_{d} \mathcal{J} \frac{g_L - 1}{g_L} \frac{1}{\mu_B} S_d \tag{5.3}$$

It is remarkable, that H_{ex} is proportional to some g_L dependent exchange factor $\frac{g_L-1}{g_L}$. So, the value of the d-f exchange increases in the direction from Lu^{3+} to La^{3+} (Fig. 5.5b). The Lande factor of the ${}^6H_{15/2}$ and ${}^7F_9$ multiplets are quite different ($g_L = 1/3$ in the case of ${}^6H_{15/2}$ and $g_L = 1/4$ in the case of ${}^7F_9$). Consequently, the photo-ionization of the Dy^{3+} into a Tb^{3+}-like ion results into an increase of the exchange interaction (Fig. 5.5c).

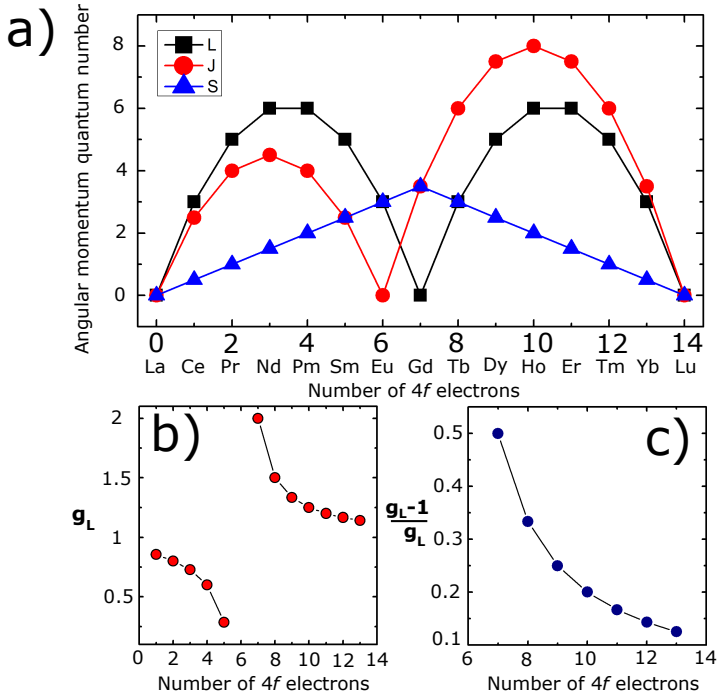

Figure 5.5: (a) Spin S, orbital L, and total angular momentum J as functions of the number of $4f$ electrons of trivalent rare earth ions. (b) Lande factor as a function of the number of $4f$ electrons of trivalent rare earth ions. (c) d-f exchange factor as a function of the number of $4f$ electrons of trivalent rare earth ions.

In the model of the Morin transition suggested in Ref. [19], the Morin temperature T_M is defined by the equality:

$$K_{Dy}\left(T_M\right) = K_{Fe}, \tag{5.4}$$

where K_{Fe} is the energy of the magnetic anisotropy which holds the Fe^{3+} spins in the xz-plane (Γ_4 phase). $K_{Dy}(T)$ is the temperature dependent d-f exchange energy,

that can be presented in the form:

$$K_{Dy} = \frac{1}{2}\chi_c H_{ex}^2 \tag{5.5}$$

Here χ_c is the effective magnetic susceptibility. The d-f exchange coupling acts as an effective anisotropy on the Fe^{+3} spins and tries to align the spins in the xy plane, along the y-axis (Γ_1 phase). According to Ref. [19]:

$$K_{Dy}(T) = K_{Dy}(0)\tanh(\frac{E_1}{2kT}), \tag{5.6}$$

where k is the Boltzman constant and $K_{Dy}(0) \sim (H_{ex})^2$.

If the concentration x of the Dy^{4+}-ions induced by light is small (xll1), the K_{Dy} can be expressed:

$$K_{Dy} = (1-x)\cdot K_{Dy^{3+}} + x \cdot K_{Dy^{4+}}. \tag{5.7}$$

Here the constants $K_{Dy^{3+}}$ and $K_{Dy^{4+}}$ account for the different Lande factors of the ions. Substituting Eq. 5.7 into the Eq. 5.4 one obtains:

$$K_{Dy}(0)(1+\frac{7}{9}x)\tanh(\frac{E_1}{2kT}) = K_{Fe}, \tag{5.8}$$

The very same equation can be written as:

$$\frac{1}{T_M}\frac{\partial T_M}{\partial x} \cong \frac{7}{9}\frac{\sinh\left(\frac{E_1}{kT_M}\right)}{\frac{E_1}{kT_M}}, \tag{5.9}$$

Equation 5.9 shows that in order to shift the Morin point over 1 K, it is sufficient to ionize about 2 % of the dysprosium ions.

5.4 Conclusion

Imaging magnetic domains in antiferromagnetic $DyFeO_3$ in the vicinity of the Morin point allows to reveal an effect of ultrashort intense laser pulses on the critical temperature of the phase transition in the orthoferrite. It is shown that excitation of the antiferromagnet with at least 10 femtosecond laser pulses at the central wavelength of 800 nm leads to a shift of the transition temperature over 1 K to higher values as if the light can effectively cool the irradiated area. The measurements at different temperatures and magnetic fields allowed us to reveal the whole phase diagram for the photo-excited crystal. It is suggested that the optical control of the Morin point can be a result of a photo-ionization of the Dy^{3+} ions.

References

[1] I. Zutic, J. Fabian, and S. Das Sarma, "Spintronics: Fundamentals and applications," Rev. Mod. Phys. **76**, 323 (2004).

[2] V. V. Kruglyak, S. O. Demokritov, and D. Grundler, "Magnonics," J. Phys. Cond. Mat. D **43**, 264001 (2010).

[3] T. Kubacka, J. A. Johnson, M. C. Hoffmann, C. Vicario, S. de Jong, P. Beaud, S. Grbel, S.-W. Huang, L. Huber, L. Patthey, Y.-D. Chuang, J. J. Turner, G. L. Dakovski, W.-S. Lee, M. P. Minitti, W. Schlotter, R. G. Moore, C. P. Hauri, S. M. Koohpayeh, V. Scagnoli, G. Ingold, S. L. Johnson, and U. Staub, Large-amplitude spin dynamics driven by a Thz pulse in resonance with an electromagnon, Science **343**, 13331336 (2014).

[4] W. J. Tabor, A. W. Anderson, and L. G. Van Uitert, "Visible and Infrared Faraday Rotation and Birefringence of Single-Crystal Rare-Earth Orthoferrites," Journal of Applied Physics, **41**, 3018-3021 (1970).

[5] D. F. Evans, "Photomagnetism of triplet states of organic molecules," Nature **176**, 777–778 (1955).

[6] E. Beaurepaire, J.-C. Merle, A. Daunois, and J.-Y. Bigot, "Ultrafast spin dynamics in ferromagnetic nickel," Phys. Rev. Lett. **76**, 4250 (1996).

[7] T. Li, A. Patz, L. Mouchliadis, J. Yan, T. A. Lograsso, I. E. Perakis, and J. Wang, "Femtosecond switching of magnetism via strongly correlated spin-charge quantum excitations," Nature **496**, 69-73 (2013).

[8] A. Kirilyuk, A. V. Kimel, and Th. Rasing, "Ultrafast optical manipulation of magnetic order," Review of Modern Physics **82**, 2731-2784 (2010).

[9] A. V. Kimel, A. Kirilyuk, A. A. Tsvetkov, R. V. Pisarev and Th. Rasing, "Laser-induced ultrafast spin reorientation in the antiferromagnet $TmFeO_3$," Nature **49**, 850 (2004).

[10] A. V. Kimel, C. D. Stanciu, P. A. Usachev, R. V. Pisarev, V. N. Gridnev, A. Kirilyuk and Th. Rasing,"Optical excitation of antiferromagnetic resonance in $TmFeO_3$," Phys. Rev. B **74**, 060403 (2006).

[11] A. V. Kimel, A. Kirilyuk, P. A. Usachev, R. V. Pisarev, A. M. Balbashov, R. V. Pisarev, and Th. Rasing, "Ultrafast non-thermal control of magnetization by instantaneous photomagnetic pulses", Nature **435**, 655 (2005).

[12] R. Iida, T. Satoh, T. Shimura, K. Kuroda, B. A. Ivanov, Y. Tokunaga, and Y. Tokura, "Spectral dependence of photoinduced spin precession in $DyFeO_3$," Phys. Rev B **84**, 064402 (2011)

[13] J. de Jong, I. Razdolski, A. M. Kalashnikova, A. Balbashov, R. V. Pisraev, A. Kirilyuk, Th. Rasing, and A. V. Kimel, "Coherent control of the route of an ultrafast magnetic phase transition via low-amplitude spin precession," Phys. Rev. Lett. **108**, 157601 (2012).

[14] P. S. Pershan, J. P. van der Ziel, and L. D. Malmstrom, "Optically-Induced Magnetization Resulting from the Inverse Faraday Effect," Phys. Rev. **143**, 574583 (1966).

[15] R. V. Mikhaylovskiy, E. Hendry, A. Secchi, J. H. Mentink, M. Eckstein, A. Wu, R. V. Pisarev, V. V. Kruglyak, M. I. Katsnelson, Th. Rasing, and A. V. Kimel, "Ultrafast optical modification of exchange interactions in iron oxides," Nature Communication 6:8190 doi: 10.1038/ncomms9190 (2015).

[16] S. O. Demokritov, N. M. Kreines, and V. I. Kudinov, "Inelastic scattering of light in the antiferromagnet EuTe," Sov. Phys. JETP **65** (1987)

[17] R. R. Subkhangulov, A. B. Henriques, P. H. O. Rappl, E. Abramof, Th. Rasing, and A. V. Kimel, "All-optical manipulation and probing of the d-f exchange interaction in EuTe," Scientific reports **4**, 4368 (2014).

[18] Wijn, H. P. J. (ed.) "Numerical Data and Functional Relationships. In Landolt-Boernstein New Series Group III,", Vol. **27**, 125-134 (1981).

[19] K. P. Belov, A. K. Zvezdin, A. M. Kadomsteva, and I. B. Krinetskii, "Orientational Transitions in Rare-Earth Magnets," Sov. Phys. JETP **40**, 980 (1974).

[20] Kurtzig A. J., "Faraday Rotation in Birefringent Crystals," Journal of Applied Physics, **42**, 3494-3498 (1971).

[21] K. Vahaplar, A. M. Kalashnikova, A.V. Kimel, D. Hinzke, U. Nowak, R. Chantrell, A. Tsukamoto, A. Itoh, A. Kirilyuk, and Th. Rasing, "All-optical magnetization reversal by circularly polarized laser pulses: Experiment and multiscale modeling," Phys. Rev. B **85**, 104402 (2012).

[22] A. K. Zvezdin and V. M. Matveev, "Theory of the magnetic properties of dysprosium orthoferrite," Sov. Phys. JETP **50**, 543-548 (1979).

[23] S.S. Mao, F. Quere, S. Guizard, X. Mao, R.E. Russo, G. Petite, and P. Martin "Dynamics of femtosecond laser interactions with dielectrics," Applied Physics A, **70**, 7, pp. 1695-1709 (2004).

[24] H. Schuchert, S. Hfner, and R. Faulhaber, "Optical investigation of $DyFeO_3$," Zeitschrift fr Physik, **220**, no. 3, pp. 273-279 (1969).

[25] E. Belorizky, M. A. Fremy, J. P. Gavigan, D.Givord, and H. S. Li, "Evidence in rareearth (R)transition metal (M) intermetallics for a systematic dependence of RM exchange interactions on the nature of the R atom," Journal of Applied Physics, **61**, 3971-3973 (1987).

[26] N.F. Kharchenko, V.V. Eremenko, S.L. Gnatchenko, R. Szymczak and H. Szymczak, "Magnetic field induced intermediate state in dysprosium orthoferrite," Solid State Communications **22**, 463-465 (1977).

Summary and Outlook

The main goal of the work, described in this Thesis, was devoted to investigations of novel approaches to trigger and launch large-amplitude magnetization dynamics by means of ultrashort laser pulses. We showed that efficient control of the photo-induced magnetization can be achieved in transparent media via optically triggering:

1. A sound wave in the gigahertz frequency range, which is strongly coupled to spins in the medium via magneto-elastic coupling,

2. A first-order magnetic phase transition from compensated collinear to canted antiferromagnetic structure, such that the net magnetization emerges on sub-100 ps timescale.

In the first experiment, we excited a magnetic mode using optically generated standing sound wave in weak ferromagnet $FeBO_3$. High efficiency of the optical excitation of the lattice-driven magnetization dynamics in $FeBO_3$ is manifested by emergence of the high order harmonics in the magnetization dynamics. The high amplitude of the pump-induced spin oscillations in combination with the high Q-factor, inherent for the lattice vibration, shows that $FeBO_3$ is a suitable material for coherent control of magnetization [1].

In the second experiment we showed that ultrafast excitation of first-order Morin phase transition in $DyFeO_3$ can induce a finite value of the net magnetization in the antiferromagnetic media. The photo-induced magnetization is present in the media long after the excitation (>3 ns). The ultrafast transition clearly demonstrates features of the magnetization dynamics intrinsic to a first-order phase transition, such as phases coexistence and presence of metastable nuclei. All-optical control of the the photo-induced magnetization can be performed not only by changing the polarization of the light pulse but also by changing the direction of the antiferromagnetic vector.

The dysprosium orthoferrite and iron borate are magnetic systems due to which the field of ultrafast optomagnetism emerged. Indeed, the femtosecond Inverse Faraday Effect was observed for the first time in $DyFeO_3$ and the Inverse Coutton-Mouton Effect in $FeBO_3$. Although a large work to reveal interaction of these materials with femtosecond laser pulses is done, discoveries of new and new look to old phenomena still make these materials attractive for femtomagnetic research. Here we would like to suggest future experiments with these materials.

In magnetism iron borate is known not-only for strong magneto-acoustic coupling but also due to the effect of the photo-induced anisotropy and photo-induced magnetization [2, 3]. The effect of the photo-induced anisotropy is manifested as light-induced emergence of the magnetic anisotropy axis, which is oriented perpendicularly to the initial magnetization orientation. Under continuous illumination this effect results in a coupled motion of the magnetization and anisotropy axis, such that rotation of the magnetization direction towards the new equilibrium results in change of the equilibrium. In the multidomain state this effect results in instability of the magnetic domain structure which is seen as motion of the magnetic domains. Although a large amount of studies was devoted to the photo-induced effect in $FeBO_3$ the microscopic nature of the effect remains unclear. The study of this phenomena on ultrafast timescale is an attractive experimental opportunity, which can shed the light on the physical mechanism responsible for the generation of the photoinduced magnetic anisotropy.

Recently it has been demonstrated, that $DyFeO_3$ subjected to high magnetic field at temperatures below the ordering of the Dy^{3+} spins (T_{Dy}=3.9 K) acquires multiferroic properties [4]. Multiferroics represent an appealing class of multifunctional materials that simultaneously exhibit several ferroic orders, such as ferroelectricity and ferromagnetism [5]. Of particular interest is existence of cross-coupling between these two order parameters named magneto-electric coupling. This coupling enables the control of electric polarization by magnetic field and conversely-the manipulation of magnetization by an external field. Interestingly, that the ferroelectricity is induced on application of large field along the $z-$axis which provokes spins to rotate and in such way initiates the Morin transition. Essential for the electric polarization emergence is the presence of the magnetic moment along the $z-$axis. In our work we show that femtosecond laser pulse can produce non-equilibrium metastable gems of the phase Γ_4 within first 3 ps. It is reasonable to assume that these gems, being created at a temperature below T_{Dy}, show multiferroic properties. Moreover, antiferromagnetic soft mode, isomorphic to the Morin transition has to possess properties of electromagnons. Thus the study of non-equilibrium Morin transition at temperatures below T_{Dy} might shed light on emergence of the magneto-electric order in multiferroic $DyFeO_3$.

Another opportunity to affect magnetization state in orthoferrites in general, and $DyFeO_3$, in particular, emerges with availability of short and intense pulses of the THz radiation. It is known that spontaneous spin-reorientational phase transitions are driven by temperature-induced repopulation of the ground multiplets of rare-earth ions [6]. In most of the orthoferrites the energy splitting between the level of the ground multipletes is in the range of 5-10 meV. This energies correspond to THz frequency range. For example, energy splitting between the lowest Dy^{3+} doublet is about 6.5 meV. This energy corresponds to 1.6 THz. Performing resonant pumping of this transition one can achieve population inversion and in such a way launch the phase transition. Contrary, to the excitation of the phase transition by means of femtosecond laser pulse the THz radiation cannot predefine direction of the induced magnetization. For this reason it is interesting to combine resonant THz radiation with ultrafast optical excitation. In such a combination it is possible to study regimes, that transition itself is launched exclusively by THz radiation.

Finally it is known that uniform spin precession of sufficiently large amplitude demonstrates instability with respect to a spatially inhomogeneous excitation, so-called Suhl instability [7]. If such a process occurs, energy is taken from the uniform spin precession and redistributed among excitation with non-zero wavevector. One can imagine an experiment in which uniform spin precession is resonantly excited and constantly maintained. If at certain moment the pump pulse is coming and provides necessary wavevector to excite instability the energy redistribution may occur. The developed technique of the femtosecond single shot imaging is suitable tool to study poorly understood non-linear regimes of the magnetization dynamics.

References

[1] E. Rozkotova, P. Nemec, N. Tesarova, P. Maly, V. Novak, K. Olejnik, M. Cukr, and T. Jungwirth, "Coherent control of magnetization precession in ferromagnetic semiconductor (Ga,Mn)As," *Applied Physics Letters*, vol. 93, no. 23, pp. –, 2008.

[2] Y. M. Fedorov, A. A. Leksikov, and A. Aksenov, "Light-induced dynamic instability of the domain structure in $FeBO_3$:Ni," *JETP Lett*, vol. 37, no. 3, 1983.

[3] M. Borovets, A. Garmonov, S. Rudov, and Y. M. Fedorov, "Photomagnetization of iron borate," *JETP Lett*, vol. 50, no. 10, 1989.

[4] Y. Tokunaga, S. Iguchi, T. Arima, and Y. Tokura, "Magnetic-field-induced ferroelectric state in $DyFeO_3$," *Phys. Rev. Lett.*, vol. 101, p. 097205, Aug 2008.

[5] S.-W. Cheong and M. Mostovoy, "Multiferroics: a magnetic twist for ferroelectricity," *Nat Mater*, vol. 6, pp. 13–20, Jan. 2007.

[6] A. Zvezdin and V. Matveev, "Theory of the magnetic properties of dysprosium orthoferrite," *ZhETF (Soviet Phys. JETP)*, vol. 77, pp. 1076–1086, 1979.

[7] A. J. Heeger and P. Pincus, "Spin-wave instability and premature saturation in antiferromagnetic resonance," *Phys. Rev. Lett.*, vol. 10, pp. 53–55, Jan 1963.

Samenvatting en vooruitblik

Het hoofddoel van het werk dat is beschreven in dit proefschrift was gericht op het bestuderen van nieuwe mechanismes voor het aan slaan van magnetisatie dynamica met een grote amplitude door middel van ultra korte laser pulsen. Wij hebben laten zien dat de fotogeenduceerde magnetisatie in een transparant medium efficient kan worden beenvloed door het optisch aan slaan van:

1. Een geluidsgolf met een frequentie in de gigahertz range, welke sterk gekoppeld is aan de spins in het medium door middel van een magnetisch elastische koppeling.

2. Een eerste order magnetische fase overgang van gecompenseerd co-lineair naar een hellend antiferromagnetische structuur zodat er netto magnetisatie ontstaat op de sub-100 ps tijdsschaal.

In het eerste experiment hebben we een magnetische mode geexciteerd gebruikmakend van een optisch geexciteerde staande geluidsgolf in de zwakke ferromagneet $FeBO_3$. Een hoge efficientie van de optische excitatie van de kristal rooster gedreven magnetisatie dynamica in $FeBO_3$ manifesteert zich met de verschijning van hogere order harmonische in de magnetisatie dynamica. De grote amplitude van de pomp geenduceerde spin oscillaties in combinatie met de hoge Q-factor, onafscheidelijk verbonden met de rooster vibraties, laat zien dat $FeBO_3$ een geschikt materiaal is voor het coherent sturen van de magnetisatie [1].

In het tweede experiment hebben we laten zien dat de ultra snelle excitatie van de eerste order Morin fase overgang in $DyFeO_3$ een netto magnetisatie met een eindige waarde kan induceren in een anti-ferromagnetisch medium. De foto geenduceerde magnetisatie tot op lange tijd na excitatie (> 3 ns) aanwezig in het medium. De ultra snelle overgang laat duidelijk eigenschappen in de magnetisatie dynamica zien die intrinsiek zijn aan een eerste order fase overgang, zoals het gelijktijdig bestaan van fasen en de aanwezigheid van meta stabiele kernen. Het volledig optisch sturen van de foto geenduceerde magnetisatie kan niet alleen bereikt worden door de polarisatie van het licht te veranderen maar ook door het veranderen van de antiferromagnetische vector.

De dysprosium orthoferriet en de ijzer boraat zijn magnetische systemen waarlangs het veld van ultra snelle optomagnetisme is ontstaan. Inderdaad was het femtosecconde omgekeerde Faraday effect voor de eerste keer waar genomen in $DyFeO_3$ en het omgekeerde Coutton-Mouton effect in $FeBO_3$. Alhoewel er al een hoop werk is gedaan

aan het in kaart brengen van de interacties in deze materialen met femtoseconde laser pulsen, maakt de ontdekking van nieuwe effecten en nieuwe inzichten van oude effecten deze materialen nog steeds interessant voor femto magnetisch onderzoek. Hier willen we graag toekomstige experimenten met deze materialen suggereren.

In magnetisme ijzer boraat is niet alleen bekend voor zijn sterke magneto-acoustische koppeling maar ook vanwege het verschijnsel van foto geenduceerde anisotropie en foto geenduceerde magnetisatie [2, 3]. Het effect van de foto geenduceerde anisotropie word gemanifesteerd door het licht geenduceerd verschijnen van een magnetische anisotropie as, welke orthogonaal georienteerd is ten opzichte van de initiele magnetische orientatie. Onder continue belichting resulteert dit effect in een gekoppelde beweging van de magnetisatie en anisotropie-as, zodat de rotatie van de magnetisatierichting naar de nieuwe evenwichtspositie resulteert in een verandering van het evenwicht. In de multidomeinstoestand resulteerd dit effect in een instabiliteit van de magnetische domein structuur, dit is zichtbaar in de vorm van het bewegen van magnetische domeinen. Alhoewel een grote hoeveelheid onderzoeken was gericht op het foto geenduceerde effect in $FeBO_3$, is de microscopische herkomst van dit effect nog steeds onduidelijk. Het onderzoek naar dit effect op een ultra snelle tijdsschaal is een aantrekkelijke onderzoeksmogelijkheid, welke licht kan schijnen op het natuurkundige mechanisme dat verantwoordelijk is voor de generatie van de foto geinduceerde magnetische anisotropie. Recentelijk heeft men laten zien dat $DyFeO_3$ multi-ferroische eigenschappen krijgt onder invloed van een hoog magnetisch veld en bij temperaturen onder de ordeningstemperatuur van de Dy^{3+} spins ($T_{Dy} = 3.9$ K)[4]. Multiferroics representeert een aantrekkelijke groep van multifunctionele materialen die simultaan verschillende ferroische orders laten zien zoals ferro-electriciteit en ferromagnetisme [5]. Met name het bestaan van een kruiskoppeling tussen deze twee order parameters, genaamd magneto-elektrische koppeling is interessant. Deze koppeling maakt het mogelijk de elektrische polarisatie te sturen met een magnetisch veld en omgekeerd. De manipulatie van de magnetisatie met een extern veld. Het is interessant dat de ferro-elektriciteit wordt gecreeerd door het aanleggen van een groot veld langs de z-as, welke de spins provoceerd om te gaan draaien en op deze manier de Morin overgang activeert. Essentieel voor het ontstaan van de elektrische polarisatie is de aanwezigheid van het magnetische moment langs de z-as. In ons werk laten we zien dat femtoseconde laser pulsen niet-evenwicht metastabiele edelstenen met een Γ_4 fase kunnen creeren binnen 3 ps. Het is redelijk om aan te nemen dat deze edelstenen, gecreerd bij temperaturen beneden T_{Dy}, multiferroische eigenschappen vertonen. Daarnaast moet de antiferromagnetisch zachte mode, isomorf aan de Morin overgang, eigenschappen van elektromagnonen laten zien. De studie van niet-evenwicht Morin overgangen op temperaturen beneden T_{Dy} zou dus mogelijk licht kunnen werpen op het ontstaan van magnetisch-elektrische orde in multiferroisch $DyFeO_3$.

Een andere mogelijkheid om de magnetische toestand in orthoferrieten in het algemeen, en $DyFeO_3$ in het bijzonder te beenvloeden ontstaat met de beschikbaarheid van korte en krachtige pulsen van THz straling. Het is bekend dat spontane spin herorienterende fase overgangen worden gedreven door temperatuur geenduceerde herpopulatie van de grond multipletten van bijzondere aarde ionen [6]. In de meeste orthoferrieten is de energie splitsing tussen de grond multiplet levels in de range van

5 tot 10 meV. Deze energieen corresponderen met de THz frequentie range. Als voorbeeld, de energie splitsing tussen de laagste Dy^{3+} doublets is rond de 6.5 meV. Deze energie komt overeen met 1.6 THz. Door deze overgang resonant te exciteren kan er populatie inversie bereikt worden en kan op deze manier de fase overgang gestart worden. Tegengesteld aan excitatie van de fase overgang door middel van femtoseconde laser pulsen, de THz straling kan de richting van de geinduceerde magnetisatie niet definieren. Om deze reden is het interessant om de resonante THz straling te combineren met ultrasnelle optische excitatie. Met zo een combinatie is het mogelijk om een regiem te onderzoeken waarin de overgang exclusief gestart wordt door de THz straling.

Ten slotte is het bekend dat uniforme spin precessie met voldoende grote amplitude een instabiliteit laat zien ten opzichte van een plaatselijk inhomogene excitatie, de zogenoemde Suhl instabiliteit [7]. Als dit proces plaats vind dan word energie van de uniforme spin precessie herverdeeld naar excitaties waarvan de golf vector een waarde ongelijk aan nul heeft. Men kan zich een experiment voorstellen waarin uniforme spin precessie resonant geexciteerd en continu onderhouden wordt. Zodra op een bepaald moment de pomp puls aankomt en de nodige golfvector aanbied om de instabiliteit te exciteren, dan zou de energie herdistributie kunnen plaats vinden. De ontwikkelde techniek van femtoseconde enkel schot beeldopname is een geschikt gereedschap om de slecht begrepen niet lineaire regio′s van magnetisatie dynamica te bestuderen.

References

[1] E. Rozkotova, P. Nemec, N. Tesarova, P. Maly, V. Novak, K. Olejnik, M. Cukr, and T. Jungwirth, "Coherent control of magnetization precession in ferromagnetic semiconductor (Ga,Mn)As," *Applied Physics Letters*, vol. 93, no. 23, pp. –, 2008.

[2] Y. M. Fedorov, A. A. Leksikov, and A. Aksenov, "Light-induced dynamic instability of the domain structure in $FeBO_3$:Ni," *JETP Lett*, vol. 37, no. 3, 1983.

[3] M. Borovets, A. Garmonov, S. Rudov, and Y. M. Fedorov, "Photomagnetization of iron borate," *JETP Lett*, vol. 50, no. 10, 1989.

[4] Y. Tokunaga, S. Iguchi, T. Arima, and Y. Tokura, "Magnetic-field-induced ferroelectric state in $DyFeO_3$," *Phys. Rev. Lett.*, vol. 101, p. 097205, Aug 2008.

[5] S.-W. Cheong and M. Mostovoy, "Multiferroics: a magnetic twist for ferroelectricity," *Nat Mater*, vol. 6, pp. 13–20, Jan. 2007.

[6] A. Zvezdin and V. Matveev, "Theory of the magnetic properties of dysprosium orthoferrite," *ZhETF (Soviet Phys. JETP)*, vol. 77, pp. 1076–1086, 1979.

[7] A. J. Heeger and P. Pincus, "Spin-wave instability and premature saturation in antiferromagnetic resonance," *Phys. Rev. Lett.*, vol. 10, pp. 53–55, Jan 1963.

List Of Publications

1. M. I. Tribrat and S. D. Pogorilyy and D. V. Afanas'ev "Approaches to parallel implementation Yen's algorithm using CUDA," IDAACS11, **1**, (2011).

2. J. H. Mentink, J. Hellsvik, D. V. Afanasiev, B. A. Ivanov, A. Kirilyuk, A. V. Kimel, O. Eriksson, M. I. Katsnelson, Th. Rasing,"Ultrafast Spin Dynamics in Multisublattice Magnets", Phys. Rev. Lett. 108 057202 (2012).

3. T.A. Ostler, J. Barker, R.F.L. Evans, R.W. Chantrell, U. Atxitia, O. Chubykalo-Fesenko, S. El Moussaoui, L. Le Guyader, E. Mengotti, L.J. Heyderman, F. Nolting, A. Tsukamoto, A. Itoh, D. Afanasiev, B.A. Ivanov, A.M. Kalashnikova, K. Vahaplar, J. Mentink, A. Kirilyuk, Th. Rasing and A.V. Kimel, "Ultrafast heating as a sufficient stimulus for magnetization reversal in a ferrimagnet," Nature-Communications 3, 666 (2012).

4. D. Afanasiev, I. Razdolski, K. M. Skibinsky, D. Bolotin, S. V. Yagupov, M. B. Strugatsky, A. Kirilyuk, T. Rasing, and A. V. Kimel, "Laser excitation of lattice-driven anharmonic magnetization dynamics in dielectric $FeBO_3$," Phys.Rev Lett. 112, 147403 (2014).

5. D. Afanasiev, B. Ivanov, A. Kirilyuk,T. Rasing, R.V. Pisarev and A. V. Kimel "Imaging and All-Optical Control of the Ultrafast Photo-Induced Magnetization Across the Morin Transition in $DyFeO_3$," to be submitted (2015).

6. D. Afanasiev, A. K. Zvezdin and A. V. Kimel "Laser-induced shift of the Morin Point in Antiferromagnetic $DyFeO_3$," Opt. Express 23, 23978-23984 (2015).

7. K. A. Brekhov, K. A. Grishunin, D. V. Afanasiev, S. V. Semin, N. E. Sherstuk, G. H. Kitaeva, E. D. Mishina, Th. Rasing and A. V. Kimel, Photo-induced dynamics and femtosecond excitation of phonon modes in ferroelectric-semiconductor $Sn_2P_2S_6$, JETP Letters (accepted).

Curriculum Vitae

Name: Dmytro V. Afanasiev
Gender: Male
Date of Birth: 06.06.1988
Place of birth: Kremenchuk, Poltava prov., Ukraine
Nationality: Ukrainian
e-mail: dima.afanasev@gmail.com

1995 – 2005: Physics and Mathematics Lyceum 4 of Kremenchuk, Poltava prov., graduated with distinction.

2005 – 2009: National Taras Shevchenko University of Kyiv, Faculty of Radiophysics.

2009: B.Sc. degree, graduated with distinction.

2010 – 2011: M.Sc. student of National Taras Shevchenko University of Kyiv, Faculty of Radiophysics (semiconductor electronics department, specialization: automation of scientific research, computer engineering), graduated with distinction.

2011 – 2015: PhD researcher at the Radboud University, Nijmegen, the Netherlands, in the group of Prof. Th. Rasing.